


Spring 5-15-2018

The Ugly Sequestosome 1: the role of p62/SQSTM1 in autophagy and multisystem proteinopathy

Eugene Lee

Washington University in St. Louis

Follow this and additional works at: https://openscholarship.wustl.edu/art_sci_etds

 Part of the [Cell Biology Commons](#), [Medicine and Health Sciences Commons](#), and the [Neuroscience and Neurobiology Commons](#)

Recommended Citation

Lee, Eugene, "The Ugly Sequestosome 1: the role of p62/SQSTM1 in autophagy and multisystem proteinopathy" (2018). *Arts & Sciences Electronic Theses and Dissertations*. 1554.

https://openscholarship.wustl.edu/art_sci_etds/1554

This Dissertation is brought to you for free and open access by the Arts & Sciences at Washington University Open Scholarship. It has been accepted for inclusion in Arts & Sciences Electronic Theses and Dissertations by an authorized administrator of Washington University Open Scholarship. For more information, please contact digital@wumail.wustl.edu.

WASHINGTON UNIVERSITY IN ST. LOUIS

Division of Biology and Biomedical Sciences
Molecular Cell Biology

The Ugly Sequestosome1: The role of SQSTM1 in autophagy and multisystem proteinopathy

Dissertation Examination Committee:

Conrad Weihl, Chair

Abhinav Diwan

Phyllis Hanson

Timothy Miller

Heather True

A dissertation presented to
The Graduate School
of Washington University in
partial fulfillment of the
requirements for the degree
of Doctor of Philosophy

May 2018
St. Louis, Missouri

© 2018, Eugene Lee

Table of Contents

| | |
|--|-----|
| List of Figures | iv |
| List of Tables | vi |
| Acknowledgments..... | vii |
| Abstract of the dissertation..... | x |
| Chapter 1: Introduction..... | 1 |
| 1.1 Overview: Multisystem proteinopathy..... | 2 |
| 1.2 Autophagy | 3 |
| 1.3 The role of SQSTM1 in autophagy..... | 4 |
| 1.4 Ubiquitination and ubiquitin-binding proteins..... | 7 |
| 1.5 Regulation of autophagic adaptor proteins by ubiquitination..... | 9 |
| 1.5 The domain of SQSTM1 and its function..... | 10 |
| 1.6 MSP disease aspect of SQSTM1..... | 12 |
| 1.7 TIA1 and stress granules..... | 13 |
| Chapter 2: The Regulation of p62/SQSTM1 via UBA domain ubiquitination | 15 |
| Preface..... | 16 |
| 2.1 Abstract | 17 |
| 2.2 Introduction | 18 |
| 2.3 Material and Methods..... | 21 |
| 2.4 Result..... | 27 |
| 2.4.1 SQSTM1's UBA domain is ubiquitinated at K420..... | 27 |
| 2.4.2 The Cul3 complex ubiquitinates SQSTM1..... | 32 |
| 2.4.3 Keap1 modulates SQSTM1 ubiquitination..... | 34 |
| 2.4.4 Keap1/Cul3-mediated ubiquitination of SQSTM1 increases sequestering activity..... | 38 |
| 2.4.5 SQSTM1 ubiquitination modulates its exchange rate..... | 44 |
| 2.4.6 Keap1/Cul3-mediated ubiquitination of SQSTM1 facilitates its role in autophagy | 48 |
| 2.4.7 UBA domain ubiquitination in SQSTM1 is diminished with disease mutations..... | 54 |
| 2.5 Discussion | 56 |
| Chapter 3: TIA1 variant drives myodegeneration in multisystem proteinopathy with SQSTM1 mutations..... | 61 |

| | |
|--|-----|
| Preface..... | 62 |
| 3.1 Abstract | 63 |
| 3.3 Introduction | 64 |
| 3.3 Material and Methods..... | 67 |
| 3.4 Result..... | 73 |
| 3.4.1 Digenic inheritance of an MSP-associated SQSTM1 mutation with a rare TIA1-N357S variant occurs in distal myopathy patients with rimmed vacuolar pathology..... | 73 |
| 3.4.2 TIA1 N357S variant promotes LLPS and impairs stress granule clearance..... | 81 |
| 3.4.3 SQSTM1 participates in stress granule protein clearance..... | 86 |
| 3.4.4 The presence of aggregated proteins increases TIA SG persistence in the presence of TIA1 mutations or loss of SQSTM1..... | 89 |
| 3.4.5 MSP associated SQSTM1 mutations impair TIA1 positive stress granule homeostasis..... | 93 |
| 3.4.6 Co-expression of MSP associated SQSTM1 mutations and TIA1-N357S is myotoxic..... | 96 |
| 3.5 Discussion | 97 |
| Chapter 4: General Conclusion and Future direction | 102 |
| 4.1 The butterfly effect of a small protein, ubiquitin..... | 103 |
| 4.2 Ubiquitination status of SQSTM1 disease mutants as a unifying disease feature | 105 |
| 4.3 SQSTM1 mediates the clearance of SGs..... | 107 |
| 4.4 Proposed model of SGs homeostasis | 108 |
| 4.5 Concluding remarks | 115 |
| References..... | 116 |

List of Figures

Chapter 1

Figure 1: The very first observed SQSTM1 body.....7

Chapter 2

Figure 1: SQSTM1 is ubiquitinated within its UBA Domain.....29

Figure S1: Schematic of SQSTM1 and expression level of SQSTM1.....31

Figure 2: The Cul3 complex ubiquitinates SQSTM1.....33

Figure 3: Keap1 modulates SQSTM1 ubiquitination.....36

Figure 4: Keap1/Cul3-mediated ubiquitination of SQSTM1 increases sequestering activity.....40

Figure S2: SQSTM1 expression level.....42

Figure S3: Endogenous SQSTM1 body size.....43

Figure 5: SQSTM1 ubiquitination modulates its exchange rate.....45

Figure S4: FRAP assay in ATG5^{-/-}MEFs.....47

Figure 6: Keap1/Cul3-mediated ubiquitination of SQSTM1 facilitates its role in autophagy.....51

Figure S5: Cell Images of mCherry-GFP-SQSTM1 Quench Assay and Co-localization of Cherry-SQSTM1 with endogenous LC3B.....53

Figure 7: SQSTM1 disease mutants have decreased ubiquitination and function.....55

Chapter 3

Figure 1: Digenic inheritance of SQSTM1 and TIA1 variants lead to a distal myopathy with RV-IBM pathology.....75

Figure S1: Histopathology of SQSTM1-TIA1 patients and controls.....76

Figure 2: TIA1-N357S variant promotes LLPS and disrupts SGs dynamics.....82

Figure S2: Immunoblot images of GFP-TIA1 and live cell images following photobleaching...84

Figure 3: SQSTM1 is necessary for SGs homeostasis.....86

Figure S3: Immunostaining of stress granules accumulating ubiquitin conjugates and bar graph of cells treated with proteasomal inhibitor (MG132) or lysosomal autophagic inhibitor (BafilomycinA)87

Figure 4: The presence of aggregated proteins increases TIA SG persistence in the presence of TIA1 mutations or loss of SQSTM1.....90

Figure 5: SQSTM1 disease mutations alter SGs kinetics and synergistically mediate myotoxicity with TIA1-N357S.....93

Chapter 4

Figure 1: UBA domain ubiquitination regulates SQSTM1's functions.....103

Figure 2: Proposed model for SGs homeostasis.....112

Figure 3: Expected result.....113

List of Tables

Chapter 3

| | |
|---|----|
| Table 1: Clinical characteristics of the patients | 77 |
| Table S1: Genotypes of PDB patients | 78 |

Acknowledgments

For last 5 years, I have been trained to look for logical rationale, scientific evidence, and ultimately a truth. I was too naïve to believe that all of Ph.D works could be done only with scientific data. However, here, I could not thank more all the people who have been supporting me during my Ph.D years. This work could not be done without them. First, I would like to thank my mentor, Chris. It was a big pleasure and honor to be his first graduate student. He is a great scientist and caring mentor, who taught me how to think, write, and speak as a scientist. Discussions with him have been fun but challenging because of his cynical but very thorough comments on my positive data. However, lots of time (since 99% of my experiments were failed), I have seen and learned his enthusiastic endeavor to analyze my negative data and step back to think about the project. I appreciate that he is a very witty person who knows the value of having a beer and taking a break. Also, my lab mates, Sara and Rocio, have been a big support for my scientific life and non-scientific life. I feel very lucky to know them. I know they are always there to help me to troubleshoot my failed experiments or just try to make me laugh. Even though sometimes we have different agenda on “room temperature” at the lab, five years being with them have been so much fun and never made me hesitating to come to the lab every morning. I still feel they’ve done lots of things to me more than what I’ve done to them. All the best wishes to them and their families. I would like to thank my committee members as well. Their patience and expertise let me grow as a more mature scientist. Lastly, I would like to thank my family. I assume it must be a big change for them too since I came here 5 years ago. I could make that decision because they always believe in me and support me to do whatever I feel right. I could not thank them more about the way they raise me to become a better person being conscious about a family, friends, other people and a society I live in.

It has been a great pleasure for me to belong in WashU community. I have met many wonderful people here and learned a lot from them too. I wish I could list all the names and thank them who became my friends and had great time together. Wish all the best to them, too.

Eugene Lee

Washington University in St. Louis

May 2018

Dedicated to my family, coffees, cookies, and milk.

ABSTRACT OF THE DISSERTATION

The Ugly Sequestosome1: The role of SQSTM1 in autophagy and multisystem proteinopathy

by

Eugene Lee

Doctor of Philosophy in Biology and Biomedical Sciences

Molecular Cell Biology

Washington University in St. Louis, 2018

Professor Conrad Weihl, Chair

Multisystem proteinopathy (MSP) defines a spectrum of degenerative diseases unified by TDP-43 pathology that affect muscle, brain and bone. Mutations in several proteins (*VCP*, *p62/SQSTM1*, *HNRNPA2B1*, *HNRNPA1*) can all cause MSP via impairments in autophagic protein degradation (*VCP* and *SQSTM1*) or RNA granule dynamics (*HNRNPA2B1* and *HNRNPA1*). Phenotypically, MSP mutations lead to variable penetrance of several phenotypes: Paget's disease of the bone (PDB), rimmed vacuolar inclusion body myopathy (RV-IBM), amyotrophic lateral sclerosis (ALS) or frontotemporal dementia (FTD). However, how a same mutation of a protein can develop different diseases remains unclear. Understanding of *p62/SQSTM1* (*SQSTM1*) function is critical to answer this question. In this dissertation, we provide evidence that *SQSTM1* is regulated via its UBA domain ubiquitination. We find that Keap1/Cullin3 ubiquitinates *SQSTM1* at lysine 420 within its UBA domain. Substitution of lysine 420 with arginine or disease-associated mutation of *SQSTM1* disrupts its ubiquitination, sequestering activity, and degradation. In contrast, overexpression of Keap1/Cullin3 in

SQSTM1-WT expressing cells increases ubiquitinated inclusion formation, SQSTM1's association with autophagosomes and rescues proteotoxicity.

We also provide evidence that the oligogenic inheritance of a disease associated SQSTM1 mutation with a rare coding variant in the low-complexity domain (LCD) of the RNA-binding protein, *TIA1* (p.N357S) can dictate a myodegenerative phenotypes. Deletion or mutation of SQSTM1 along with *TIA1* disease mutants synergistically impairs RNA stress granules clearance and their dynamics. These findings demonstrate a pathogenic connection between SG homeostasis and ubiquitin mediated autophagic degradation that defines the penetrance of a MSP phenotype.

Chapter 1: Introduction

1.1 Overview: Multisystem proteinopathy

“The Ugly Duchess” painted by Quentin Matsys around 1513 is a portrait of an old grotesque woman holding a red rose with her wrinkled face skin and breasts. This painting had been thought to be a satire of an old lady trying to seduce her younger lover. More than 150 years later, one surgeon finally suggested that this woman suffered from Paget’s disease of the bone (PDB) with deformed joints and bones. The most common genetic causes of PDB is a mutation in *p62/SQSTM1 (SQSTM1)*, whose function has been established in protein homeostasis.

Protein homeostasis is regulated by a complex network of chaperones, ubiquitin, proteases, and other factors. Cellular protein homeostasis has evolved to battle with cellular stresses including heat shock, oxidative stress, chemical stress, viral/bacterial invaders, and even their own inevitable event, aging [1]. Protein homeostasis should be more tightly regulated in differentiated cells since they are incapable of diluting toxic materials by mitosis.

Multisystem proteinopathy (MSP) defines inherited degenerative diseases that affect muscle, central nervous system (CNS) and bone [2]. MSP mutations in some genes lead to a variable penetrance of different disease phenotypes: PDB, rimmed vacuolar inclusion body myopathy (RV-IBM), amyotrophic lateral sclerosis (ALS) or frontotemporal dementia (FTD). One distinctive feature of MSP pedigrees is that patients with the same mutation and even the same mutation within a family can have different disease phenotypes (i.e. PDB in one sibling and ALS in another sibling). It is not surprising that MSP is mostly a late-onset disease since aging accelerates somatic mutations and protein homeostasis collapse of all tissues. The vast majority of MSP-affected tissues showed nucleocytoplasmic transport defect, misfolding/aggregation of proteins, and dysfunctional protein degradation. They are accumulated

with ubiquitinated aggregates in the cytoplasm that contain RNA-binding proteins with low-complexity domain (LCD) such as TDP-43, FUS and may include autophagy related proteins such as VCP, SQSTM1 [2]. Interestingly, genes associated with MSP or related to MSP can be distinguished into two categories: autophagic degradation proteins (*VCP*, *p62/SQSTM1*) or RNA-binding proteins (*HNRNPA2B1*, *HNRNPA1*, *TIA1*, *MATR3*). However, how a same mutation of a protein can cause different diseases is unclear. For example, one disease associated *SQSTM1* mutation that has been demonstrated to cause the full spectrum of MSP phenotypes (PDB, RV-IBM, ALS and FTD) is a proline to a leucine mutation at residue 392 (P392L) in the UBA domain [3-6]. This single mutation is the most common genetic cause of PDB but is incompletely penetrant suggesting that other genetic or environmental factors are needed for the phenotypic manifestation of PDB, RV-IBM, ALS or FTD. Thus, understanding a MSP-associated protein is critical to answer these two questions: how does a MSP-protein, SQSTM1, contribute to pathogenesis of MSP? What other factors are involved in MSP pathogenicity?

1.2 Autophagy

Autophagy is a highly conserved degradative mechanism in eukaryotic cells. The term “autophagy” means “self-eating” in Greek to describe the presence of single- or double-membraned intracellular vesicles containing cellular compartments or organelles [7]. Under basal condition, autophagy plays a critical role to maintain homeostasis to recycle nucleic acids, lipids, proteins, carbohydrate, and organelles. With internal or external stress, cellular materials or invading bacteria/virus are recognized by autophagic adaptor proteins and sequestered into double-layered phagopores, which become autophagosomes after the membrane closure. These autophagosomes fuse with lysosomes and their engulfed cargoes are degraded.

Autophagosomes formation is a rapid process but requires more than 100 proteins [8]. Briefly, a ULK/Beclin-1/VPS34 complex localizes the site of autophagosome initiation. Active VPS34 phosphorylates the lipid to generate phosphatidylinositol 3-phosphate (PtdIns(3)P) on the phagopore. PtdIns(3)P on the surface of phagopore is recognized by ATG12, which directly interact with ATG16L1. ATG16L1 and ATG12-ATG5 to form a complex that activates ATG7 and ATG3. Together with ATG16L1/ATG12/ATG5, ATG3 and ATG7 covalently conjugates phosphatidylethanolamine (PE) to LC3-I, which is a maturation form of LC3 after proteolytic cleavage at its c-terminus. Lipidated LC3 known as LC3-II is attached on membranes, allowing cargoes uptake upon interaction with several autophagic adaptor proteins and the membrane closure. While autophagic structure grows, various cellular sources such as the endoplasmic reticulum (ER), Golgi, recycling endosomes, mitochondria, and plasma membrane will supply autophagic membrane materials [9].

1.3 The role of SQSTM1 in autophagy

In addition to the identification of MSP-associated autophagy genes, autophagy has been linked to MSP since tissue-specific ablation of autophagy genes in mice and other models mimics a key pathological feature of MSP: the accumulation of ubiquitin-positive inclusion bodies in the cytoplasm [10-13]. Since autophagy genes knock-out mouse models (*ATG5*^{-/-} or *ATG7*^{-/-} mice) die soon after birth, neural-cell-specific *ATG5*^{-/-} mice was generated. In this mouse model, SQSTM1-positive ubiquitinated proteins were accumulated in central nervous system. In addition, they showed motor and behavioral deficits, suggesting that the autophagy in basal level maintain protein homeostasis to prevent from neurodegeneration [10]. In muscle-specific *ATG7*^{-/-} mice, SQSTM1-positive ubiquitinated proteins and vacuolar structures were accumulated in

muscle fibers together with disrupted sarcomere and other muscle structures, indicating that these mice have myopathy [13].

Autophagy can be a selective degradative process via the utilization of various autophagic adaptor proteins. SQSTM1 is one of such autophagic adaptor proteins, which selectively recognize ubiquitinated cargoes and deliver them to growing autophagosomes for their degradation. SQSTM1 had been initially identified as a polyubiquitin shuttling protein to the 26S proteasome [14]. However, two types of cytoplasmic SQSTM1 inclusions (SQSTM1 bodies) with ubiquitin aggregates were consistently observed: small membrane-less bodies and larger bodies with autolysosomes (Figure1) [15-17]. These observations suggest the role of SQSTM1 in autophagy. More specifically, SQSTM1 directly binds to ubiquitinated protein aggregates via its UBA domain and sequesters them into inclusion bodies via its PB1 domain. SQSTM1 also interacts with autophagosomes via its LC3-interacting (LIR) motif [16, 18]. Depletion of SQSTM1 in cell, mice and *Drosophila* models leads to the accumulation of soluble ubiquitinated proteins without the formation of inclusion bodies, suggesting that SQSTM1 is required for the formation and degradation of inclusion bodies in the cytoplasm [11, 12, 16, 18].

Cargo trafficking to autophagosomes is not solely driven by one autophagic adaptor protein alone. Different autophagic adaptor proteins cooperate to each other to select specific cargoes [9]. For example, SQSTM1 teams up with NBR1 to recognize aggregated proteins [19]. NDP52 and optineurin (OPTN) aid SQSTM1 to get rid of invading bacteria [20-22]. Depletion of a certain autophagic adaptor protein does not always guarantee the impairment of a selective autophagic process, suggesting the complementary but selective function of autophagic adaptors. However, a regulatory mechanism for autophagic adaptors is not yet well-established.

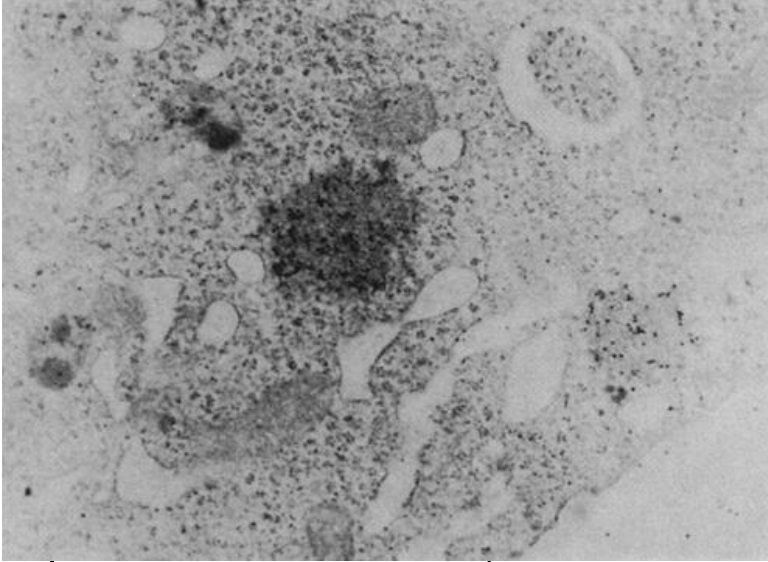


Figure 1. The very first observed SQSTM1 body [17].

1.4 Ubiquitination and ubiquitin-binding proteins

Ubiquitin is a versatile modification protein that controls a various cellular process. A protein degradation function was the first identified function of ubiquitin, but it has been expanded to various cellular functions including inflammation, DNA repair, signal transduction, endocytosis and autophagy [23, 24]. Covalently binding of ubiquitin to a target protein requires E1/E2/E3 enzymes. E1 enzymes (two have been identified in human) activate ubiquitin to form an E1-ubiquitin thioester in an ATP-dependent manner. They are transferred to E2 enzymes (~40 have been identified in human) to form an E2-ubiquitin thioester. Finally, E3 ligases (~600 have been identified in human) interact with the E2-ubiquitin thioester and a target protein. E3 ligases catalyze them to form the isopeptide bond between the c-terminal glycine of ubiquitin and lysine residue of a target protein. Deubiquitinating enzymes (DUB; ~100 have been identified) remove tagged ubiquitins from the target proteins.

The modification by ubiquitin (referred to as ubiquitination) on a target protein can be varies from a single molecule attachment (monoubiquitination), several single attachments (multiple monoubiquitination) to a ubiquitin chain attachment (polyubiquitination).

Polyubiquitination occurs when a glycine residue of ubiquitin repeatedly links to one of seven lysine residues (K6, K11, K27, K29, K33, K48, and K63) within a neighboring ubiquitin. The function of each mono- and poly-ubiquitination chain has not been well-studied, but it is believed that different ubiquitin chains can dictate various cellular functions [25, 26]. K48-linked polyubiquitination is a classic example that targets a protein to the proteasome for their degradation. The multisubunit 26S proteasome is a cylinder complex that recognizes, unfolds and transfers polyubiquitinated proteins into its hollow core where the substrates are catalyzed

into small peptides. In contrast, K6-linked polyubiquitination does not destabilize its target protein or increase its abundance upon proteasomal inhibition, suggesting its proteasome-independent function. K63-linked polyubiquitination is known as a preferential signal of protein aggregates for their autophagic/lysosomal degradation. Also, K63-linked polyubiquitination can increase interaction of a target protein with other proteins while monoubiquitination can inhibit the interaction.

Along with different ubiquitin conjugation systems, the specificity of ubiquitin signaling is also achieved by post-modifications on ubiquitin molecules and/or multiple ubiquitin-binding proteins [23]. Ubiquitin-binding proteins contain ubiquitin-binding domains such as UIM, CUE, UBAN, and UBA domains, which non-covalently bind to a hydrophobic patch (Ile 36 or Ile44 patch) of ubiquitin. Ubiquitin-binding proteins are frequently regulated by its ubiquitination. For example, monoubiquitination of a UIM-domain containing protein, eps15 alters its binding to ubiquitin and disturbs its function during endocytosis [27, 28]. Thus, the combinational use of ubiquitination and ubiquitin-binding proteins endlessly but selectively expands cellular regulatory modules.

The collaborative practice of various ubiquitin chains and ubiquitin-binding proteins may also contribute to the selective autophagy. Mitophagy is the best example that the outer membrane of damaged mitochondria can be tagged with K6, K11, K48, and K63-linked polyubiquitination catalyzed by Parkin E3 ligase *in vivo* and *in vitro* in different cells [29]. The ubiquitin chains are recognized by several ubiquitin-binding autophagy adaptors such as SQSTM1, OPTN, NBR1, NDP52, and Tax1-binding protein1. However, which type of ubiquitin chain is specifically recognized by autophagic adaptors remains elucidated. Recent studies suggested that post-translational modification regulates the preferential binding of autophagic

adaptors during selective autophagy. Two different studies demonstrated that TBK1-mediated phosphorylation within/adjacent to ubiquitin-binding domain (UBAN) of OPTN selectively increases its binding affinity to K48 and K63-linked polyubiquitin chains during mitophagy [30, 31]. Similarly, casein kinase2 phosphorylates SQSTM1's UBA domain, increasing its binding affinity to K63-linked polyubiquitin *in vitro* [32].

1.5 Regulation of autophagic adaptor proteins by ubiquitination

Autophagic adaptor proteins directly associate with ubiquitinated proteins via its ubiquitin-binding domain. Accumulating evidence supports that ubiquitination also regulates the function of autophagic adaptor proteins. For example, K48-linked ubiquitination of the autophagic adaptor OPTN by HACE1 increases its association with SQSTM1 and enhances autophagic flux [33]. Also, several studies suggest that ubiquitination of SQSTM1 modulates its functions. RPN26 ubiquitinates SQSTM1's UBA domain at the ER membrane leading to an increase in SQSTM1's capture of ubiquitinated endosomes [34]. However, it is not clear which lysine within SQSTM1's UBA domain is ubiquitinated by RPN26. During xenophagy, RNF166 catalyzes K33-linked ubiquitination of SQSTM1 and recruits SQSTM1 and another autophagic adaptor, NDP52 to ubiquitinated bacteria [35]. RNF166 may target multiple lysine sites within different domains of SQSTM1 including K91 in the PB1 domain. Parkin and TRIM21 also ubiquitinate SQSTM1's PB1 domain [36, 37]. Parkin catalyzes ubiquitination of K13, promoting SQSTM1's degradation. TRIM21 ubiquitinates SQSTM1 at K7 within the PB1 domain, abrogating SQSTM1's oligomerization and sequestering activity. Other E3 ligase, NEDD4 is also reported to ubiquitinate SQSTM1 via its PB1 domain, affecting SQSTM1 body formation [38]. Notably,

an E2 complex, UBE2D2/UBE2D3 catalyzes ubiquitination at K420 within SQSTM1's UBA domain [39]. This E2 ligase complex directly interacts with SQSTM1 via residues adjacent to the LIR motif.

1.5 The domain of SQSTM1 and its function

SQSTM1 directly interacts with another E3 ligases complex, Keap1/Cullin (Cul3) to regulate cell signaling pathways via its Keap1-interacting motif (KIR) [40-42]. Cul3 is one of Cullin-RING E3 ligases, which may need an E3 ligase adaptor to catalyze its substrate. One of such E3 ligase adaptors is Keap1, which interacts with Cul3 via its BR-C, ttk and bab (BTB) domain at the N-terminus [43]. The most well-established substrate of Keap1/Cul3 complex is a transcription factor NF-E2 p45-related factor 2 (Nrf2). In basal level, the Kelch domain of Keap1 recognizes the DLG and ETGE motifs of Nrf2. Consequently, Nrf2 is ubiquitinated by Keap1/Cul3 complex and delivered for proteasomal degradation. However, upon the generation of reactive oxidative stress (ROS) or electrophile in cells, the Keap1 binding to Nrf2 is destabilized. Stabilized Nrf2 enters the nucleus to activate the expression of genes regulated by antioxidant response elements (AREs) [44]. Several studies demonstrated that SQSTM1 sequesters Keap1 into aggregates under conditions of autophagic inhibition [40-42, 45]. This SQSTM1-Keap1 interaction also disturbs Keap1 interaction with Nrf2 and subsequently diminishes Cul3-catalyzed ubiquitination on Nrf2. Thus, it allows Nrf2 to activate AREs genes.

The UBA domain mediates several functions including sequestering activity, ubiquitin binding, and self-dimerization. UBA domain dimerization inactivates ubiquitin binding since it shares interfaces for dimerization and ubiquitin binding [46]. Phosphorylation of the UBA domain disrupts this self-dimerization and increases its binding affinity to ubiquitin [32, 47].

Similarly, a purified SQSTM1 carrying the K420R mutation abolishing its ubiquitination along with an E409K mutation, which destabilizes the UBA dimerization increased poly-ubiquitin association *in vitro*, as compared to purified SQSTM1-WT. A purified ubiquitinated SQSTM1-WT also bound more poly-ubiquitin than unmodified SQSTM1-WT *in vitro* [39].

There is accumulating evidence that the oligomerization of autophagic adaptor proteins is critical for recognizing polyubiquitinated protein aggregates and interacting with phagophores [48-51]. Autophagic adaptor protein in yeast, Cue5 (human homolog Tollip) oligomerizes via its UBA domain and this oligomerization process allows its ubiquitinated aggregates to be degraded via autophagy, not via the proteasome [48]. However, a proteasomal protein, Dsk2 (human homolog UBQN2) does not self-associate despite the presence of its UBA domain and ubiquitinated aggregates accumulate in these cells.

The formation and degradation of ubiquitinated protein aggregates or organelles require SQSTM1's oligomerization [16, 52]. The oligomerization of SQSTM1 is required for sequestering damaged mitochondria after Parkin catalyzes K63-linked polyubiquitination on them (Narendra et al., 2010). This sequestering activity is mediated by SQSTM1's UBA domain and PB1 domain that regulates SQSTM1's self-association [51]. This self-association of SQSTM1 is necessary for the formation of a filamentous SQSTM1 scaffold that then allows for the interaction with LC3 and development of phagophore membrane [53]. The deletion of either the PB1 or UBA domains disrupts the self-association of SQSTM1 and reduces cell viability against proteotoxicity [16]. In addition, the high-ordered SQSTM1 structure can be altered in presence of different types of ubiquitin [50, 51, 54]. SQSTM1 filaments are fragmented in the presence of polyubiquitin [51]. Recently, Zaffagnini and colleagues demonstrated that SQSTM1 spontaneously oligomerizes with polyubiquitin *in vitro* (Zaffagnini et al., 2018). Interestingly,

polyubiquitin and SQSTM1 respectively have different dynamics *in vitro*, suggesting that SQSTM1 oligomer is a dynamic high-ordered structure but may change its dynamics in presence of ubiquitin.

1.6 MSP disease aspect of SQSTM1

Dominantly inherited deletion or missense mutations of SQSTM1 are predominantly within its UBA domain in several degenerative diseases, including PDB, ALS, FTD, and RV-IBM [55]. The common pathological feature among these different tissues is the accumulation of ubiquitin/SQSTM1-positive protein aggregates. However, how SQSTM1 mutations contribute to pathogenesis is not clear but disrupted ubiquitin binding *in vitro* may explain it. For example, purified SQSTM1-M404V and SQSTM1-G425R proteins diminished ubiquitin binding *in vitro* [56]. SQSTM1 mutations are recently identified in KIR motif and LIR motif from PDB and ALS patients. These KIR disease mutants decreased the interaction with Keap1 while LIR disease mutants diminished LC3 binding [57, 58].

The most common genetic cause of PDB is SQSTM1-P392L mutation in the UBA domain. This mutation has been identified to cause all other MSP-spectrum diseases: RV-IBM, ALS, and FTD [3-6]. However, this single point mutation showed incomplete penetrance with all these MSP diseases, suggesting other genetic or environmental factors are involved. One study showed that transgenic mice co-expressing SQSTM1-P392L mutation along with measles virus nucleocapsid gene developed PDB phenotypes and PDB patients with SQSTM1-P392L mutation also carry measles virus nucleocapsid gene, suggesting that this measles virus gene may dictate bone-specific phenotypes of SQSTM1 diseases [59]. However, what dictates other SQSTM1-associated disease phenotypes such as RV-IBM, ALS, and FTD still remains unclear.

1.7 TIA1 and stress granules

The accumulation of RNA-binding proteins such as TDP-43 in cytoplasmic inclusion bodies is one of distinguished features of MSP [2]. In addition, several MSP mutations have been identified in low-complexity domain (LCD) of RNA-binding proteins such as TDP-43, FUS, HNRNPA2B1, TIA1, etc [60-65]. The MSP disease mutation-clustered LCD domain contains repeats mostly enriched for glycine and uncharged polar amino acids, which are intrinsically disordered [66]. Recent findings suggest that multivalent weak interactions between different LCD domains mediate liquid-liquid phase separation (LLPS) of membrane-less organelles such as stress granules (SGs) between soluble and liquid-droplet states [67, 68]. When LCD domain-containing proteins undergo LLPS, these proteins demix from homogenous solutions and separate into two phases: dense phase and dilute phase to form liquid droplets. However, the LCD domain mutations or/and stress conditions promote LLPS and convert the proteins into fibers.

SGs are dynamic membrane-less organelles containing untranslated mRNA, RNA-binding proteins and other initiation factors [68, 69]. SGs are evolutionally conserved in multiple organisms and may serve several protective roles against cellular stress such as viral infection, oxidative stress, heat shock, and proteasomal/autophagic inhibition, etc [70]. During the translation inhibited by those stresses, mRNA and RNA-binding proteins are stalled and assemble as SGs. Upon cellular stress dissipation, SGs disassemble into translating mRNA and RNA-binding proteins to re-initiate the translation. Interestingly, MSP-associated mutations in LCD domain of RNA-binding proteins alter their biophysical properties and increase their fibrilization via LLPS, impairing SGs clearance. TIA1, a key component of SGs, is one of such

examples. Dominantly inherited TIA1 mutations within its LCD domain manifest MSP phenotypes including ALS/FTD and distal myopathy termed Welander distal myopathy [60, 61]. These TIA1 mutations promote LLPS and increase its fibrilization. TIA1 aggregates within SGs along with TDP-43 and impairs the clearance of SGs.

Autophagy has been linked to SGs homeostasis. Recent studies show that SGs clearance is impeded in autophagy-deficient or autophagy-inhibited cells. In these studies, they also showed that a MSP-associated protein, VCP may be required for the clearance of SGs. VCP is a ubiquitin segregase that mediates autophagic degradation of ubiquitinated proteins along with its co-factors. VCP is the first identified MSP-associated protein that causes RV-IBM, ALS, FTD and/or PDB. SGs clearance is impaired in VCP-depleted cells or VCP disease-mutations carrying cells. Recent study showed that another MSP-associated protein, SQSTM1 accumulates within SGs along with FUS disease-mutants in autophagy-deficient cells [71]. After heat shock or other SG inducers treatment, SQSTM1 is recruited to SGs containing misfolded proteins [72, 73]. However, the mechanism of SGs clearance is still unclear.

Chapter 2: The Regulation of
p62/SQSTM1 via UBA domain
ubiquitination

Preface

This chapter has been previously published.

Title: Keap1/Cullin3 Modulates p62/SQSTM1 Activity via UBA Domain Ubiquitination.

YouJin Lee, Tsui-Fen Chou, Sara K. Pittman, Amy L. Keith, Babak Razani, Conrad C. Weihl

Lee Y, Chou TF, Pittman SK, Keith AL, Razani B, Weihl CC. (2017) *Cell Reports*. DOI:

<http://dx.doi.org/10.1016/j.celrep.2017.03.030>

2.1 Abstract

p62/SQSTM1 (SQSTM1) is a scaffolding protein that facilitates the formation and degradation of ubiquitinated aggregates via its self-interaction and ubiquitin binding domains. The regulation of this process is unclear but may relate to the post-translational modification of SQSTM1. In the present study, we find that Keap1/Cullin3 ubiquitinates SQSTM1 at lysine 420 within its UBA domain. Substitution of lysine 420 with an arginine diminishes SQSTM1 sequestration and degradation activity similar to that seen when the UBA domain is deleted. Overexpression of Keap1/Cullin3 in SQSTM1-WT expressing cells increases ubiquitinated inclusion formation, SQSTM1's association with LC3 and rescues proteotoxicity. This effect is not seen in cells expressing a mutant SQSTM1 that fails to interact with Keap1. Interestingly, SQSTM1 disease mutants have diminished or absent UBA domain ubiquitination. These data suggest that the ubiquitination of SQSTM1's UBA domain at lysine 420 may regulate SQSTM1's function and be disrupted in SQSTM1 associated disease.

2.2 Introduction

Autophagic degradation can be a selective process targeting distinct cargoes via autophagic receptor proteins [74]. p62/SQSTM1 (SQSTM1) is an autophagic receptor that interacts with ubiquitinated cargo via its ubiquitin association (UBA) domain and recruits them via its LC3-interacting motif into the growing autophagosome membrane [11, 16, 18]. Autophagic degradation of ubiquitinated proteins requires SQSTM1 to sequester them into inclusion bodies. This property is mediated by SQSTM1's UBA domain but also via a PB1 domain that facilitates homo-oligomerization [16, 51, 53].

The oligomerization of SQSTM1 may serve several different roles in both inclusion body formation and autophagy. For example, SQSTM1 oligomers may organize along with ubiquitinated proteins sequestering them into inclusions [16]. In addition, SQSTM1 forms filamentous structures via its PB1 domain that may serve as a site for phagophore membrane development [53]. Interestingly, SQSTM1 filaments are fragmented in the presence of polyubiquitin [51]. This fragmentation is mediated via SQSTM1's UBA domain and suggests that higher-ordered oligomeric SQSTM1 structures may dynamically change in the setting of ubiquitin.

Consistent with SQSTM1's role in the handling of ubiquitinated protein aggregates, dominantly inherited missense or deletion mutations within SQSTM1's UBA domain are associated with degenerative diseases including Paget's disease of the bone (PDB), amyotrophic lateral sclerosis (ALS), fronto-temporal dementia and more recently inclusion body myopathy [55, 75]. The common pathogenic feature among these disparate tissues is the accumulation of

SQSTM1 aggregates and ubiquitinated inclusions. How SQSTM1 mutations contribute to disease pathogenesis is unclear but may relate to diminished ubiquitin binding activity [76].

The post-translational modification of SQSTM1 has been demonstrated to regulate its function. Phosphorylation at one of two different serines within SQSTM1's UBA domain enhances its association with ubiquitinated proteins promoting sequestering activity and rescue from proteotoxic stress [32, 47]. Ubiquitination of SQSTM1 also occurs. Mass spectrometry approaches have identified multiple ubiquitination sites on SQSTM1 that include lysine residues within the PB1 and UBA domains [36, 77].

Ubiquitination of SQSTM1 can also modulate its function. Recently, studies identified ubiquitin ligases that depending upon their site of ubiquitination inhibited or facilitated SQSTM1's function [34, 35, 37]. The E3 ubiquitin ligase TRIM21 ubiquitinates SQSTM1 at lysine 7 within its PB1 domain. This ubiquitination abrogates SQSTM1 oligomerization thus inhibiting SQSTM1's sequestration activity [37]. SQSTM1 is also ubiquitinated within its UBA domain by the E3 ligase RNF26 although the exact residue in the UBA domain was not determined. This ubiquitination event was proposed to enhance SQSTM1's interaction with other ubiquitin adaptors such as, TOLLIP, thus facilitating vesicular cargo sorting [34]. In addition, RNF166 ubiquitinates SQSTM1 at residues K91 and K189 [35]. Interestingly, these events involve atypical ubiquitin chains that are K29- and K33-linked. RNF166 mediated ubiquitin ligase activity facilitates SQSTM1's role in the xenophagic degradation of intracellular bacteria [35].

SQSTM1 also associates with E3 ligases to regulate cell signaling pathways. Keap1 is an E3 ligase adaptor that contains a BR-C, ttk and bab (BTB) domain at its N-terminus, which mediates interaction with Cullin3 (Cul3) [43]. One substrate of the Keap1/Cul3 complex is Nrf2. When Keap1 is destabilized by oxidative stress, Nrf2 stabilizes and translocates to the nucleus where it activates the expression of genes regulated by antioxidant response elements [44]. Several studies demonstrate that SQSTM1 binds to Keap1; sequestering it into aggregates under conditions of autophagic inhibition [40-42]. This SQSTM1-Keap1 interaction titrates Keap1 away from Nrf2, stabilizing Nrf2 by decreasing Cul3 mediated ubiquitination and allowing Nrf2 mediated activation of the antioxidant response pathway.

In this thesis dissertation work, we find that SQSTM1 is ubiquitinated at lysine 420 within its UBA domain. This ubiquitination is mediated by the Keap1/Cul3 E3 ligase complex. Moreover, mutation of lysine 420 or disease mutations within SQSTM1's UBA domain affect its ubiquitination and diminish its sequestration activity. The ubiquitination of ubiquitin binding proteins such as SQSTM1 is emerging as a novel regulatory mechanism for autophagic adaptor proteins.

2.3 Material and Methods

Reagents and antibodies

N-Etylmalimide (NEM; #3876), BafilomycinA (#B1793) and cycloheximide (#C7698) is from Sigma. MLN4924 (#B1036) is from ApexBio. Anti-HA monoclonal antibody (Covance #MMS-101P, 1:1000 for WB), anti-HA polyclonal antibody (Abcam #9110, 1:1000 for WB), anti-Flag monoclonal antibody (Sigma #F1804, 1:1000 for WB, 1:100 for IF), anti-Flag polyclonal antibody (Sigma #F7425, 1:1000 for WB, 1:100 for IF), anti-SQSTM1 monoclonal antibody (Novus #H00008878-M01, 1:1000 for WB, 1:100 for IF), anti-SQSTM1 polyclonal antibody (Proteintech #18420-1-AP, 1:1000 for WB, 1:100 for IF), anti-Ub monoclonal antibody (FK2; Biomol #PW-8810, 1:500 for WB, 1:100 for IF), anti-Ub polyclonal antibody (Dako #Z0458, 1:5000 for WB, 1:100 for IF), anti-Gapdh polyclonal antibody (Cell Signaling #2118, 1:1000 for WB), anti-myc monoclonal antibody (Cell Signaling #2276, 1:1000 for WB), Anti-V5 HRP antibody (Invitrogen #B96125, 1:1000 for WB), anti-LC3B polyclonal antibody (Sigma #L7543, 1:500 for WB), anti-Keap1 polyclonal antibody (SantaCruz #sc15246, 1:500).

Cell culture and transient transfection

Immortalized wild type and SQSTM1^{-/-}-MEFs were a kind gift by Dr. Komatsu, Niigata University [11]. Keap1^{-/-}-MEFs were from Dr. Wakabayashi, University of Pittsburgh [78]. ATG5^{-/-}-MEFs were from Dr. Virgin, Washington University in St. Louis. MEFs were maintained in in Dulbecco's modified Eagle's medium (DMEM, Gibco #11965-084), 10% fetal bovine serum (FBS, Atlanta Biologicals #S10350H), and 50 µg/mL penicillin and streptomycin (P/S, Sigma #P4333), 1% sodium pyruvate (Gibco #11360070), and 1% non-essential amino

acid (Gibco #11140050) at 37°C with 5% CO₂. U2OS cells were maintained in DMEM with 10% FBS, 50 µg/mL P/S at 37°C with 5% CO₂. Transfection was performed with lipofectamine2000 (Life Technologies #11668019) according to the manufacturer's instruction. 24hr post-transfection, cells were washed three times with ice-chilled PBS and harvested in lysis buffer. HA-human SQSTM1-WT gift from Dr. Moscat, Sanford-Burnham Medical Research Institute [79], HA-SQSTM1 K420R, HA-SQSTM1 ΔUBA, ΔPB1, D69A P392L, M404V, G411S, G425R generated using Quik Change Mutagenesis Kit (Agilent Technologies #200517). HA-SQSTM1 6 K/R commercially synthesized by Genewiz and HA-SQSTM1 7 K/R generated by mutagenesis. pDEST-mCherry-human SQSTM1 WT and pDEST-mCherry-eGFP-SQSTM1 WT gifted from Dr. Johansen, The Arctic University of Norway [18]. pDEST-mCherry-human SQSTM1 P392L, M404V, G411S, G425R generated by mutagenesis. Flag-Ub-WT from Dr. Yarden, Weizmann Institute of Science [80]. V5-Cul3, Cul3-Flag and Myc-Keap1 gifted from Dr. Diehl, University of South Carolina [81]. DN-CUL3-FLAG from Addgene (#15820). HttQ72-CFP previously described [82]. His-Ub purchased from Addgene (#31815).

Immunoprecipitation and Western blotting

Cells were harvested in NP-40 lysis buffers (50mM Tris pH7.7, 150mM NaCl, 1% NP-40) or RIPA buffers (50mM Tris pH 7.7, 150mM NaCl, 1% NP-40, 0.5% sodium deoxycholate, 0.1% sodium dodecyl sulfate) with protease inhibitor cocktails (PIC; Sigma#P8340), 20mM NEM and phenylmethylsulfonyl fluoride (PMSF; Sigma#P7626) and washed with ice-chilled PBS. Lysates were centrifuged for 15mins at 4°C, 16,000g. The supernatants were collected. Some lysates were incubated with Usp2cc (1µg Usp2cc per 100µg cell lysates; R&D #O75604). 200µg of cell lysates were pre-cleared for 1hr with end-over-end rotator with 10µg of dynabeads M-270 Epoxy (Life Technologies #14302D) at 4°C. Samples were placed on a magnet and the supernatants

were collected. The supernatants were incubated with antibody-conjugated Dynabeads on the rotator at 4°C for 2hrs. For antibody conjugation, dialyzed antibodies were coupled to Dynabeads M-270 Epoxy beads (Life Technologies #14311D) according to the manufacturer's instruction. After 2hr incubation, the samples were placed on the magnet and washed three times with lysis buffer.

In the case of denaturing conditions, the assay was performed as previously described [37]. Briefly, 10% of sample was kept as “input” samples. The rest of samples were mixed with equal volume of 6M guanidine buffer (6M guanidine-HCl, 100mM sodium phosphate, 600mM NaCl, 30mM imidazole, 0.05% Tween-20, pH 8.0). The mixed samples were pre-cleared for 1hr on end-over-end rotator with 10µg of Dynabeads M-270 Epoxy at 4°C. The samples were placed on a magnetic stand and the supernatants were collected. The supernatants were incubated with HisPur Ni-NTA Magnetic Beads (Thermo Sci#88831) on the rotator for 2hrs at 4°C. The samples were placed on a magnetic stand and washed twice with 8M urea buffer (8M urea, 100mM sodium phosphate, 10mM Tris-Base, 50mM imidazole, pH 8.0). After all urea buffer completely removed, the samples containing beads were incubated with elution buffer (250mM imidazole, 100mM sodium phosphate, 600mM NaCl) for 30mins on a rotator. The samples were mixed with β-mercaptoethanol containing sample buffer and boiled at 95°C for 5mins. The Western blot analysis was performed as previously described [83].

***In vitro* ubiquitination assay**

Recombinant E2 enzyme (UbcH5a/UBE2D1; #E2-616) and ubiquitylation kit containing E1 enzyme (#K-995) were purchased from Boston Biochem. Recombinant fragment of Histidine tagged human SQSTM1 (#SQSTM1-29505TH) containing amino acids 83-440 and was purchased from Biomart. Cells were transfected with Cul3 WT-Flag or Cul3-D.N.-Flag. 24hrs

after, cells were harvested in RIPA buffer and immunoprecipitated with Flag-antibody-conjugated Dynabead for 2hrs at 4°C. The samples were washed three times with lysis buffer and incubated with E1, E2, ubiquitin and His-SQSTM1 (500ng) at 37°C for 1hr. The samples were mixed with β -mercaptoethanol containing sample buffer and boiled at 95°C for 5mins.

Fractionation assay

SQSTM1^{-/-}MEFs were grown in 10cm dishes at ~80% confluency. After three washes with ice-chilled PBS, cells were harvested in RIPA buffer with PIC, PMSF, and NEM. The cells were sonicated for 10s, two times at 4°C. 10% of sample was taken from the lysate as a ‘total’ fraction. The remaining sample was centrifuged at 100,000g for 30mins at 4°C. After centrifugation, the supernatant was transferred to a new tube and labeled as a ‘supernatant’ fraction. The rest of sample was resuspended in 200 μ l of 7M urea buffer (7M urea, 2M thiourea, 4% CHAPS, 30mM Tris, pH 8.5) and re-sonicated for 10s, two times at 4°C. The samples were re-centrifuged at 100,000g for 30mins at 4°C. The supernatant was transferred to a new tube and labeled as a ‘pellet’ fraction and the debris was discarded.

Cell viability assay

SQSTM1^{-/-}MEFs grown at ~80% confluency were co-transfected with HttQ72-CFP and HA-SQSTM1. 24hr after the transfection, cells were washed three times with PBS. The assay was performed according to the manufacturer’s instruction (Life Technologies #L-3224).

Immunocytochemistry and fluorescence microscopy

Cells were grown on glass coverslips prior to transfection with plasmid constructs. 24hrs after the transfection, cells were washed three times with PBS, fixed in 4% PFA for 10mins and permeabilized with 0.1% Triton X-100 in PBS for 10mins. After washing three times with PBS,

cells were blocked with 2% BSA in PBS for 30mins-1hr at room temperature (RT). Cells were stained with primary antibody at 4°C overnight followed by three-times washing with PBS. Cells were incubated with Alexa 555 or 488 Fluor-conjugated secondary antibody at RT for 1hr and mounted with Mowiol media containing DAPI. 10 random fields were taken with 20x objective equipped in a NIKON Eclipse 80i fluorescence microscopy. Co-transfected cells were counted as a total number of cells, and the cells containing ubiquitin-positive aggregates were counted using ImageJ software (NIH). The images were presented in pseudo-color. For Cherry-eGFP-SQSTM1 assay, SQSTM1^{-/-}-MEFs were transfected with Cherry-eGFP-SQSTM1-WT, K420R, or T350A along with or without Myc-Keap1/V5-Cul3 for 24hrs. Cells were washed two times with PBS and mounted with Mowiol media containing DAPI without fixation to avoid pH disruption [57]. Pearson's coefficient between red and green channel was measured by ImageJ.

Fluorescence recovery after photobleaching

SQSTM1^{-/-}-MEFs were grown on 1.5 Glass bottom 35mm dishes (MatTek #P35G-1.5-10-C) and transfected with pDest-mCherry-SQSTM1 for 24hrs prior to imaging. Immediately before imaging, the medium was replaced with Phenol Red-free medium (Gibco #21063029) containing 10% FBS, 50 µg/mL P/S, 1% sodium pyruvate, and 1% non-essential amino acid. The live cell samples were placed on a heated chamber at 37°C with 5% CO₂. The imaging and photobleaching were performed with 40x oil objective using an NIKON A1Rsi confocal microscopy. Before bleaching, the images of pre-bleached SQSTM1 bodies were taken. 561nm laser was used to photobleach SQSTM1 bodies for 500ms. Immediately after the bleaching, the images were collected every 2s for a total of 5mins as a post-bleached sample. The fluorescence intensities of post-bleached SQSTM1 bodies were individually measured. In the meantime, the fluorescence intensities of non-bleached SQSTM1 bodies were measured as a control. An

average of SQSTM1 bodies in different cells ($n \geq 7$ cells containing SQSTM1 bodies) was calculated. The relative fluorescence intensities were calculated as the average fluorescence intensities of photobleached SQSTM1 bodies divided by the average fluorescence intensities of pre-bleached samples.

Cycloheximide assay

Keap1^{-/-} or control MEFs was transfected at ~80% confluency with empty vector or Myc-Keap1/V5-Cul3. 24hrs after the transfection, cells were treated with 10 μ g/mL cycloheximide for varying time.

Statistical analysis

A two-tailed Student's t-test was performed. For all tests, p-values < 0.05 were considered statistically significant. Data are represented as mean \pm SEM.

2.4 Result

2.4.1 SQSTM1's UBA domain is ubiquitinated at K420.

SQSTM1 associates with ubiquitinated proteins in cells [16]. We co-expressed HA-SQSTM1 and Flag-ubiquitin (Flag-Ub) in SQSTM1^{-/-} mouse embryonic fibroblasts (MEFs) for 24 hours and then immunoprecipitated with an HA antibody. Both SQSTM1 and Flag-Ub were detected within the immunoprecipitate (Figure 1A). Interestingly, whereas Flag-Ub migrated as a high molecular weight (HMW) species in the cell lysate, it migrated at ~75kDa in the HA immunoprecipitant (Figure 1A). Moreover, an immunoblot of SQSTM1 from similar lysates demonstrated both a 65kDa band and several HMW species (Figure 1A). This data suggested that Flag-Ub was conjugated to SQSTM1. Treatment of cell lysates with the catalytic domain of ubiquitin specific protease 2 (Usp2cc) collapsed the HMW species above SQSTM1 and abolished the presence of Flag-Ub within the HA immunoprecipitant (Figure 1A). N-ethylmaleimide (NEM) increased the amount of ubiquitinated SQSTM1 and inhibited the effect of Usp2cc (Figure 1A).

We co-expressed both Flag-Ub and a HA-SQSTM1 construct that lacks its UBA domain, SQSTM1- Δ UBA, and immunoprecipitated with an antibody to HA in SQSTM1^{-/-} MEFs. SQSTM1- Δ UBA failed to co-immunoprecipitate any Flag-Ub even in the presence of NEM (Figure 1B). A similar experiment was performed that co-expressed Flag-Ub and a HA-SQSTM1 construct that lacks its N-terminal PB1 domain, SQSTM1- Δ PB1. Similar to SQSTM1- Δ UBA, SQSTM1- Δ PB1 failed to co-immunoprecipitate any Flag-Ub (Figure 1C). To see if this related to a lack of a critical lysine residue such as K7 or K13 that have been previously reported to be ubiquitinated or related to a lack of SQSTM1 dimerization that is mediated via the PB1 domain,

we performed the same experiment with HA-SQSTM1-D69A that fails to dimerize but maintains all N-terminal lysines (Figure 1D) [36, 37]. Again, similar to SQSTM1- Δ PB1 no Flag-Ub was immunoprecipitated suggesting that the dimerization of SQSTM1 may be critical for the ubiquitination of SQSTM1's C-terminal region.

To identify the principal lysine that is ubiquitinated on SQSTM1, we selected seven sites as determined by mass spectrometry analysis and previous proteomic studies [36, 77, 84, 85]. We generated multiple HA-SQSTM1 mutant constructs with a lysine to arginine substitution (K/R; Figure S1A). Notably, the HA tag does not contain a lysine. HA-SQSTM1 constructs were co-transfected with Flag-Ub into SQSTM1^{-/-}-MEFs for 24 hours and then immunoprecipitated with HA antibody in the presence of NEM. Mutation of all selected lysines, HA-SQSTM1-7K/R, abolished the ubiquitination of SQSTM1 as seen by the absence of Flag-Ub in the immunoprecipitant (Figure 1E). However, immunoprecipitation of SQSTM1 with mutations of 6 lysine residues (HA-SQSTM1-6K/R) that retains the C-terminal K420 residue demonstrates Flag-Ub in a pattern similar to SQSTM1-WT (Figure 1E). Changing the lysine at amino acid 420 to an arginine (HA-SQSTM1-K420R) diminished the amount of Flag-Ub in the immunoprecipitant similar to HA-SQSTM1- Δ UBA expression suggesting that the principal ubiquitinated lysine resides at K420 (Figure 1E).

To confirm that ubiquitin was indeed covalently attached to SQSTM1, we co-transfected HA-SQSTM1-WT, HA-SQSTM1-K420R or SQSTM1- Δ UBA with histidine tagged ubiquitin (His-Ub) into SQSTM1^{-/-}-MEFs for 24 hours and performed purification using a nickel charged affinity resin in the presence of 6M guanidine. Consistent with our results in RIPA buffer, only HMW HA-SQSTM1-WT was present in the affinity-purified lysate (Figure 1F).

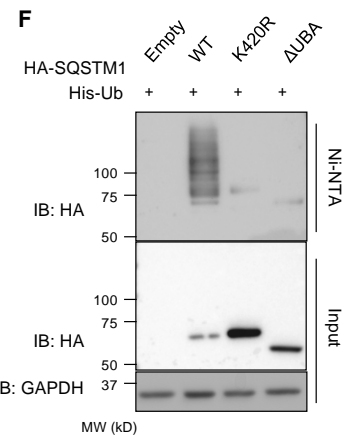
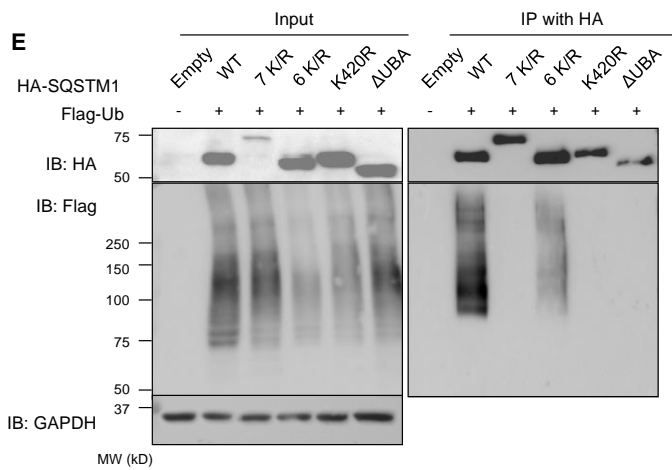
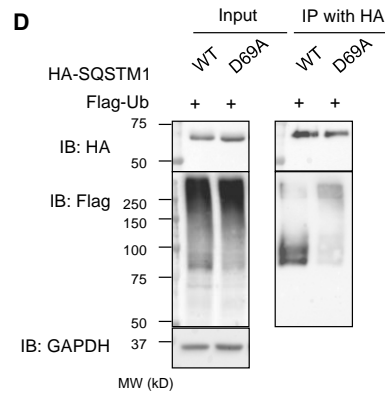
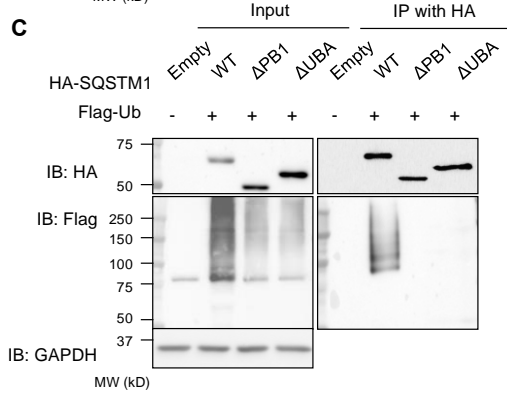
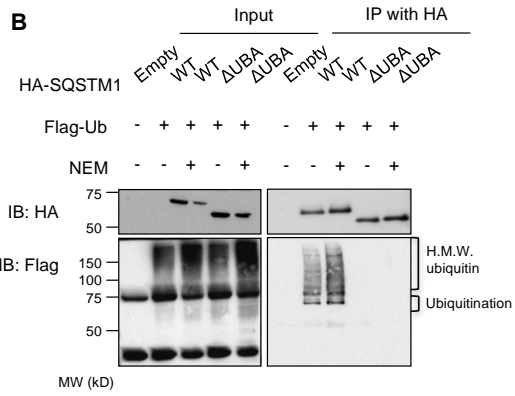
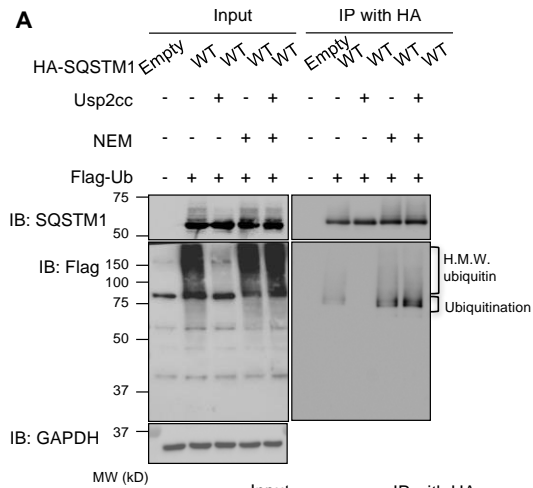


Figure1. SQSTM1 is ubiquitinated within its UBA domain. (A) anti-SQSTM1 and anti-Flag immunoblots of HA-immunoprecipitated lysates from SQSTM1^{-/-}-MEFs expressing HA-SQSTM1 and Flag-Ub. Some lysates were incubated with Usp2cc or NEM. (B) anti-SQSTM1 and anti-Flag immunoblots of HA-immunoprecipitated lysates from SQSTM1^{-/-}-MEFs expressing HA-SQSTM1-WT or HA-SQSTM1- Δ UBA and Flag-Ub. Some lysates were treated with NEM. (C) anti-HA and anti-Flag immunoblots of HA-immunoprecipitated lysates from SQSTM1^{-/-}-MEFs expressing HA-SQSTM1-WT, HA-SQSTM1- Δ PB1, or HA-SQSTM1- Δ UBA and Flag-Ub. (D) anti-HA and anti-Flag immunoblots of HA-immunoprecipitated lysates from SQSTM1^{-/-}-MEFs expressing HA-SQSTM1-WT or HA-SQSTM1-D69A along with Flag-Ub. (E) anti-HA and anti-Flag immunoblots of HA-immunoprecipitated lysates from SQSTM1^{-/-}-MEFs expressing HA tagged SQSTM1-WT, K/R, 6K/R, K420R or Δ UBA and Flag-Ub. Anti-GAPDH serves as loading control for blots. (F) anti-HA immunoblots from SQSTM1^{-/-}-MEFs expressing HA, HA-SQSTM1-WT, HA-SQSTM1-K420R, or HA-SQSTM1- Δ UBA and histidine tagged ubiquitin (His-Ub). Anti-GAPDH serves as a loading control.

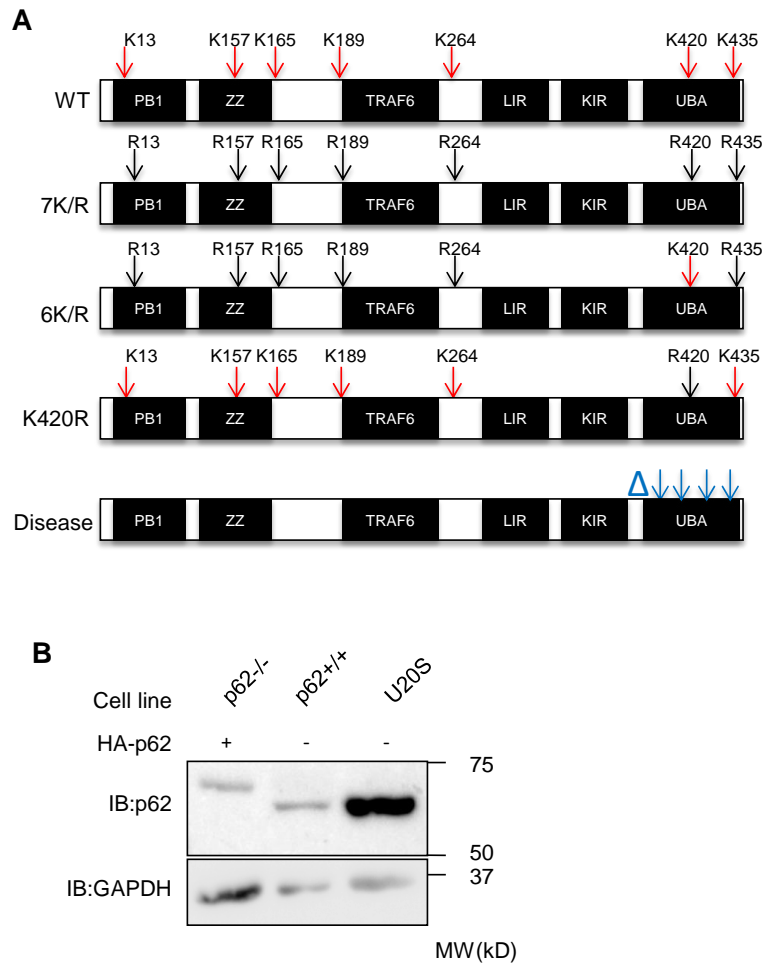


Figure S1. Schematic of SQSTM1 and expression level of SQSTM1 (A) Schematic of 7 putative ubiquitination sites on SQSTM1 and the three lysine to arginine constructs utilized; SQSTM1-7K/R, SQSTM1-6K/R and SQSTM1-K420R. Bottom schematic illustrates the site of SQSTM1 disease mutations including deletion of the UBA domain. (B) Anti-SQSTM1 immunoblot in SQSTM1^{-/-}-MEFs expressing HA-SQSTM1-WT, SQSTM1^{+/+}-MEFs, and U2OS cells. Anti-GAPDH was used as a loading control.

2.4.2 The Cul3 complex ubiquitinates SQSTM1.

Since SQSTM1 interacts with Keap1, an adaptor for the E3 ligase Cul3, we expressed HA-SQSTM1-WT, HA-SQSTM1-K420R and HA-SQSTM1- Δ UBA with Flag-Ub and Myc-Cul3 in SQSTM1^{-/-}MEFs (Figure 2A) [40]. After 24 hours, immunoblotting for SQSTM1 demonstrated an increase in ubiquitinated SQSTM1 in Myc-Cul3 expressing cells as evidenced by an increase in HMW SQSTM1 bands that were not present in HA-SQSTM1-K420R or HA-SQSTM1- Δ UBA expressing lysates (Figure 2A).

To further demonstrate that SQSTM1 could be ubiquitinated by Cul3 we transfected SQSTM1^{-/-}MEFs with an expression construct containing a Flag tagged Cul3-WT or an inactive Cul3 that lacks its C-terminus (Cul3-DN) and immunoprecipitated Cul3 with an anti-Flag antibody. Purified His-SQSTM1 lacking the first 84 amino acids of SQSTM1 and thus does not contain two previously reported ubiquitination sites on SQSTM1 adjacent to the PB1 domain (K7 or K13) was incubated with ubiquitin, immunoprecipitated Flag-Cul3 and recombinant E1/E2 enzymes. Consistent with His-SQSTM1 ubiquitination there was an increase in its molecular weight when Flag-Cul3-WT and not Flag-Cul3-DN was included in the reaction (Figure 2B).

To function in ubiquitination reactions, Cul3 must be activated by, and bound to, NEDD8, in a process called neddylation [86]. Cul3 activity can be inhibited using a nonspecific neddylation inhibitor, MLN4924 [87]. Treatment of SQSTM1^{-/-}MEFs expressing HA-SQSTM1 and Flag-Ub with MLN4924 and subsequent immunoprecipitation of HA-SQSTM1 abolished SQSTM1 ubiquitination as assessed by Flag immunoblot (Figure 2C).

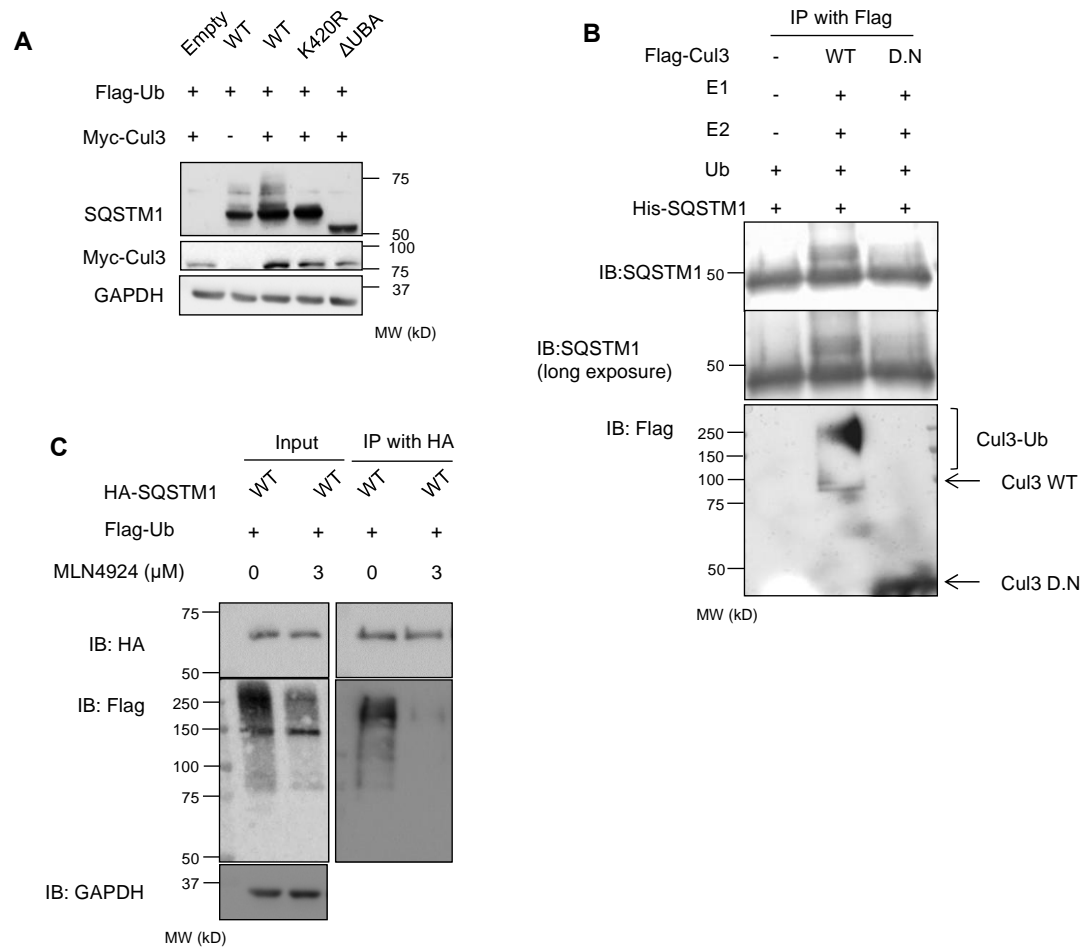


Figure 2. The Cul3 complex ubiquitinates SQSTM1. (A) anti-SQSTM1 and anti-myc immunoblots of lysates from SQSTM1^{-/-}-MEFs expressing HA tagged SQSTM1-WT, K420R or Δ UBA, Flag-Ub and myc-Cul3. A representative blot is from three independent experiments. (B) Anti-Flag and anti-SQSTM1 immunoblot of recombinant SQSTM1 (Δ N84) following *in vitro* ubiquitination with immunoprecipitated Flag-Cul3-WT or Cul3-DN from SQSTM1^{-/-}-MEFs. (C) anti-HA and anti-Flag immunoblots of HA-immunoprecipitated lysates from SQSTM1^{-/-}-MEFs expressing HA tagged SQSTM1-WT and Flag-Ub. Some cells were treated for 24hrs with 3 μ M MLN4924. Anti-GAPDH serves as loading control for blots. A representative blot is from three independent experiments.

2.4.3 Keap1 modulates SQSTM1 ubiquitination.

Since SQSTM1 associates with Keap1, an adaptor of the Cul3 ligase complex, we reasoned that SQSTM1 ubiquitination may be diminished in the absence of Keap1. We expressed HA-SQSTM1 and Flag-Ub in Keap1^{-/-}-MEFs with or without Myc-Keap1 for 24 hours and immunoprecipitated the lysates with an HA antibody. The amount of ubiquitinated SQSTM1 was increased when Myc-Keap1 was expressed in Keap1^{-/-}-MEFs (Figure 3A).

Immunoprecipitation of HA-SQSTM1 in SQSTM1^{-/-}-MEFs expressing Flag-Ub, V5-Cul3 and Myc-Keap1 demonstrated more ubiquitinated SQSTM1 as compared with expression of HA-SQSTM1 and Flag-Ub alone (Figure 3B). This ubiquitination was abrogated when Myc-Keap1- Δ BTB that lacks its BTB domain, which is necessary for Cul3 association was expressed along with V5-Cul3 further suggesting that the Keap1/Cul3 complex mediates ubiquitination of SQSTM1 (Figure 3B).

SQSTM1 binds to Keap1 via its Keap1 interacting region (KIR). A single point mutation in SQSTM1, T350A, abolishes this interaction [40]. To further establish that SQSTM1 ubiquitination is facilitated via Keap1, we expressed HA-SQSTM1-WT, HA-SQSTM1-T350A or HA-SQSTM1- Δ UBA along with Flag-Ub in Keap1^{-/-}-MEFs with or without Myc-Keap1 for 24 hours and immunoprecipitated the lysates with an HA antibody. Whereas Myc-Keap1 co-expression increased ubiquitinated HA-SQSTM1-WT as detected by Flag antibody, there was no augmentation of HA-SQSTM1-T350A when Myc-Keap1 was also expressed (Figure 3C).

Since the previous studies used an overexpressed human SQSTM1 construct in knockout mouse cells (see Figure S1B for level of overexpression as compared to control lines), we wanted to establish that endogenous SQSTM1 was indeed ubiquitinated. To do this, we

expressed His-Ub in U2OS cells treated with vehicle or MLN4924 for 24 hours and performed purification using a nickel charged affinity resin in the presence of 6M guanidine.

Immunoblotting of the purified lysate with an antibody to SQSTM1 demonstrated a HMW smear in His-Ub transfected cells that was reduced when MLN4924 was added to the cells (Figure 3D).

Similarly, we expressed Myc-Keap1 and V5-Cul3 in U2OS cells or treated these cells with MLN4924. Lysates were then immunoblotted with a polyclonal antibody to SQSTM1. Myc-Keap1/V5-Cul3 co-expression increased the amount of a second band migrating above SQSTM1 and this band disappeared with MLN4924 treatment (Figure 3E).

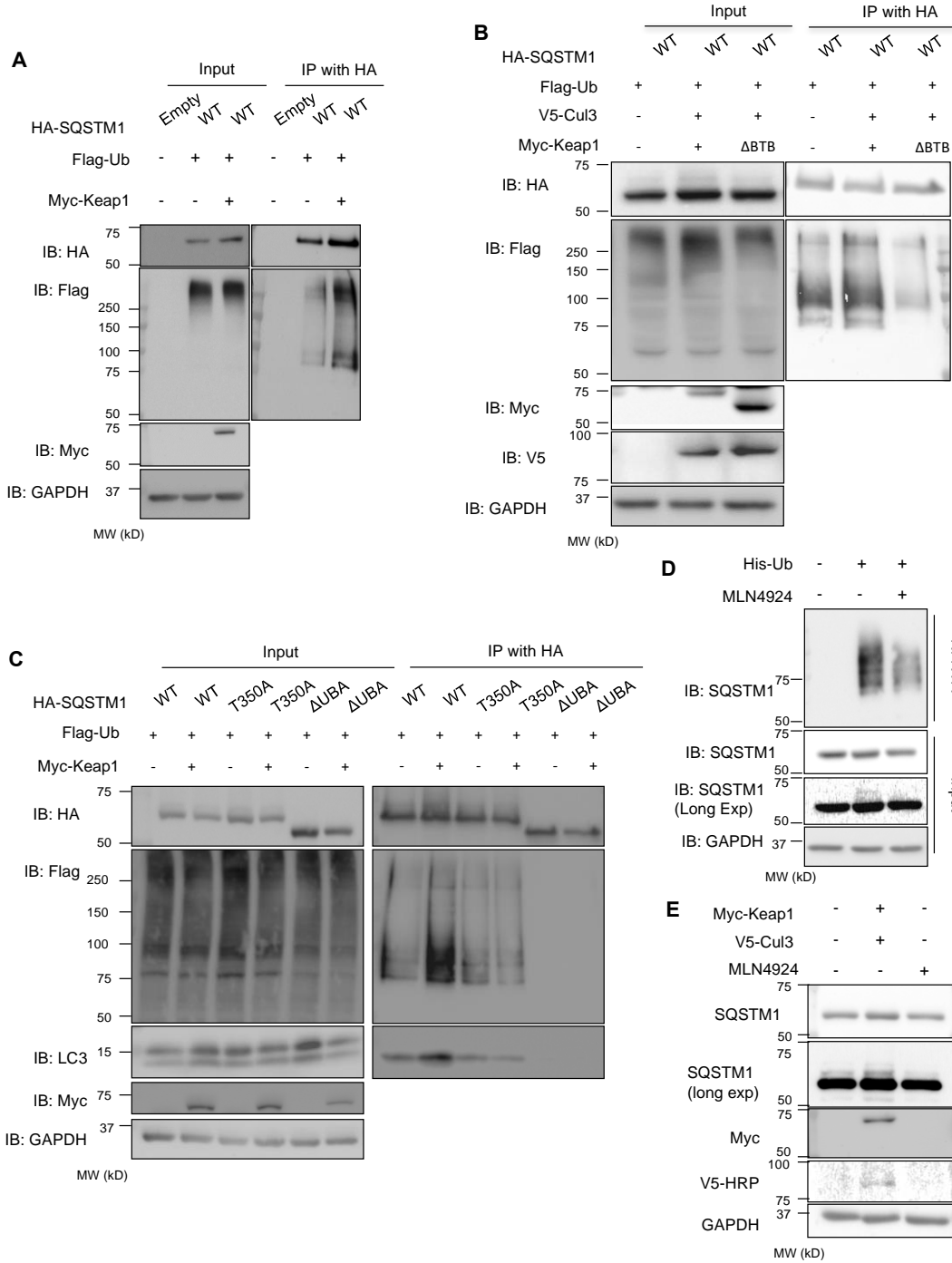


Figure 3. Keap1 modulates SQSTM1 ubiquitination. (A) Anti-HA and anti-Flag immunoblots of HA-immunoprecipitated lysates from Keap1^{-/-}-MEFs expressing HA-SQSTM1-WT, Flag-Ub and myc-Keap1. (B) Anti-HA and anti-Flag immunoblots of HA-immunoprecipitated lysates from SQSTM1^{-/-}-MEFs expressing HA-SQSTM1, Flag-Ub, V5-cul3 and myc-Keap1-WT or myc-Keap1- Δ BTB. (C) Anti-HA, anti-Flag, and LC3 immunoblots of HA-immunoprecipitated lysates from Keap1^{-/-}-MEFs expressing Flag-Ub, HA-SQSTM1-WT, HA-SQSTM1-T350A or HA-SQSTM1- Δ UBA with or without myc-Keap1. (D) anti-SQSTM1 immunoblot of nickel resin purified lysates from U2OS cells expressing His-Ub and treated with DMSO or MLN4924. (E) Anti-SQSTM1 immunoblot of lysates from U2OS cells with or without Myc-Keap1/V5-Cul3 expression or treated with MLN4924. Anti-GAPDH serves as loading control for blots.

2.4.4 Keap1/Cul3-mediated ubiquitination of SQSTM1 increases sequestering activity.

SQSTM1's sequestering activity is required for ubiquitinated inclusion body formation in the setting of autophagic impairment and loss of SQSTM1 leads to a reduction of insoluble ubiquitinated proteins with a concomitant accumulation of soluble ubiquitinated proteins [11]. To explore this function, we expressed control vector, HA-SQSTM1-WT, HA-SQSTM1-K420R and HA-SQSTM1- Δ UBA in SQSTM1^{-/-}-MEFs and fractionated cell lysates via ultracentrifugation (Figure 4A). In the absence of SQSTM1, ubiquitinated proteins remain in the supernatant and do not shift to the pelleted fraction. HA-SQSTM1-WT was enriched in the pelleted fraction along with HMW ubiquitinated proteins. In contrast, HA-SQSTM1-K420R and HA-SQSTM1- Δ UBA were enriched in the supernatant fraction and did not shift ubiquitinated proteins to the pelleted fraction.

Expression of HA-SQSTM1-WT in SQSTM1^{-/-}-MEFs generated multiple punctate ubiquitin positive inclusions throughout the cytoplasm. In contrast, HA-SQSTM1- Δ UBA and HA-SQSTM1-K420R had markedly fewer ubiquitin positive inclusions (Figure 4B-C). The co-expression of Myc-Keap1, V5-Cul3 or Myc-Keap1/V5-Cul3 increased the percentage of HA-SQSTM1-WT expressing cells containing ubiquitinated aggregates that did not occur in cells expressing HA-SQSTM1-K420R (Figure 4B and Figure S2). Similarly, we expressed mCherry-SQSTM1-WT and mCherry-SQSTM1-K420R in SQSTM1^{-/-}-MEFs or ATG5^{-/-}-MEFs and quantitated the average size of SQSTM1 bodies. mCherry-SQSTM1-WT formed larger SQSTM1 bodies and this was greater in ATG5^{-/-}-MEFs (Figure 4D-E). Co-expression of Myc-Keap1/V5-Cul3 further increased mCherry-SQSTM1-WT body size in both cell types but mCherry-SQSTM1-WT body size did not increase when Myc-Keap1- Δ BTB/V5-Cul3 was co-expressed. In control fibroblasts, co-expression of Myc-Keap1/V5-Cul3 increased mCherry-

SQSTM1-WT body size but this augmentation did not occur with mCherry-SQSTM1-T350A expression (Figure 4F). Co-expression of Myc-Keap1/V5-Cul3 increased the size of endogenous SQSTM1 bodies, and MLN4924 treatment significantly decreased the size in U20S cells (Figure S3).

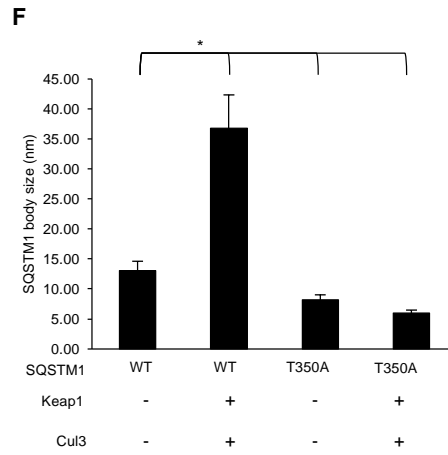
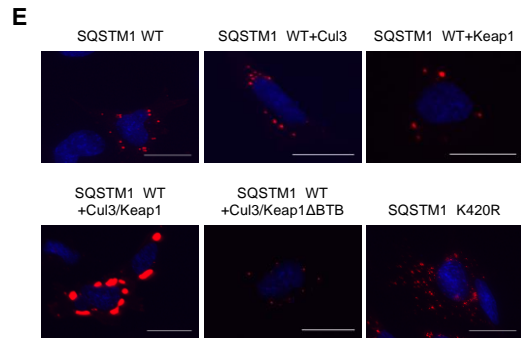
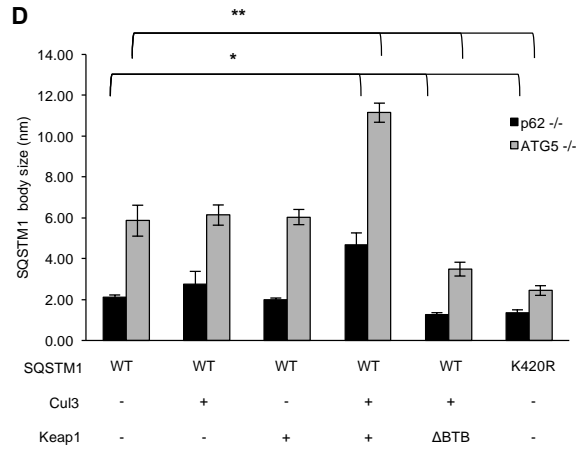
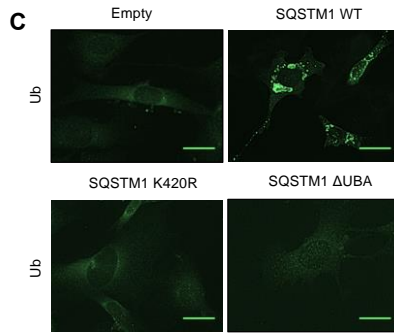
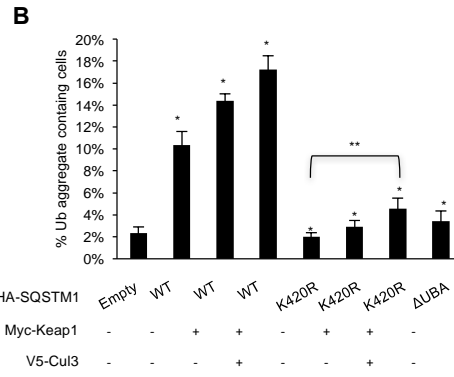
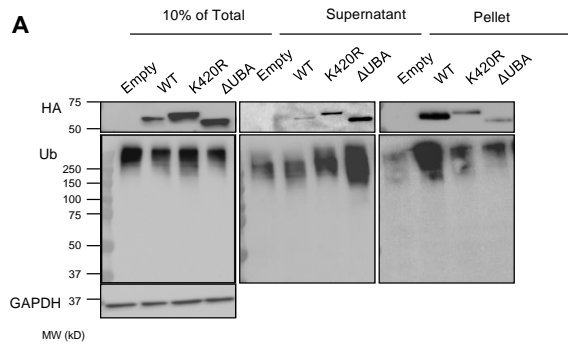


Figure 4. Keap1/Cul3-mediated ubiquitination of SQSTM1 increases sequestering activity. (A) Anti-HA and anti-ubiquitin immunoblots of cellular lysates (10% of total, supernatant and pellet) from SQSTM1^{-/-}-MEFs expressing empty HA vector, HA-SQSTM1-WT, HA-SQSTM1-K420R, or HA-SQSTM1-ΔUBA. (B) Quantitation of SQSTM1^{-/-}-MEFs expressing HA-SQSTM1-WT, HA-SQSTM1-K420R, HA-SQSTM1-ΔUBA or co-transfected with myc-Keap1 and myc-Keap1/V5-cul3 containing ubiquitinated inclusions. Representative data is pooled from four independent experiments. All data are represented as mean ± SEM. *p<0.05. (C) Anti-Ub immunostaining of SQSTM1^{-/-}-MEFs expressing empty vector, HA-SQSTM1-WT, K420R or ΔUBA. The scale bar indicates 1 μm. (D) Quantitation of SQSTM1 body size in SQSTM1^{-/-} and ATG5^{-/-} MEFs expressing mCherry tagged SQSTM1-WT or -K420R with myc-Keap1, myc-Keap1- ΔBTB and V5-Cul3. All data are represented as mean ± SEM. *p<0.05. (E) Representative images of ATG5^{-/-}-MEFs expressing Cherry-SQSTM1-WT or K420R along with Myc-Keap1/V5-Cul3. The scale bar indicates 1 μm. (F) Quantitation of SQSTM1 body size in MEFs expressing mCherry tagged SQSTM1-WT or T350A with or without myc-Keap1/V5-cul3. All data are represented as mean ± SEM. *p<0.05.

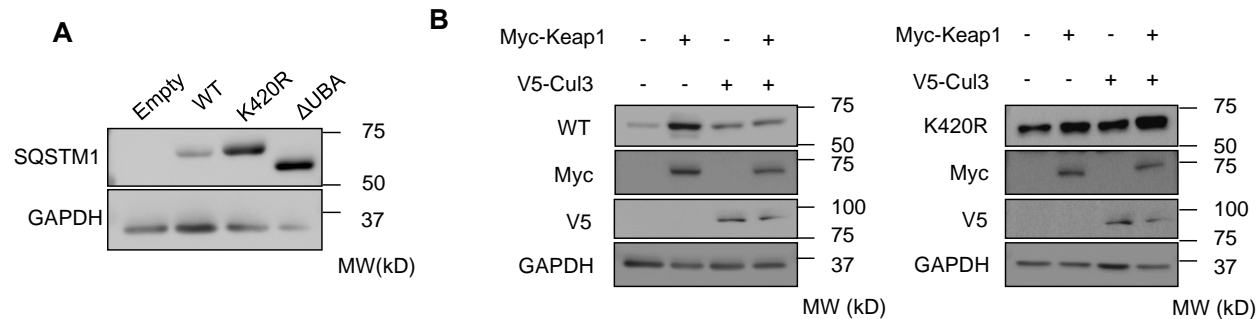


Figure S2. SQSTM1 expression level. (A) Anti-SQSTM1 immunoblot of SQSTM1^{-/-}MEFs expressing empty vector, HA-SQSTM1-WT, K420R or ΔUBA. Anti-GAPDH was used as a loading control. (B) Anti-SQSTM1, anti-Myc and anti-V5-HRP immunoblots of SQSTM1^{-/-}MEFs expressing HA-SQSTM1-WT or K420R along with Myc-Keap1/V5-Cul3. Anti-GAPDH was used as a loading control.

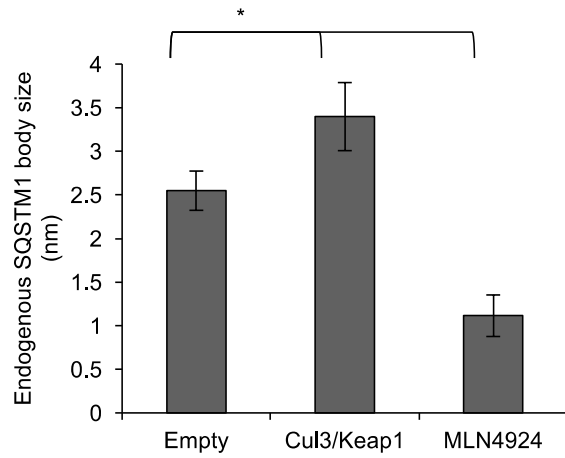


Figure S3. Endogenous SQSTM1 body size. Quantitation of endogenous SQSTM1 body size in U2OS cells expressing myc-Keap1/V5-cul3 or treated with 3 μ M MLN4924 for 24hrs. All data are represented as mean \pm SEM. * $p < 0.05$. ($n \geq 100$)

2.4.5 SQSTM1 ubiquitination modulates its exchange rate

mCherry-SQSTM1-WT or SQSTM1-K420R was expressed in SQSTM1^{-/-}-MEFs and live cell imaging was performed to evaluate fluorescence recovery after photobleaching (FRAP) of individual puncta. The initial rapid phase of recovery has been suggested to correlate with SQSTM1's sequestering activity [32]. The fluorescence exchange rate of mCherry-SQSTM1-K420R was more rapid than mCherry-SQSTM1-WT and co-expression of Myc-Keap1/V5-Cul3 decreased fluorescence recovery whereas co-expression of Myc-Keap1- Δ BTB/V5-Cul3 increased fluorescence recovery (Figure 5A-B). In a similar experiment, the co-expression of Myc-Keap1/V5-Cul3 failed to decrease the fluorescence recovery of mCherry-SQSTM1-T350A (Figure 5C). The differences in fluorescent recovery were not due to SQSTM1 presence within an autophagosome since an experiment performed in ATG5^{-/-}-MEFs gave similar results (Figure S4A-B).

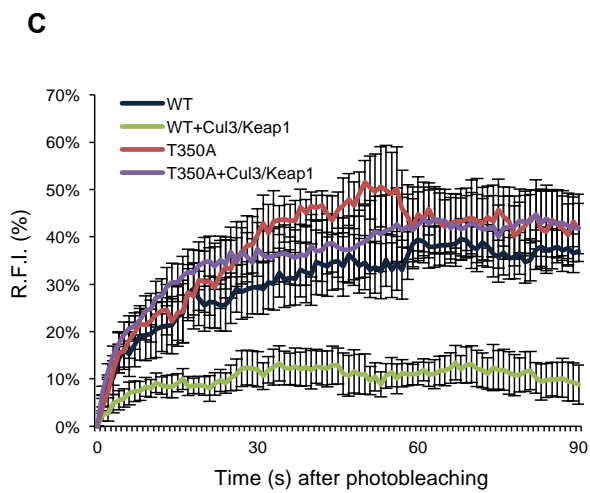
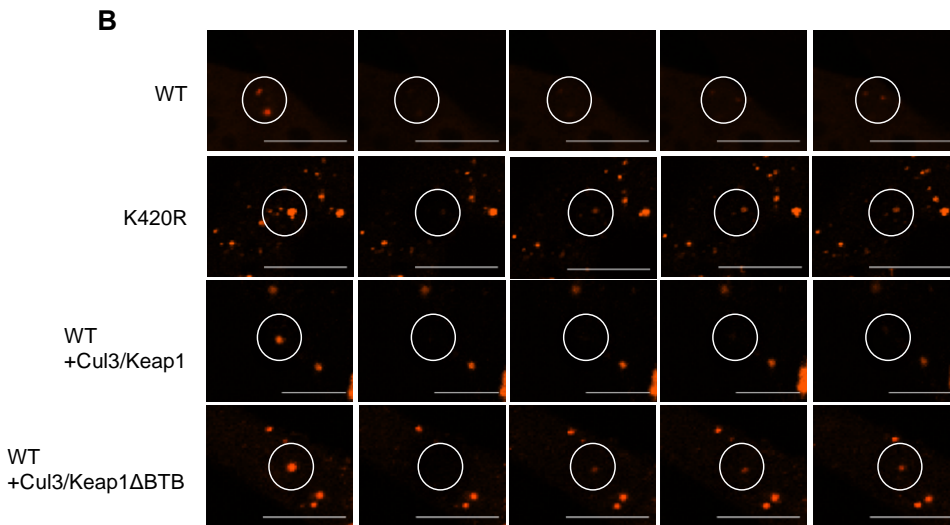
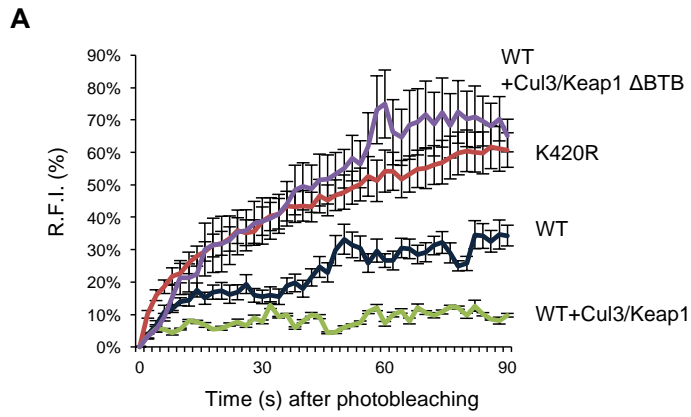


Figure 5. SQSTM1 ubiquitination modulates its exchange rate. (A) The average RFI following photobleaching from SQSTM1^{-/-}-MEFs expressing mCherry-SQSTM1-WT or K420R and V5-Cul3 with myc-Keap1-WT or myc-Keap1- Δ BTB. Representative data is pooled from four independent experiments. (B) Representative live cell images of mCherry-SQSTM1-WT or K420R and V5-cul3 with myc-Keap1-WT or myc-Keap1- Δ BTB following photobleaching and fluorescent recovery. The circle indicates the photobleached area. The scale bars indicate 1 μ m. (C) The average RFI following photobleaching from SQSTM1^{-/-}-MEFs expressing mCherry-SQSTM1-WT or T350A and V5-Cul3 with myc-Keap1-WT. Representative data is pooled from three independent experiments.

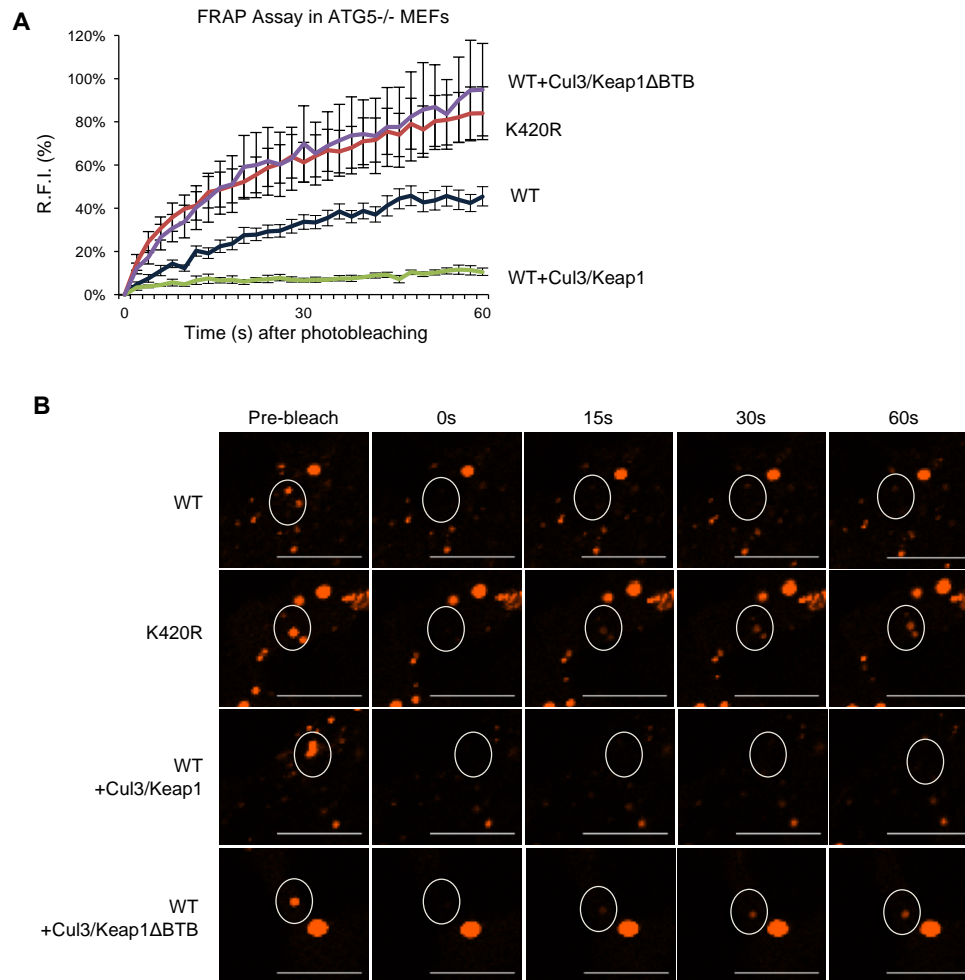


Figure S4. FRAP assay in ATG5^{-/-}MEFs. (A-B) Cherry-SQSTM1 WT or K420R was transfected into ATG5^{-/-}MEFs for 24hrs and then subjected to FRAP assay. Also, SQSTM1 WT along with Cul3 and Keap1, or Keap1 Δ BTB were transfected. R.F.I. was measured at each time point. The circle in (B) indicates the photobleached area. Data are represented as mean \pm SEM. The scale bar indicates 1 μ m ($n \geq 7$ cells containing SQSTM1 bodies).

2.4.6 Keap1/Cul3-mediated ubiquitination of SQSTM1 facilitates its role in autophagy

We reasoned that the increased SQSTM1 exchange rate seen with mCherry-SQSTM1-K420R as compared with mCherry-SQSTM1-WT may reduce phagophore association with SQSTM1. To test this, we expressed HA-SQSTM1-WT or HA-SQSTM1-K420R with Flag-Ub in SQSTM1^{-/-} MEFs for 24 hours. Cell lysates were immunoprecipitated with an anti-HA antibody and immunoblotted for HA and LC3B. HA-SQSTM1-K420R immunoprecipitants had less LC3BII as compared with HA-SQSTM1-WT (Figure 6A). Consistent with this, cell lysates immunoprecipitated with anti-HA from SQSTM1^{-/-} MEFs expressing HA-SQSTM1-WT with Flag-Ub, Myc-Keap1 and V5-Cul3 in SQSTM1^{-/-} MEFs had an increase in LC3BII association as observed on immunoblots probed with HA and LC3 (Figure 6B). Similarly, whereas Myc-Keap1/V5-Cul3 co-expression increased HA-SQSTM1-WT association with LC3B, this was not seen for HA-SQSTM1-T350A (Figure 3C).

To further explore the role of UBA domain ubiquitination by Keap1/Cul3 on SQSTM1's degradation, we expressed tandem tagged mCherry-GFP-SQSTM1-WT in SQSTM1^{-/-} MEFs for 24 hours with and without BafilomycinA (BafA) (Figure 6C). When mCherry-GFP-SQSTM1-WT is in the cytosol as an inclusion body or within the non-acidic environment of an autophagosome, both mCherry and GFP fluorescence is present [18]. However, when mCherry-GFP-SQSTM1-WT enters an acidic environment such as an autolysosome, GFP fluorescence quenches leaving only mCherry fluorescence. Consistent with this, the degree of mCherry:GFP co-localization was increased in BafA-treated cells as compared with untreated cells (Figure 6C and Figure S5A-B). In addition, co-expression of Myc-Keap1/V5-Cul3 with mCherry-GFP-SQSTM1-WT decreased the degree of mCherry:GFP co-localization suggesting that SQSTM1

ubiquitination enhances its autophagic degradation (Figure 2.4.6C). This effect was not seen in the presence of BafA.

The ratio of mCherry:GFP co-localization in SQSTM1^{-/-}-MEFs expressing mCherry-GFP-SQSTM1-K420R or mCherry-GFP-SQSTM1-T350A was significantly increased as compared to mCherry-GFP-SQSTM1-WT suggesting that fewer SQSTM1-K420R or SQSTM1-T350A puncta were within autolysosomes (Figure 6C). In contrast to mCherry-GFP-SQSTM1-WT puncta, there was not a decrease in mCherry:GFP co-localization with Myc-Keap1/V5-Cul3 expression in mCherry-GFP-SQSTM1-K420R or mCherry-GFP-SQSTM1-T350A expressing SQSTM1^{-/-}-MEFs (Figure 6C).

We reasoned that the increase in mCherry:GFP co-localization in SQSTM1^{-/-}-MEFs expressing mCherry-GFP-SQSTM1-K420R or mCherry-GFP-SQSTM1-T350A was due to its cytoplasmic accumulation in inclusion bodies rather than accumulation within autophagosomes. Consistent with this, SQSTM1^{-/-}-MEFs expressing mCherry-SQSTM1-K420R or mCherry-SQSTM1-T350A had a reduction in co-localization with co-expressed GFP-LC3B as compared to mCherry-SQSTM1-WT expressing SQSTM1^{-/-}-MEFs (Figure 6D). Moreover, expression of Myc-Keap1/V5-Cul3 increased the GFP-LC3B or endogenous LC3B co-localization with mCherry-SQSTM1-WT but failed to do so in mCherry-SQSTM1-K420R or mCherry-SQSTM1-T350A expressing SQSTM1^{-/-}-MEFs (Figure 6D and Figure S5C).

Further studies demonstrated that the stability of endogenous SQSTM1 was increased in Keap1^{-/-}-MEFs as compared with control MEFs when cell lysates were immunoblotted for SQSTM1 from cells treated with cycloheximide for varying times (Figure 6E). This increase in

SQSTM1 stability was abrogated in Keap1^{-/-}-MEFs that were transfected with Myc-Keap1/V5-Cul3 expression constructs.

The expression of HttQ72-CFP in SQSTM1^{-/-}-MEFs is toxic with only ~5% of transfected cells remaining viable 24 hours post transfection (Figure 6F). This toxicity is rescued when HA-SQSTM1-WT is expressed but not by HA-SQSTM1-K420R, HA-SQSTM1-ΔUBA or HA-SQSTM1-T350A (Figure 6F). The expression of Myc-Keap1 and/or V5-Cul3 without HA-SQSTM1-WT in SQSTM1^{-/-}-MEFs did not significantly change HttQ72-CFP toxicity. However, the co-expression of Myc-Keap1/V5-Cul3 along with HA-SQSTM1-WT enhanced cell viability. This effect was not seen in the setting of HA-SQSTM1-K420R, HA-SQSTM1-ΔUBA or HA-SQSTM1-T350A (Figure 6F).

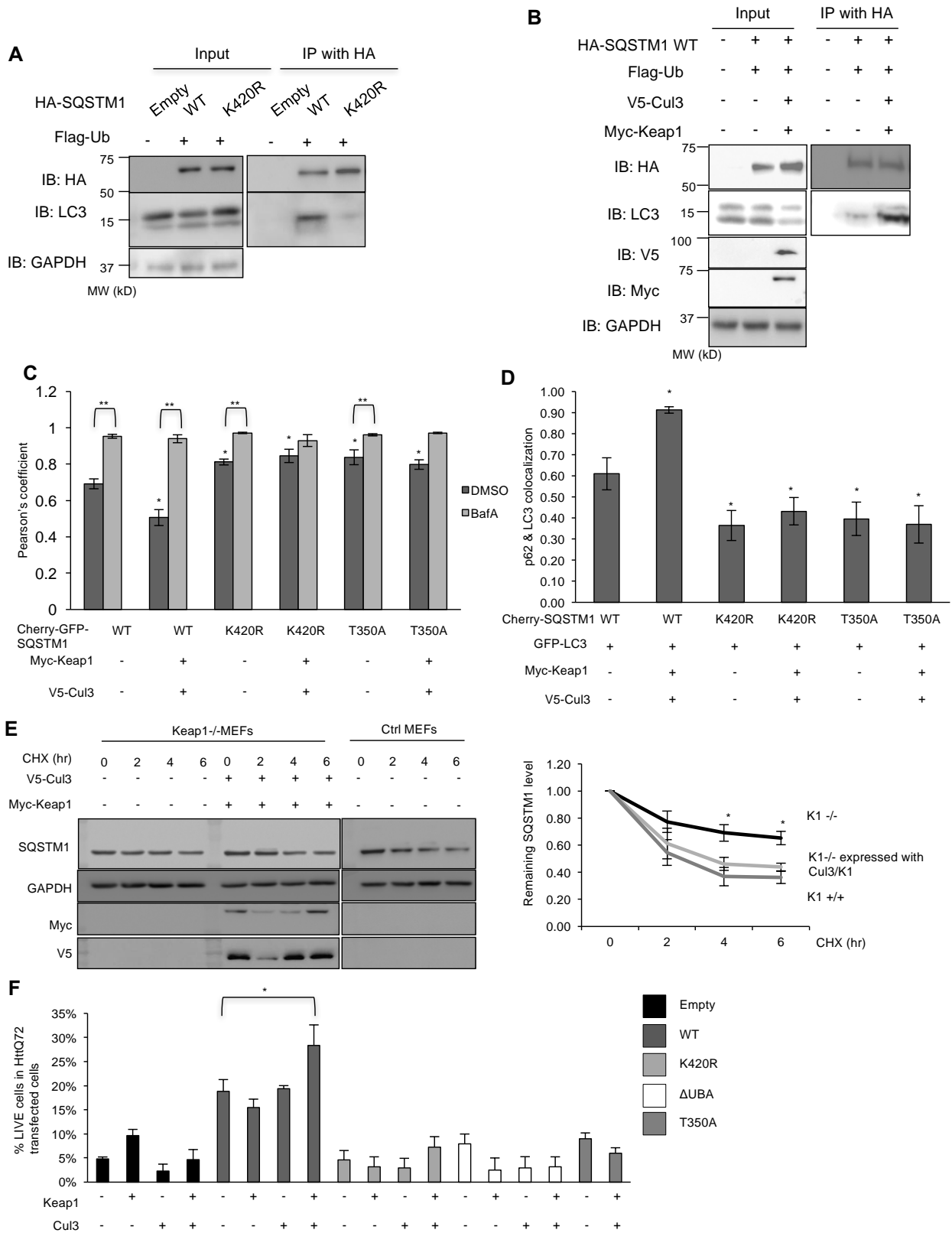


Figure 6. Keap1/Cul3-mediated ubiquitination of SQSTM1 facilitates its role in autophagy. (A) Anti-HA and anti-LC3 immunoblots of HA-immunoprecipitated lysates from SQSTM1^{-/-}MEFs expressing HA-SQSTM1-WT or K420R and Flag-Ub. (B) Anti-HA and anti-LC3 immunoblots of HA-immunoprecipitated lysates from SQSTM1^{-/-}MEFs expressing HA-SQSTM1-WT and Flag-Ub with and without Myc-Keap1 and V5-Cul3. (C) Graph of the Pearson's coefficient of co-localization of mCherry:GFP fluorescence in SQSTM1^{-/-}MEFs expressing a dual fluorescent reporter mCherry-GFP fused to SQSTM1-WT, K420R or T350A with or without myc-Keap1 and V5-Cul3. Some cells were also with BafA. Representative data is pooled from three independent experiments. (D) Quantitation of the percent of mCherry-SQSTM1 bodies that co-localize with GFP-LC3 in SQSTM1^{-/-}MEFs expressing mCherry fused SQSTM1-WT, K420R or T350A with or without Myc-Keap1 and V5-Cul3. Representative data is pooled from three independent experiments. (E) Anti-SQSTM1 immunoblot of lysates from control or Keap1^{-/-}MEFs treated with cycloheximide for the indicated times. Some cells were also transfected with Myc-Keap1 and V5-Cul3. The percent of remaining SQSTM1 was quantified from three independent experiments and is represented graphically. (F) Quantitation of the percent of HttQ72-CFP positive SQSTM1^{-/-}MEFs expressing HA-SQSTM1-WT, K420R, Δ UBA, T350A or co-expressing myc-Keap1 and V5-cul3. All data are represented as mean \pm SEM. *p<0.05. Anti-GAPDH serves as loading control for blots. Representative data is pooled from three independent experiments.

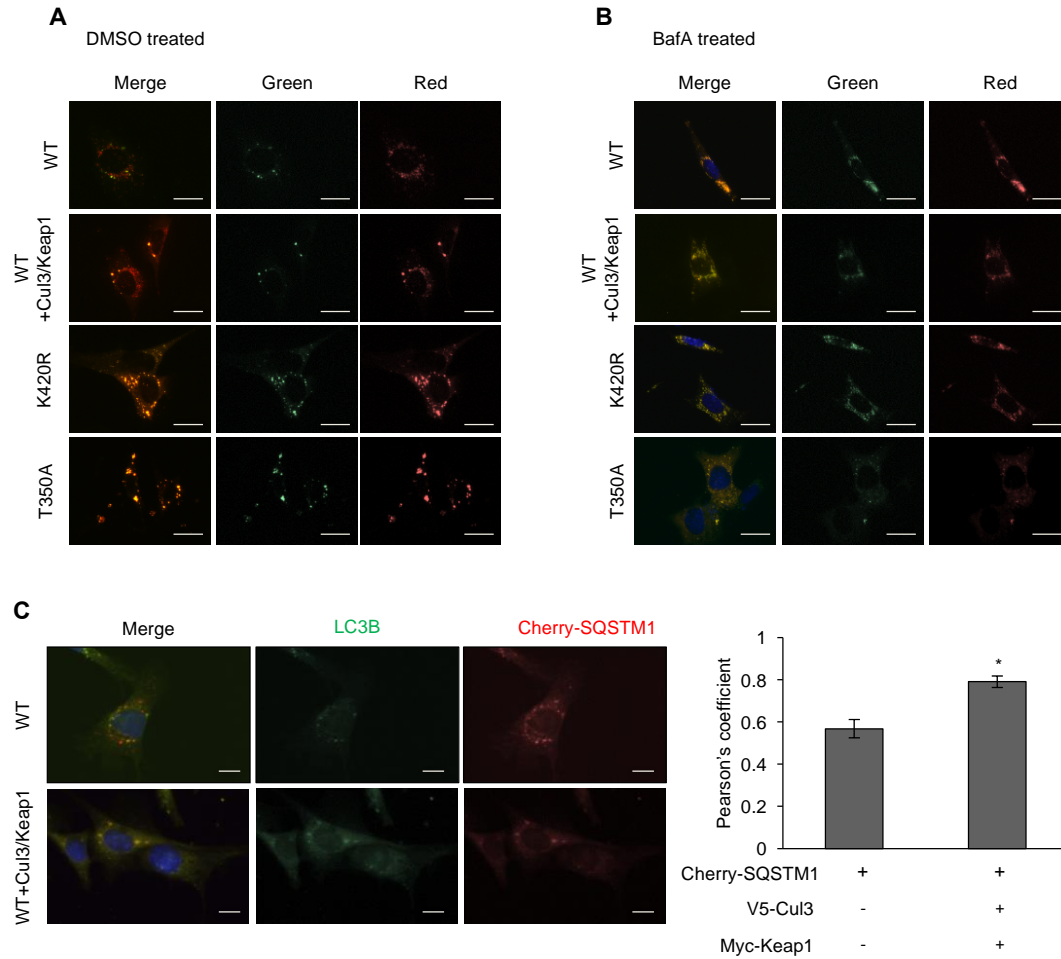


Figure S5. Cell Images of mCherry-GFP-SQSTM1 Quench Assay and Co-localization of Cherry-SQSTM1 with endogenous LC3B. (A) Representative live cell images of SQSTM1^{-/-}MEFs expressing mCherry-GFP-SQSTM1-WT, K420R or T350A along with Myc-Keap1/V5-Cul3. Cells were treated with DMSO or (B) BafA for 4hrs. The scale bar indicates 1 μ m. (C) Anti-LC3B immunostaining of SQSTM1^{-/-}MEFs expressing Cherry-SQSTM1-WT along with Myc-Keap1/V5-Cul3. The scale bar indicates 1 μ m. The graph indicates the Pearson's coefficient of Cherry-SQSTM1-WT and LC3B (n \geq 50). All data are represented as mean \pm SEM. *p<0.05.

2.4.7 UBA domain ubiquitination in SQSTM1 is diminished with disease mutations.

Some SQSTM1 disease mutations reside within its UBA domain (Figure S1A) [55]. We expressed HA-SQSTM1-WT, SQSTM1-K420R and 5 different disease mutations, SQSTM1-A390X (equivalent to SQSTM1- Δ UBA used above), SQSTM1-P392L, SQSTM1-M404V, SQSTM1-G411S, and SQSTM1-G425R along with Flag-Ub in SQSTM1^{-/-}-MEFs (Figure 7A). Following 24 hours, we immunoprecipitated cell lysates with an HA antibody and immunoblotted for Flag and HA. Immunoprecipitants from HA-SQSTM1-WT but not HA-SQSTM1-K420R or HA-SQSTM1-A390X had Flag immunoreactive bands (Figure 7A). In addition, all expressed SQSTM1 disease mutants showed an absence or reduction in Flag immunoreactivity (Figure 7A). FRAP analysis of mCherry-SQSTM1-WT, SQSTM1-P392L, SQSTM1-M404V, SQSTM1-G411S or SQSTM1-G425R in SQSTM1^{-/-}-MEFs demonstrated that fluorescence recovery was more rapid with all disease mutants as compared with mCherry-SQSTM1-WT (Figure 7B). HA-SQSTM1-WT increased the number of live cells expressing HttQ72-CFP and this was augmented with co-expression of Keap1/Cul3 in SQSTM1^{-/-}-MEFs (Figure 7C). Whereas, expression of SQSTM1 disease mutants, with the exception of HA-SQSTM1-P392L, significantly decreased cell viability compared to HA-SQSTM1-WT. Co-expression of Keap1/Cul3 in SQSTM1 disease mutant-expressing cells reduced cell death.

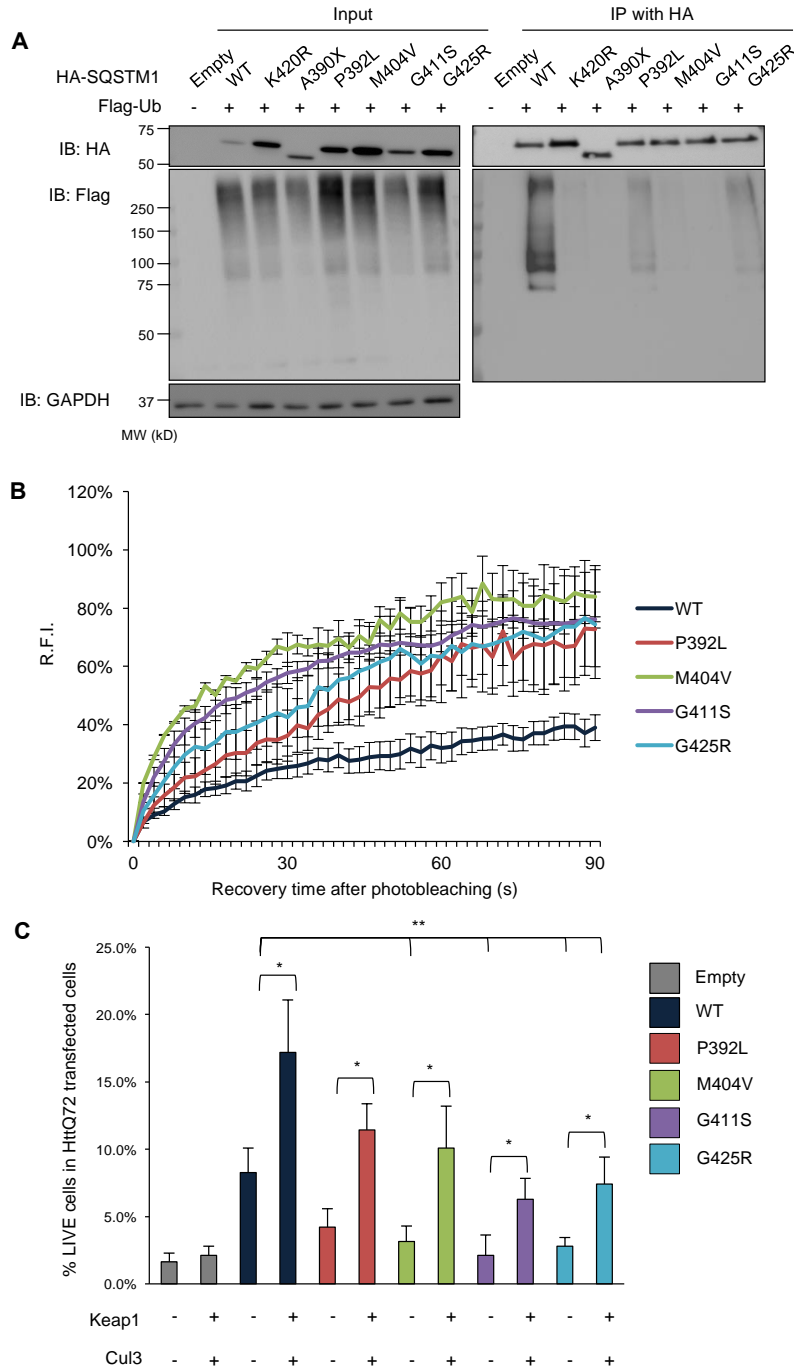


Figure 7. SQSTM1 disease mutants have decreased ubiquitination and function. (A) Anti-HA and anti-Flag immunoblots of HA-immunoprecipitated lysates from SQSTM1^{-/-}MEFs expressing HA-SQSTM1-WT, SQSTM1-K420R, SQSTM1-ΔUBA, SQSTM1-P392L, SQSTM1-M404V, SQSTM1-G411S, SQSTM1-G425R and Flag-Ub-WT. Anti-GAPDH is used as loading control. (B) The average RFI following photobleaching from SQSTM1^{-/-}MEFs expressing mCherry-SQSTM1-WT, SQSTM1-P392L, SQSTM1-M404V, SQSTM1-G411S or SQSTM1-G425R. (C) Quantitation of the percent of HttQ72-CFP positive SQSTM1^{-/-}MEFs expressing HA-SQSTM1-WT, P392L, M404V, G411S, G425R or co-expressing myc-Keap1 and V5-Cul3. All data are represented as mean ± SEM. *p<0.05. Representative data is pooled from three independent experiments.

2.5 Discussion

The present study finds that SQSTM1 is ubiquitinated at a highly conserved lysine within its UBA domain (K420) by Keap1/Cul3. Substitution of K420 to arginine, deletion of the UBA domain or mutation of the KIR domain in SQSTM1 decreases ubiquitinated inclusion formation, its LC3 interaction and cell viability. In contrast, Keap1/Cul3 expression can increase ubiquitinated inclusion formation, SQSTM1 inclusion body size and rescue cells from proteotoxic stress. Moreover, Keap1/Cul3 increases SQSTM1's association with LC3B and its subsequent degradation. We propose that the ubiquitination of SQSTM1's UBA domain by Keap1/Cul3 enhances its sequestration activity, subsequent phagophore association and degradation.

The molecular assembly of SQSTM1 oligomers is necessary for its function in autophagy. How this assembly is regulated is not fully understood. Recent studies support a model where the self-association of SQSTM1 occurs via its PB1 domain [51]. This interaction is a nidus for the extension of a filamentous SQSTM1 scaffold that allows the engulfing phagophore membrane to bind the LIR domain and degrade ubiquitinated proteins [53]. Deletion of the PB1 domain abrogates the self-association of SQSTM1 reducing SQSTM1's sequestration activity and cellular function [16]. Similarly, deletion of SQSTM1's UBA domain impairs SQSTM1 body formation even in the setting of an intact PB1 domain. SQSTM1's UBA domain can also self-associate as a dimer [46]. Phosphorylation of serines 403 and 409 within the UBA domain destabilize this dimer and regulates SQSTM1's activity [32, 47]. These studies suggest that SQSTM1's molecular assembly is dependent upon both its PB1 and UBA domains.

The UBA domain of SQSTM1 has a shared interface that mediates dimerization and ubiquitin binding. Ubiquitin binding and UBA domain dimerization are mutually exclusive with dimerization “inactivating” ubiquitin binding [46]. Amino acid K420 resides at the C-terminus of helix 2. Structural studies have demonstrated that this region of SQSTM1’s UBA domain interacts with residues in loop 1. Indeed, point mutations in loop 1 residues (E409K, G410K) or helix 2 (T419K) disrupt dimerization (Long et al., 2010). Whether ubiquitination of K420 disrupts dimerization allowing for increased ubiquitin binding is unclear. Alternatively, K420 ubiquitination may serve as means for increased oligomer formation via interaction of a SQSTM1 UBA domain with an adjacent SQSTM1’s ubiquitinated UBA domain or interactions with other proteins harboring ubiquitin-binding motifs.

More recently, it was demonstrated that polyubiquitin could fragment SQSTM1 filaments suggesting that the oligomeric structure of SQSTM1 was dynamic and could change with the addition of ubiquitinated cargo [51]. Our data extends this model and suggests that the ubiquitination status of SQSTM1’s UBA domain may alter SQSTM1’s oligomeric structure thus promoting inclusion body formation. This higher ordered SQSTM1 oligomer would then further promote SQSTM1’s sequestration activity, subsequent phagophore assembly and autophagic degradation. We suggest that by refining SQSTM1’s oligomeric structure via UBA domain ubiquitination, autophagic degradation and sequestration activity can be activated or inhibited locally within the SQSTM1 inclusion body.

The ubiquitination of autophagic adaptors is emerging as a means of regulating their function. Ubiquitination of optineurin by HACE1 increases its association with SQSTM1 enhancing autophagic flux and suppressing tumor growth [33]. TRIM21 ubiquitinates SQSTM1 on its N-terminal PB1 domain inhibiting SQSTM1 oligomerization and sequestration activity

[37]. This event would antagonize Keap1/Cul3 mediated ubiquitination at the C-terminal UBA domain suggesting that the ubiquitination of SQSTM1 can both positively and negatively affect its sequestration function. Recently, the E3 ligase RPN26 was found to recruit and ubiquitinate SQSTM1's UBA domain at the ER membrane [34]. This event enhanced SQSTM1's ability to capture a subset of endosomes via binding to ubiquitin binding domains on endocytic adaptors. Whether RPN26 ubiquitinates K420 or another lysine within the UBA domain is not established.

Previous studies have found that a Keap1 homodimer binds to two sites on Nrf2 facilitating Cul3 mediated ubiquitination. Oxidative stress destabilizes Keap1 and abrogates its interactions with Nrf2. Keap1 binds SQSTM1 at a single KIR domain. The affinity for this interaction becomes greater as SQSTM1 accumulates under conditions of impaired autophagy, sequestering Keap1 from Nrf2 leading to its stabilization [40, 42, 45]. Similarly, Keap1 accumulates under conditions of impaired autophagy or in the setting SQSTM1 knockdown [88]. Autophagic degradation of Keap1 through its interaction with SQSTM1 may help to maintain redox homeostasis [89]. In fact, Keap1 itself enhances SQSTM1 mediated ubiquitin aggregate clearance [90]. This may further serve to regulate Keap1 levels and its interactions with both Nrf2 and SQSTM1.

Our data suggests that Keap1/Cul3 can ubiquitinate SQSTM1 and enhance its autophagic activity. Only dimeric SQSTM1 is able to be ubiquitinated since SQSTM1 with a PB1 domain deletion or SQSTM1-D69A fail to be ubiquitinated (Figure 1C and 1D). This would suggest that a Keap1 homodimer binds to two high affinity KIR motifs on a SQSTM1 dimer leading to its ubiquitination. This model is similar to alternative models of Keap1 which suggests that a homodimer can associate with two Nrf2 molecules or with Nrf2 and a second protein with a KIR motif, such as PGAM5 which then targets this complex to the mitochondria [91, 92].

Interestingly, loss of Keap1 stabilizes SQSTM1 whereas increased expression of Keap1/Cul3 increases SQSTM1 inclusion formation and subsequent degradation. Whether Keap1 is further degraded along with SQSTM1 is not known. However, Keap1/Cul3 mediated ubiquitination and subsequent enhancement of SQSTM1 degradation would be an efficient means by which Keap1 could decrease the levels of SQSTM1 thus releasing its antagonistic interaction.

Dominantly inherited mutations in SQSTM1 are associated with several degenerative diseases ranging from PDB to ALS [55]. More recently, homozygous loss of function mutations in SQSTM1 were identified in patients with childhood onset neurodegeneration [93]. Some SQSTM1 disease mutations reside within or lead to premature truncations of the UBA domain [55]. One unifying feature for these mutations is variable degrees of impaired ubiquitin binding *in vitro* [76]. Our data finds that UBA domain associated SQSTM1 disease mutations also have a reduction in UBA domain ubiquitination. More recently, several SQSTM1 missense mutations associated with PDB and ALS have been identified within the Keap1 interacting region [58, 94]. These mutations lead to a loss of Keap1 interaction and a reduction in Nrf2 signaling. It is intriguing to speculate that these mutations may also affect Keap1/Cul3 associated ubiquitination of SQSTM1's UBA domain further unifying the pathogenic mechanism of SQSTM1 mutations. Alternatively, xenophagy associated phosphorylation of SQSTM1 at serine 349 can be disrupted by a point mutation within the UBA domain that diminishes its ubiquitin binding function [95]. The phosphorylation of serine 349 on SQSTM1 then increases SQSTM1's affinity for Keap1 [41]. It is also conceivable that UBA domain associated disease mutations in SQSTM1 affect serine 349 phosphorylation abrogating Keap1/Cul3 mediated ubiquitination of the UBA domain.

The modulation of SQSTM1 activity via Keap1/Cul3 offers an attractive therapeutic target. Expression of Keap1/Cul3 increases SQSTM1's sequestration activity. In the case of

SQSTM1 associated disease mutations, Keap1/Cul3 expression restored SQSTM1's cytoprotective role in polyglutamine toxicity. Whether Keap1/Cul3 mediated ubiquitination of SQSTM1 further enhances the sequestration of Keap1 resulting in the non-canonical activation of Nrf2, which may further enhance cell viability remains to be established. Indeed, activation of Nrf2 is cytoprotective in models of polyglutamine toxicity [96]. Our present data further connects SQSTM1-mediated autophagy with the Keap1-Nrf2 signaling pathway.

**Chapter 3: TIA1 variant drives
myodegeneration in multisystem
proteinopathy with SQSTM1 mutations**

Preface

This chapter has been previously published.

Title: TIA1 variant drives myodegeneration in multisystem proteinopathy with SQSTM1 mutations.

YouJin Lee, Per Harald Jonson, Jaakko Sarparanta, Johanna Palmio, Mohona Sarkar, Anna Vihola, Anni Evilä, Tiina Suominen, Sini Penttilä, Marco Savarese, Mridul Johari, Marie-Christine Minot, David Hilton-Jones, Paul Maddison, Patrick Chinnery, Jens Reimann, Cornelia Kornblum, Torsten Kraya, Stephan Zierz, Carolyn Sue, Hans Goebel, Asim Azfer, Stuart H. Ralston, Peter Hackman, Robert C. Bucelli, J. Paul Taylor, Conrad C. Weihl*, and Bjarne Udd.
(2018) *Journal of Clinical Investigation*. Doi:10.1172/JCI97103

*Corresponding author.

3.1 Abstract

Disturbances of stress granule (SG) dynamics and autophagic protein degradation underlie the pathogenesis of a spectrum of degenerative diseases that affect muscle, brain and bone termed multisystem proteinopathy (MSP). Specifically, identical mutations in the autophagic adaptor *SQSTM1* can cause varied penetrance of four distinct phenotypes; amyotrophic lateral sclerosis, frontotemporal dementia, Paget's disease of the bone and distal myopathy. It has been hypothesized that clinical pleiotropy relates to additional genetic determinants, but thus far evidence has been lacking. Here, we provide evidence that a *TIA1* (p.N357S) variant dictates a myodegenerative phenotype when inherited along with a pathogenic *SQSTM1* mutation. Experimentally, the *TIA1*-N357S variant significantly enhances liquid-liquid phase separation *in vitro* and impairs SG dynamics in living cells. Depletion of *SQSTM1* or introduction of a mutant version of *SQSTM1* similarly impairs SG dynamics. *TIA1*-N357S persistent SGs exhibit increased association with *SQSTM1*, accumulation of ubiquitin conjugates and additional aggregated proteins. Synergistic expression of the *TIA1*-p.N357S variant and a *SQSTM1*-p.A390X mutation in myoblasts exhibit impaired SG clearance and myotoxicity relative to control myoblasts. These findings demonstrate a pathogenic connection between SG homeostasis and ubiquitin mediated autophagic degradation that defines the penetrance of a MSP phenotype.

3.3 Introduction

Pathogenic mutations in some genes lead to a spectrum of variably penetrant phenotypes that span different organs and postmitotic tissue [2, 62, 75, 97]. For example the same mutation in the autophagic adaptor protein, *SQSTM1* (also known as p62), can cause Paget's disease of the bone (PDB), rimmed vacuolar inclusion body myopathy (RV-IBM), amyotrophic lateral sclerosis (ALS) or frontotemporal dementia (FTD) [75]. The term multisystem proteinopathy (MSP) has become useful to describe this growing family of genetic diseases that so far have been reported with dominant mutations in the pleiotropic genes *VCP*, *HNRNPA2B1*, *HNRNPA1* and *SQSTM1* [2, 62, 75, 97]. Other disease associated genes with variably penetrant phenotypic expression of RV-IBM, ALS and FTD, yet no association with PDB, include *TIA1* and *MATR3* [60, 61, 98]. One distinctive feature of MSP pedigrees is that patients with the same mutation and even the same mutation within a family can manifest with different phenotypes (i.e. PDB in one sibling and ALS in another sibling). MSP also unifies two key pathologic features in affected tissue, ubiquitinated aggregates and the accumulation of RNA binding proteins with low complexity sequence domains (LCD) such as TDP-43 [2].

Mutations in several proteins that facilitate ubiquitin-dependent autophagy such as *VCP*, *SQSTM1*, *UBQLN2*, and *OPTN* are associated with PDB, RV-IBM, ALS and FTD [75, 97, 99, 100]. Disease mutations in these proteins impair the degradation and clearance of ubiquitinated inclusions resulting in their accumulation. *SQSTM1* is an autophagic adaptor protein with a UBA domain and autophagosome interacting motif [101]. Most pathogenic variants in *SQSTM1* are missense mutations within or truncations of the UBA domain [55]. These mutations affect *SQSTM1*'s oligomerization and ability to recruit ubiquitinated aggregates to the autophagosome

suggesting that the pathogenesis of MSP and its related diseases are due in part to alterations in protein homeostasis and particularly autophagic degradation of ubiquitinated proteins in vulnerable tissues [55]. One disease associated *SQSTM1* mutation that has been demonstrated to cause the full spectrum of MSP phenotypes (PDB, RV-IBM, ALS and FTD) is a proline to a leucine mutation at residue 392 (P392L) in the UBA domain [3-6]. This single mutation is the most common genetic cause of PDB but is incompletely penetrant suggesting that other genetic or environmental factors are needed for the phenotypic manifestation of PDB, RV-IBM, ALS or FTD [102].

One distinctive pathologic feature seen in MSP affected tissues is accumulation of cytoplasmic inclusions of RNA-binding proteins such as TDP-43 [2]. Indeed, mutations in RNA-binding proteins with LCDs, including *TARDBP*, *FUS*, *HNRNPA2B1*, *HNRNPA1*, *TIA1* and *HNRPDL* cause dominantly inherited forms of MSP, ALS, FTD and RV-IBM [60-65]. These RNA-binding proteins promote the assembly of membrane-less organelles such as stress granules through the biophysical process of liquid-liquid phase separation (LLPS) that is mediated via the LCD [67]. Importantly, disease-causing mutations in the LCD of these RNA-binding proteins alters their biophysical properties, increase their propensity to undergo LLPS and result in the accumulation of poorly dynamic stress granules that are believed to underlie cellular dysfunction and evolve into the pathological inclusions characteristic of these diseases [60, 67, 103]. Notably, TIA1 is a key component of cytosolic stress granules [60]. Dominantly inherited mutations within TIA1's LCD cause MSP or more discreet clinical manifestations of either ALS-FTD or a distinctive form of distal myopathy termed Welander distal myopathy (WDM) [60, 61]. As with hnRNPA1, hnRNPA2B1, and TDP-43, disease mutations in the LCD

of TIA1 alter its biophysical properties, promote LLPS, enhance fibrillization and impair stress granule clearance as a mechanism of their pathogenicity [60, 61].

RV-IBMs are defined by a core set of pathologic features; rimmed vacuoles (RVs) and inclusion bodies, seen in degenerative myopathies [104]. RVs are present within some myofibers and contain autophagic and membranous debris, such as SQSTM1 and MAP1LC3. Many proteins have been identified to accumulate as inclusions in RV-IBM tissue. These proteins include ubiquitin, β -amyloid and TDP-43; with TDP-43 aggregation being specific for RV-IBMs [104]. In many cases, protein inclusions and vacuolar debris are stained by Congo red and demonstrate birefringence suggesting they are true amyloid. Accumulating studies now establish that the presence of SQSTM1 and/or TDP-43 within myofibers serve as markers of muscle degeneration in RV-IBMs [105-108].

The relationship between stress granule homeostasis and autophagic protein degradation has been demonstrated in cell culture [73, 109]. Specifically, autophagy participates in stress granule clearance. Autophagy mediated stress granule clearance may also require the ubiquitin-segregase VCP [73, 109]. Autosomal dominantly inherited mutations in *VCP* cause MSP but whether its pathogenesis is mediated via its effect on stress granule homeostasis is not known [97]. The present study identifies a rare variant in *TIA1* that dictates the tissue specificity associated with *SQSTM1* mutations. Digenic inheritance of a *TIA1*-N357S variant with a pathogenic *SQSTM1* mutation causes a distal myopathy with RV-IBM pathology. This finding connects stress granule homeostasis with ubiquitin dependent autophagic degradation as a key mediator of phenotypic outcome within the spectrum of RV-IBM, ALS and FTD, and shows the relevance of oligogenic mechanisms as one cause of neurodegenerative-neuromuscular disease.

3.3 Material and Methods

Genetic studies

A cohort of 1293 presumed inherited myopathy patients was sequenced using a targeted high-throughput sequencing panel called MYOcap. The panel covered the exons, as well as some 3' and 5' UTRs of selected genes either reported to cause muscle disease, or genes functionally related to such genes [6]. The MYOcap panel has been regularly updated and samples of the cohort were sequenced with four versions covering 180, 236, 265 and 297 genes respectively. Details are available upon request. The TIA1 and SQSTM1 genes were included in all versions. Specific probes were manufactured by Roche NimbleGen (SeqCap EZ Choice Library). DNA was extracted from blood by standard methods and enrichment, and sequencing was done at FIMM, Biomedicum, Helsinki, Finland and at The Wellcome Trust Centre for Human Genetics (WTCHG) Oxford, England with the HiSeq1500 and 2000 platforms. The sequencing raw data was mapped against the human reference genome GRCh37/hg19. Data analysis was performed using an in-house pipeline as described earlier [6].

Indexed genomic DNA (gDNA) libraries were prepared from gDNA using TruSeq DNA Preparation kit (Illumina, San Diego, CA) and exome capture using TruSeq Exome Enrichment kit (Illumina, San Diego, CA) according to manufacturer's protocol. Sequencing was performed with 100bp paired-end reads on a HiSeq2000 (Illumina, San Diego, CA). Reads were aligned to the human reference genome with NovoAlign or Burrows-Wheeler Aligner. Variants were called with SAMtools and annotated with SeattleSeq. Coverage across genomic intervals was calculated using BEDTools. Genomic coordinates for regions targeted by the whole-exome capture kit were provided by Illumina. High-throughput sequencing results were verified by Sanger sequencing. Primer sequences are available upon request.

Allele frequencies for the general population were taken from gnomAD [110].

Protein purification, In Vitro Fibrilization, and phase diagram

Recombinant DNA for TIA1-WT, N387S, E384K constructs were cloned into pETite N-His SUMO Kan vector (Lucigen Corporation). Plasmids were chemically transformed into BL21_DE3 cells (Lucigen Corporation). Protein purification, In Vitro Fibrilization and phase diagram protocols described in Mackenzie et al.[60] were followed. For phase diagram, the spectrum of BSA (non-amyloid fibril forming) was measured as a baseline. That baseline has been subtracted from all the WT, E384K and N357S spectra at each time point respectively.

Muscle pathology, reagent and antibodies

Frozen muscle sections were processed for routine histochemical staining, including H&E, modified Gomori trichrome, combined succinate dehydrogenase–cytochrome oxidase, ATPase at pH 9.2, pH 4.3 and reduced nicotinamide adenine dinucleotide–tetrazolium reductase.

Anti-TIA1 polyclonal antibody (SantaCruz #sc-1751, 1:500 for WB, 1:100 for IF), anti-G3BP1 polyclonal antibody (Proteintech #13057-2-AP, 1:100 for IF), anti-p62 polyclonal antibody (Proteintech #18420-1-AP, 1:1000 for WB, 1:100 for IF), anti-GFP polyclonal antibody (Sigma #G1544, 1:500 for WB), anti-Ub monoclonal antibody (FK2; Biomol #PW-8810, 1:500 for WB, 1:100 for IF), anti-Ub polyclonal antibody (Dako #Z0458, 1:5000 for WB, 1:100 for IF), anti-Gapdh polyclonal antibody (Cell Signaling #2118, 1:1000 for WB). For detecting endogenous proteins in patient muscle biopsy, the following antibodies were used for IF: anti-TIA1 polyclonal (Abcam ab61700, 1:100) and anti-p62 polyclonal (Sigma-Aldrich P0067, 1:100).

Cell culture and transient transfection

Immortalized control and p62^{-/-}-MEFs were from Dr. Komatsu, Niigata University (Komatsu et al., 2007). MEFs were maintained in in Dulbecco's modified Eagle's medium (DMEM, Gibco #11965-084), 10% fetal bovine serum (FBS, Atlanta Biologicals #S10350H), and 50 µg/mL penicillin and streptomycin (P/S, Sigma #P4333), 1% sodium pyruvate (Gibco #11360070), and 1% non-essential amino acid (Gibco #11140050) at 37°C with 5% CO₂. C2C12 cells were maintained in DMEM, 20% FBS, and 50 µg/mL P/S. Transfection was performed with lipofectamine2000 (Life Technologies #11668019) according to the manufacturer's instruction. 24hr post-transfection, cells were washed three times with ice-chilled PBS. pDEST-mCherry-human p62 WT was gifted from Dr. Johansen, The Arctic University of Norway [18]. pDEST-mCherry-human p62 P392L, M404V, A390X generated by mutagenesis. GFP-human TIA1 WT (isoform A) has been previously reported and GFP-human TIA1 E384K and N357S were generated by mutagenesis [60].

Immunocytochemistry and fluorescence microscopy

Cells were grown on glass coverslips prior to transfection with plasmid constructs. 24hrs after the transfection, cells were washed three times with PBS, fixed in 4% PFA for 10mins and permeabilized with 0.05% Triton X-100 in PBS for 10mins. After washing three times with PBS, cells were blocked with 2% BSA in PBS for 30mins-1hr at room temperature (RT). Cells were stained with primary antibody at 4°C overnight followed by three-times washing with PBS. Cells were incubated with Alexa 555 or 488 Fluor-conjugated secondary antibody at RT for 1hr and mounted with Mowiol media containing DAPI. 10 random fields were taken with 20x objective equipped in a NIKON Eclipse 80i fluorescence microscopy. A blue channel was separated and used to count the total number of DAPI-stained cells in Figure 3B, 5B and S3B. Cells co-stained both with TIA1 (green) and G3BP1 (red) were counted in a merge channel. For Figure 2C-D and

5A, individual cells shown in a green or red channel were considered as GFP-TIA1 or mCherry-SQSTM1 expressing cells and counted as a total. GFP-TIA1 expressing cells stained with SQSTM1 (red) or mCherry-SQSTM1 expressing cells stained with TIA1 (green) were manually counted in a merge channel. For Figure 5D, C2C12 cells expressing both mCherry-SQSTM1 and GFP-TIA1 were counted as a total in each red or green channel while those C2C12 cells containing GFP-TIA1 puncta were counted in a merge channel. In Figure 3C-D, individual SGs puncta stained with TIA1 (green) were counted in a green channel as a total while TIA1 SGs co-localized with SQSTM1 (red) were counted in a merge channel. For Figure 4A-B and 4C-D, individual endogenous TIA1 or GFP-TIA1 SGs puncta (green) were counted as a total in a green channel while TIA1 SGs co-localized DRiPs (red) were counted in a merge channel. For Figure 4E-F, individual TIA1 puncta (green) were counted as a total in a green channel and TIA1/TDP-43 positive puncta were counted in a merge channel. Cells or individual SGs puncta were manually counted using ImageJ software (NIH). Frozen muscle biopsy sections (8 μ m) were prepared on slides, fixed in 4% PFA for 15 min and immunostained using similar protocol as for cultured cells.

Heat Shock, inhibitor treatment and DRiPs labeling

MEFs cells or C2C12 cells were incubated at 42°C with 5% CO₂ for 1hr and returned to 37°C for the indicated time points. For AsIII (Sigma #38150) treatment, control MEFs cells were treated with 0.5mM AsIII for 1hr and AsIII-containing media was replaced for the indicated time point. To label DRiPs, control or p62^{-/-} cells were incubated at 42°C with 5% CO₂ for 1hr and simultaneously treated with 25 μ M op-PURO for 30mins. For recovery experiments, cells were returned to 37°C and op-PURO-containing media was replaced for the indicated time. Fixation and Click-iT reaction were performed with Alexa Azide 594 according to the manufacturer's

instruction (Life Technologies #C10399). MG132 (#C2211) and BafA (#B1793) were purchased from Sigma. 20 μ M MG132 or 200nM BafA were treated to control MEFs and p62^{-/-}-MEFs for 1hr at 37°C with 5% CO₂ after 1hr HS at 42°C.

Fluorescence recovery after photobleaching

Control MEFs were grown on 1.5 Glass bottom 35mm dishes (MatTek #P35G-1.5-10-C) and transfected with GFP-human TIA1 for 24hrs prior to imaging. Immediately before imaging, the medium was replaced with Phenol Red-free medium (Gibco #21063029) containing 10% FBS, 50 μ g/mL P/S, 1% sodium pyruvate, and 1% non-essential amino acid. The live cell samples were treated with 0.5mM AsIII for 1hr and placed on a heated chamber at 37°C with 5% CO₂. The imaging and photobleaching were performed with 40x oil objective using an NIKON A1Rsi confocal microscopy. Before bleaching, the images of pre-bleached TIA1 aggregates were taken. 488nm laser was used to photobleach TIA1 aggregates for 500ms. Immediately after the bleaching, the images were collected every 1s for a total of 150seconds as a post-bleached sample. The fluorescence intensities of post-bleached TIA1 aggregates (Ft) were individually measured. In the meantime, the fluorescence intensities of non-bleached TIA1 aggregates were measured as a reference control (Fref). Also, the fluorescence intensities of non-bleached and non-transfected background were measured as a background control (Fb). The photobleaching rate (r) was calculated by comparing the fluorescence of the reference before (Fref0) and after (Fref) photobleaching. $r = Fref/Fref0$. An average of TIA1 aggregates fluorescence intensities (F) in different cells ($n \geq 5$ cells containing TIA1 aggregates) was calculated as followed. $F = (Ft - Fb)/r$.

LDH Assay

C2C12 cells were transfected with Cherry-p62-WT, or AX along with GFP-TIA1-WT, NS, or EK 24hrs prior to LDH assay. Cells were split into 96-well plate in 2×10^5 cells/well as triplicates. Cells were incubated in 1hr at 42°C with 5% CO₂ and returned to 37°C with 5% CO₂ for 1hr recovery. LDH assay was performed according to the manufacturer's instruction (Roche #04 744 926 001).

Statistical analysis

A two-tailed Student's t-test was performed. For all tests, p-values < 0.05 were considered statistically significant. Data are represented as mean \pm SEM.

Study approval

All examinations and genetic studies were conducted according to approval of the Human Studies Committee at Washington University and Helsinki University IRB and with informed consent of the patients following the Helsinki declaration.

3.4 Result

3.4.1 Digenic inheritance of an MSP-associated SQSTM1 mutation with a rare TIA1-N357S variant occurs in distal myopathy patients with rimmed vacuolar pathology.

We have previously described two unrelated families with distal myopathy and RV-IBM pathology due to a c.1165+1 G>A splice donor variant in *SQSTM1* [75]. This variant generates a truncated SQSTM1 protein that lacks its UBA domain and has been identified in patients with PDB and ALS [3, 4]. Subsequent to this discovery, we identified an additional three patients with a distal myopathy and a *SQSTM1* p.P392L variant [6]. This *SQSTM1* p.P392L variant has similarly been associated with dominantly inherited PDB, ALS and FTD, phenotypes that were not present in our patients [3-5]. Interestingly, these three patients had been previously identified in our cohort of distal myopathy patients carrying a rare *TIA1* c.1070A>G; p.N357S; rs116621885 variant with a MAF 0.007. Surprisingly, our three previously reported *SQSTM1* c.1165+1 G>A patients also carried the same rare *TIA1* p.N357S variant. Dominant mutations in *TIA1* are associated with WDM, a distal myopathy with RV-IBM pathology, and more recently, ALS and FTD [60, 61]. Notably, similar to the WDM and ALS/FTD associated *TIA1* mutations, the *TIA1* p.N357S variant was present within the LCD at conserved residues (Figure 1A).

To identify more myopathy patients with *SQSTM1* mutations and the *TIA1* p.N357S variant, we utilized two approaches. First, we analyzed our neuromuscular disease gene panel sequencing results that included *SQSTM1* and *TIA1* in 1294 patients with a presumed hereditary muscle disease [6]. In addition, we Sanger sequenced *SQSTM1* in 14 undetermined distal myopathy patients with a WDM phenotype that we had previously identified with *TIA1* p.N357S variant. These approaches identified a total of eight patients from six families with the common

SQSTM1 p.P392L mutation of which seven also carried the *TIA1* p.N357S variant. Notably, none of them had PDB and all had a distal myopathy with RV-IBM pathology, with the exception of one single patient that carried only the *SQSTM1* p.P392L mutation without the *TIA1* p.N357S variant. This patient had a proximal phenotype without RV-IBM muscle pathology and had been characterized as limb-girdle muscular dystrophy.

We also identified three patients from two families with a previously reported *SQSTM1* p.M404V mutation that is associated with PDB and dementia [111, 112]. These patients also carried the *TIA1* p.N357S variant and had a late onset distal predominant myopathy with RV-IBM pathology and no evidence of PDB. One additional distal myopathy with RV-IBM pathology patient carried a rare synonymous *SQSTM1* variant c.1083C>T, p.S361S that has been previously identified in a patient with early onset dementia and the *TIA1* p.N357S variant [112]. This synonymous mutation has a MAF of 0.00008 and is predicted to be disease causing.

MRI imaging of patients' lower extremities demonstrated extensive fatty degenerative changes in distal muscles shown by focal involvement of lower leg gastrocnemius and soleus muscles in Figure 3.4.1C. Patient muscle biopsies demonstrated variation in fiber size and rimmed vacuoles consistent with RV-IBM (Figure 1D and S1B). In pathologically normal muscle, *SQSTM1* is diffusely sarcoplasmic and TDP-43 and *TIA1* are myonuclear (Figure S1A). In contrast, *SQSTM1* and *TIA1* accumulate in patient muscle sarcoplasm and had some co-localization at RVs as determined by immunohistochemistry (Figure 1E). In addition, *TIA1* accumulated with other RNA binding proteins such as TDP-43 and HNRNPA2B1 (Figure 1E and S1C). Western blot analysis of skeletal muscle from one patient, found normal steady state levels for *SQSTM1* and *TIA1* (Figure S1D). Table 1 denotes the clinical and laboratory characteristics for all *SQSTM1*-*TIA1* patients included in this study. Digenic inheritance was

demonstrated in three families in which only examined affected family members carried both a *SQSTM1* p.P392L or a *SQSTM1* p.M404V mutation and a *TIA1* p.N357S variant whereas family members carrying only a *TIA1* p.N357S variant were unaffected (Figure 1B).

Importantly, sequencing of 50 patients (26 male, 24 female: average age 73.7+/-7.3years) with previously reported pathogenic *SQSTM1* mutations including 40 with a *SQSTM1*-P392L mutation and two with a *SQSTM1*-M404V mutation manifesting with PDB but no muscle weakness did not reveal any *TIA1*-N357S variant supporting that both variants are necessary for a muscle phenotype with RV-IBM pathology (Supplemental Table S1) [113].

Although patients in these small pedigrees with only the *TIA1* p.N357S variant had no evidence of weakness, we reasoned that the rare *TIA1* p.N357S variant may itself be enriched in patients with a distal myopathy phenotype. Indeed, in our large sequencing project of 1293 presumed inherited myopathy patients, 41 (3%) had the N357S variant (allele frequency 0.0162 versus 0.007 in the general population), and when this was stratified to those with a distal myopathy phenotype involving also upper limbs, 17/86 (20%) of these patients carried the variant, including one patient that was homozygous for the *TIA1* p.N357S variant making the allele frequency 0.1 for distal myopathy. A similar overrepresentation of this *TIA1* p.N357S variant was seen in 5 patients from a second cohort of 51 undiagnosed myopathy patients following whole exome sequencing. All 5 patients had a distal predominant phenotype with RV-IBM pathology including two patients with an additional c.1165+1 G>A splice donor variant in *SQSTM1* [75].

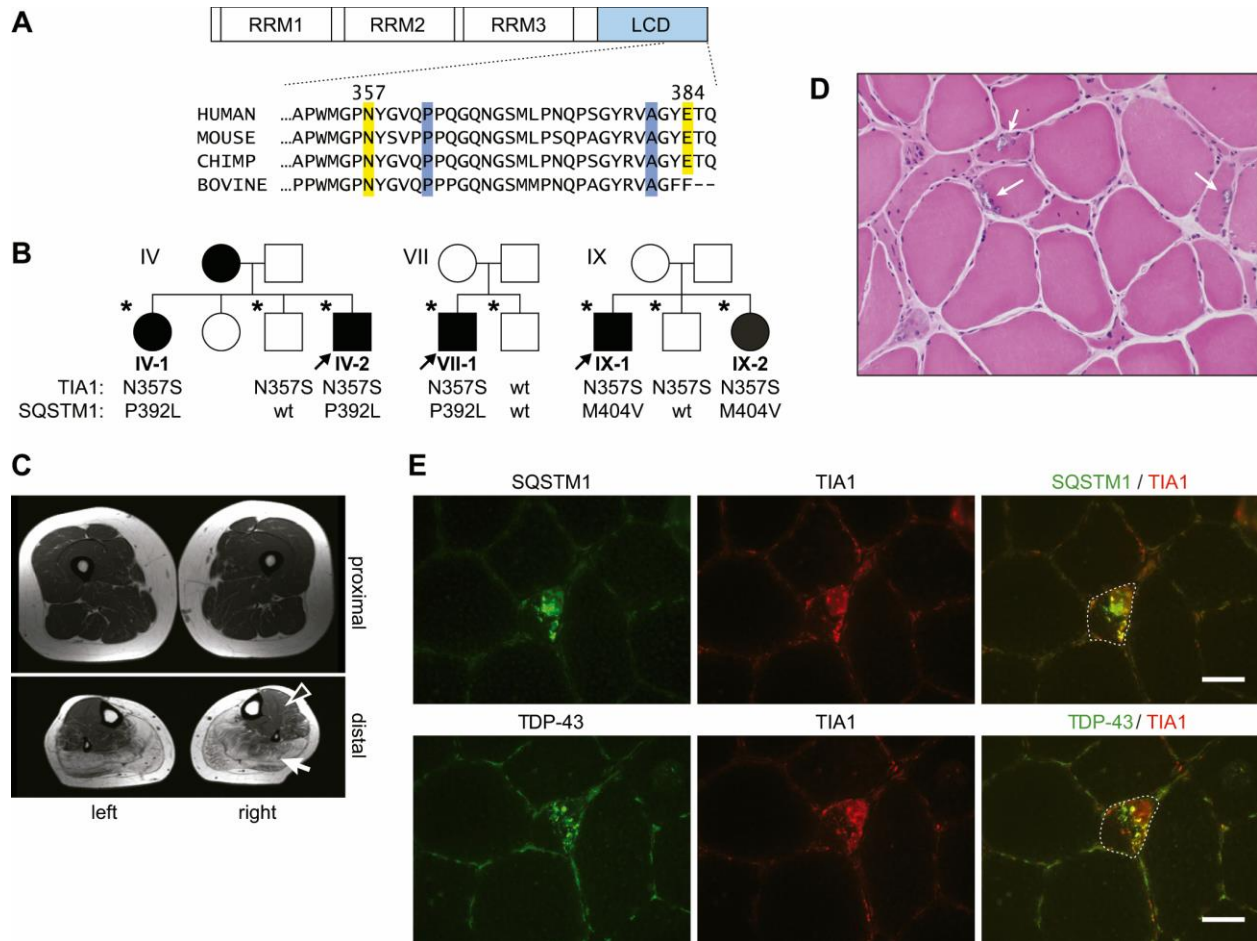


Figure 1. Digenic inheritance of SQSTM1 and TIA1 variants lead to a distal myopathy with RV-IBM pathology. A) Linear diagram of TIA1 protein highlighting conserved regions of the LCD. Distal myopathy associated variant positions are shown in yellow and ALS/FTD variants in blue. B) Pedigrees of families IV, VII and IX showing segregation. DNA was only available for patients marked with *. C) Muscle imaging findings of patient V-2 at age 54. Severe involvement of all calf muscles is seen on MRI T1-weighted images. Filled arrow denotes normal muscle and open arrow indicates atrophic muscle with fatty replacement. D) H&E staining of a muscle biopsy of the right tibialis from patient XII-1 showing several fibers with rimmed vacuoles (arrows). E) Immunofluorescent staining of TIA1 (red) with SQSTM1 (green in upper panel) or TDP-43 (green in lower panel) revealed accumulation and partial co-localization of these proteins in patient V-2 muscle biopsy. Both images show a rimmed vacuolar fiber. Dotted line denotes affected fiber.

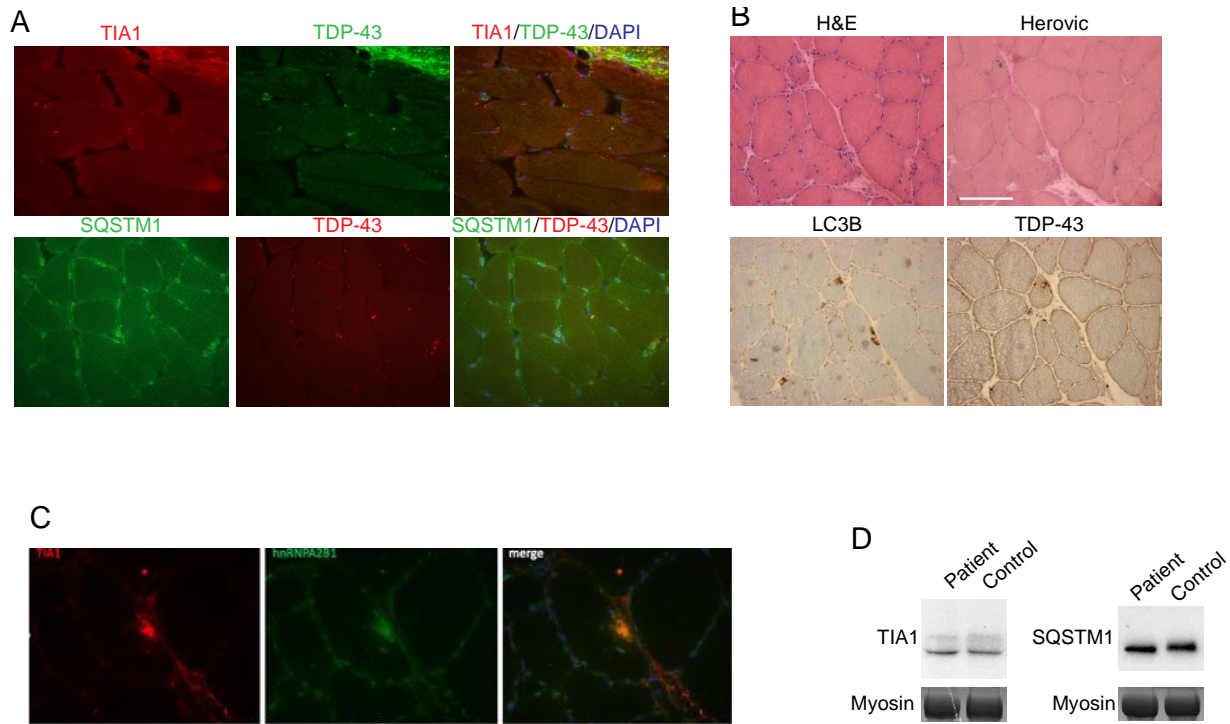


Figure S1. Histopathology of SQSTM1-TIA1 patients and controls. A) Immunofluorescent staining of TIA1 (red in upper panel) or TDP-43 (green) and SQSTM1 (green in lower panel). B) Serial sections from patient muscle biopsy histochemically stained with hematoxylin and eosin (H&E) and Herovici staining demonstrating myopathy with rimmed vacuoles. Immunohistochemistry of similar sections stained with antibodies against autophagic marker LC3B and TDP-43. C) Co-immunofluorescent staining of patient muscle with antibodies to TIA1 (red) and HNRNPA2B1 (green). D) Patient and control muscle immunoblot for TIA1 and SQSTM1. Myosin is shown as a loading control.

| | | | | | | | | | | | | |
|--------------------|--------|----|-----|--------|---|-----------|--------------------------------|----------------------------|--|-----|---------------------------------------|-------------------------------|
| I-1 ^A | Male | 63 | 52 | + | Asymmetric; ankle dorsiflexion; wrist and finger extension; scapular winging | 419 | myopathic | RVs, myofibrillar disarray | NA | -/- | c.1165+1 G>A; p.Glu389delinsAspLysTer | c.1070A>G; p.N357S |
| I-2 ^A | Male | 47 | 42 | + | Asymmetric; ankle dorsiflexion; shoulder abduction; wrist extension | 143 | myopathic | ND | NA | -/- | c.1165+1 G>A; p.Glu389delinsAspLysTer | c.1070A>G; p.N357S |
| II-1 ^A | Male | 60 | 50 | - | Asymmetric; ankle dorsiflexion; shoulder abduction; scapular winging | 346 | myopathic | RVs; myofibrillar disarray | TA, Gmed, S | -/- | c.1165+1 G>A; p.Glu389delinsAspLysTer | c.1070A>G; p.N357S |
| III-1 ^B | Male | 65 | 35 | - | Ankle plantar and dorsiflexion; wrist and finger extension; scapular winging; proximal lower limbs | NA | NA | RVs | TA, EDL/EHL, Gmed, Glat, S | -/- | c.1175C>T; p.P392L | c.1070A>G; p.N357S |
| IV-1 | Female | 68 | NA | + | Ankle dorsiflexion; finger extension | NA | NA | NA | NA | -/- | c.1175C>T; p.P392L | c.1070A>G; p.N357S |
| IV-2 | Male | 62 | 41 | + | Ankle dorsiflexion; finger extension; scapular winging; abdominal and ankle plantar flexion | NA | NA | Myofibrillar disarray | S, mild Gmed | -/- | c.1175C>T; p.P392L | c.1070A>G; p.N357S |
| V-2 | Female | 57 | 45 | - (+?) | Finger extension; thumb adduction/abduction; facial weakness | 2xUNL | NA | RVs | Gmed, Glat, S, peronei | -/- | c.1175C>T; p.P392L | c.1070A>G; p.N357S |
| VI-1 | Male | 69 | 50 | - | Ankle dorsiflexion; wrist and finger extension | 3XUNL | myopathic/ neurogenic (PNP) | RVs | TA, Gmed, Glat | -/- | c.1175C>T; p.P392L | c.1070A>G; p.N357S |
| VII-1 | Male | 50 | 48 | - | Ankle dorsiflexion; wrist and finger extension | 2xUNL | myopathic | RVs | TA, Gmed, Glat, S, glutei, paraspinal | -/- | c.1175C>T; p.P392L | c.1070A>G; p.N357S |
| VIII-1 | Female | 69 | 45 | + | Asymmetric ankle dorsiflexion; finger extension | ND | ND | ND | ND | -/- | c.1175C>T; p.P392L | c.1070A>G; p.N357S |
| IX-1 | Male | 76 | 45 | + | Ankle dorsiflexion; wrist and finger extension | 500 | myopathic | NA | NA | ? | c.1210A>G p.M404V | c.1070A>G; p.N357S |
| IX-2 | Female | 62 | 50 | + | Ankle dorsiflexion; wrist and finger extension | NA | NA | Myofibrillar disarray | NA | ? | c.1210A>G p.M404V | c.1070A>G; p.N357S |
| X-1 | Male | 68 | 55? | ? | Distal lower extremities | NA | NA | Myofibrillar disarray | TA, Gmed | | c.1210A>G p.M404V | c.1070A>G; p.N357S |
| XI-1 | Male | 74 | 68 | - | Asymmetric finger extension; thumb abduction; mild finger flexion; ankle dorsiflexion; mild toe extension/flexion | 1.5 x UNL | myopathic | RVs, myofibrillar disarray | Asymmetric TA, S, Gmed | -/- | c.1083C>T, p.S361S | c.1070A>G; p.N357S |
| XII-1 | Female | 54 | 40 | - | Distal weakness in upper and lower extremities | NA | myopathic | NA | All lower leg muscles except left Glat, deep toe flexors | -/- | - | c.1070A>G; p.N357S homozygous |

Table 1. Clinical characteristics of the patients. EDL/EHL, long toe extensors; Gmed, gastrocnemius medialis; Glat, gastrocnemius lateralis; NA, not available; ND, not done; PNP, polyneuropathy; S, soleus; TA, tibialis anterior; UNL, upper normal limit. Previously reported patients. *[75]**[6]

| Patient | Gender | Age | Onset | <i>SQSTM1</i> | <i>TIAI</i> SNP |
|----------------|---------------|------------|--------------|----------------------|------------------------|
| 1 | F | 67 | 67 | P392L/WT | WT/WT |
| 2 | F | 71 | 56 | G425R/WT | WT/WT |
| 3 | M | 66 | 53 | P392L/WT | WT/WT |
| 4 | F | 83 | 63 | P392L/WT | WT/WT |
| 5 | M | 68 | 60 | P392L/WT | WT/WT |
| 6 | M | 59 | 56 | G425R/I424S | WT/WT |
| 7 | F | 69 | 55 | G425R/WT | WT/WT |
| 8 | F | 71 | 55 | M404V/WT | WT/WT |
| 9 | F | 74 | 47 | P392L/WT | WT/WT |
| 10 | F | 78 | 69 | P392L/WT | WT/WT |
| 11 | F | 81 | 49 | P392L/WT | WT/WT |
| 12 | M | 74 | 45 | P392L/WT | WT/WT |
| 13 | M | 74 | 64 | P392L/WT | WT/WT |
| 14 | M | 71 | 66 | P392L/WT | WT/WT |
| 15 | F | 69 | 50 | M404T/WT | WT/WT |
| 16 | M | 91 | 54 | P392L/WT | WT/WT |
| 17 | M | 72 | 58 | P392L/WT | WT/WT |
| 18 | M | 80 | 78 | P392L/WT | WT/WT |
| 19 | F | 62 | 54 | G425R/WT | WT/WT |
| 20 | M | 64 | 54 | P392L/WT | WT/WT |
| 21 | F | 67 | 48 | P392L/WT | WT/WT |
| 22 | M | 82 | 57 | P392L/WT | WT/WT |
| 23 | M | 76 | 72 | P392L/WT | WT/WT |
| 24 | F | 73 | 45 | P392L/WT | WT/WT |
| 25 | F | 72 | 67 | P392L/WT | WT/WT |

| | | | | | |
|----|---|----|----|----------|-------|
| 26 | M | 73 | 70 | P392L/WT | WT/WT |
| 27 | M | 89 | 60 | P392L/WT | WT/WT |
| 28 | F | 85 | 84 | P392L/WT | WT/WT |
| 29 | M | 83 | 54 | E396X/WT | WT/WT |
| 30 | F | 82 | 75 | P392L/WT | WT/WT |
| 31 | M | 72 | 26 | I424S/WT | WT/WT |
| 32 | F | 84 | 79 | P392L/WT | WT/WT |
| 33 | F | 74 | 64 | M404V/WT | WT/WT |
| 34 | M | 72 | 55 | P392L/WT | WT/WT |
| 35 | F | 86 | 76 | P392L/WT | WT/WT |
| 36 | M | 62 | 55 | P392L/WT | WT/WT |
| 37 | M | 75 | 63 | P392L/WT | WT/WT |
| 38 | M | 71 | 72 | P392L/WT | WT/WT |
| 39 | F | 80 | 70 | P392L/WT | WT/WT |
| 40 | M | 79 | 41 | P392L/WT | WT/WT |
| 41 | F | 70 | 70 | P392L/WT | WT/WT |
| 42 | M | 74 | 50 | P392L/WT | WT/WT |
| 43 | F | 67 | 54 | P392L/WT | WT/WT |
| 44 | M | 76 | 59 | P392L/WT | WT/WT |
| 45 | F | 59 | 51 | P392L/WT | WT/WT |
| 46 | F | 66 | 40 | P392L/WT | WT/WT |
| 47 | F | 78 | 52 | P392L/WT | WT/WT |
| 48 | M | 72 | 70 | P392L/WT | WT/WT |
| 49 | F | 71 | 66 | P392L/WT | WT/WT |
| 50 | F | 73 | 67 | P392L/WT | WT/WT |

Table S1. Genotypes of PDB patients.

3.4.2 TIA1 N357S variant promotes LLPS and impairs stress granule clearance.

To examine the impact of the TIA1-N357S (NS) mutation on LLPS, we constructed a phase diagram by measuring the co-existence line of protein-depleted light phase and protein-enriched dense phase as a function of temperature and protein concentration. Similar to the previously characterized TIA1-E384K (EK) mutant, the TIA1-NS mutation caused a significant leftward shift in the co-existence line to a lower protein concentration, indicating an increased propensity of mutant TIA1 to phase separate, due to stronger intermolecular protein-protein interactions (Figure 2A). Although the promotion of LLPS with TIA1-EK was associated with an increased rate of amyloid-like fibril formation as demonstrated by a time dependent increase in thioflavin-T incorporation when compared to TIA1-WT, this increase was not seen with purified TIA1-NS (Figure 2B).

The effect of TIA1-NS and EK variants on LLPS in vitro suggested that these variants might affect the dynamics of SGs in vivo. To test this hypothesis, we expressed GFP-TIA1-WT, -NS, or -EK in mouse embryonic fibroblasts (MEFs) for 24hrs. Immunoblotting confirmed similar levels of expression for GFP-TIA1-WT, -NS, or -EK (Figure S2A). MEFs expressing GFP-TIA1 were fixed and stained with the SG marker, G3BP1. Individual GFP-TIA1 expressing cells were considered as a total number of cells while cells containing GFP-TIA1/G3BP1 SGs were counted. Untreated GFP-TIA1-WT expressing cells did not form SGs while some SGs were detected in GFP-TIA1-NS or-EK expressing cells (Figure 2C-D). 42°C heat shock (HS) induces SG formation in MEFs expressing GFP-TIA1-WT, -NS, or -EK after 1 hour. Upon return to 37°C for 30 minutes ~10% of GFP-TIA1-WT expressing MEFs contained SGs as compared to ~40% of MEFs expressing GFP-TIA1-NS or -EK (Figure 2C-D). TIA1 in SGs is normally in rapid equilibrium with TIA1 in the surrounding cytoplasm. We investigated whether TIA1-NS

mutation affects its mobility within SGs. MEFs expressing GFP-TIA1-WT, -NS, or -EK were treated with 0.5mM arsenite (AsIII) for 1hr and GFP-TIA1 SGs were subject to fluorescence recovery after photobleaching (FRAP). Following photobleaching, ~65% of GFP-TIA1-WT fluorescence rapidly recovers whereas GFP-TIA1-NS and -EK recover to ~40 and 60% respectively (Figure 2E and Figure S2B).

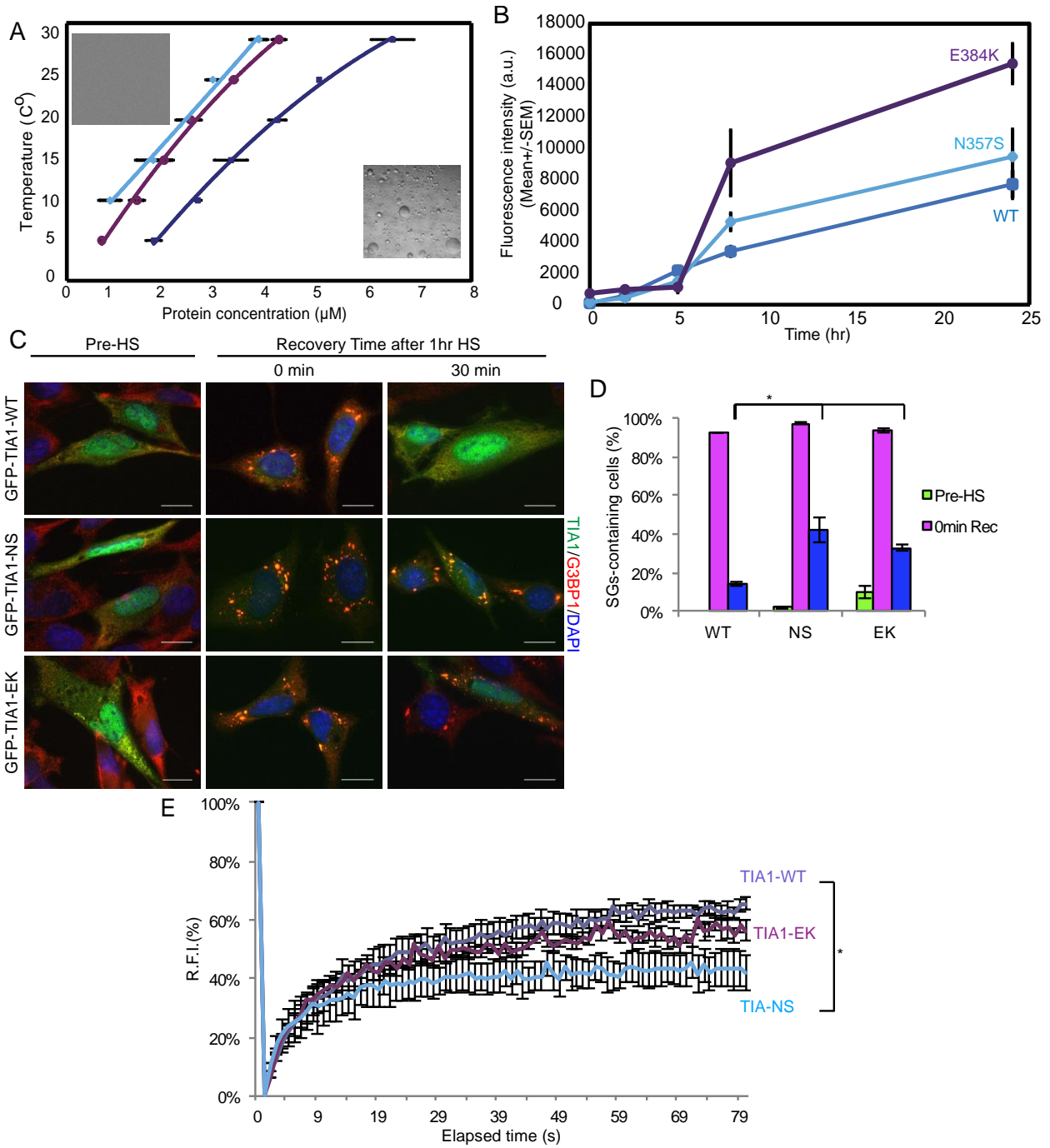


Figure 2. TIA1 N357S variant promote liquid-liquid phase separation and disrupts stress granule dynamics.

A) Phase diagram TIA1-WT, EK and NS are mapped at physiological conditions. Mean concentration of light phase (protein depleted phase) and SE are plotted. A quadratic equation is used to fit the trendlines (R^2 , WT and NS = 0.99, EK = 0.98, $P < 0.003$ for NS vs WT and $P < 0.0002$ for EK vs WT were obtained by chi-squared test). Insets show characteristics DIC images of light, diffused phase and dense phase droplets respectively. Concentration of light phase of NS variant at 5°C was below detection limit. B) Fluorescence intensity of amyloid fibrils monitored by Thioflavin T (ThT), in light phase regime at 2.5 μ M of TIA1-WT, EK and NS variants taken. Samples were agitated at RT for 24h. Each time point was measured, and mean and SE of mean, of ThT fluorescent intensity at 480 nm are plotted. The spectrum of BSA (non-amyloid fibril forming) was measured as a baseline. That baseline has been subtracted from all the WT, EK and NS spectra at each time point respectively. *** denote p value < 0.001 . C) Immunofluorescent images of mouse embryonic fibroblasts (MEFs) expressing GFP-TIA1-WT, NS, or EK immunostained with anti-G3BP1 (red) prior to 1 hour heat shock (HS) at 42°C, immediately post HS or following 30 minutes of HS recovery at 37°C. Blue color indicates DAPI nuclear staining. Scale is 5 μ m. D) Bar graph of the percentage of cells containing TIA1/G3BP1 positive stress granules under the conditions in (B). Representative data were pooled from three independent experiments (n=150~200). E) Graphical representation of the average relative fluorescent intensity (RFI) following photobleaching of individual SGs from MEFs expressing GFP-TIA1-WT, NS, or EK and treated for one hour with 0.5mM arsenite. Representative data were pooled from three independent experiments (n=20~30). All error bars are mean \pm SEM, * $P < 0.05$.

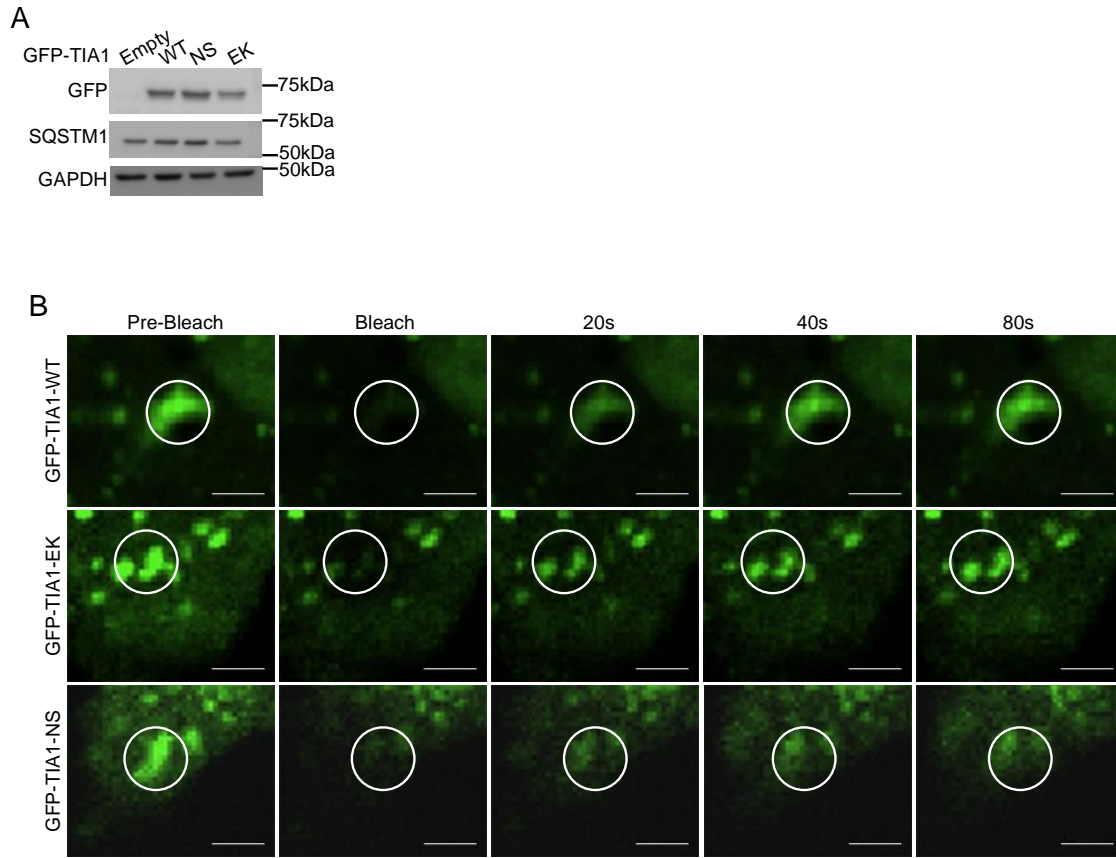


Figure S2. Immunoblot images of GFP-TIA1 and live cell images following photobleaching. A) Immunoblot from control MEFs expressing GFP-TIA1-Empty, WT, NS, or EK for GFP and SQSTM1. GAPDH is shown as a loading control. B) Representative fluorescence images of GFP-TIA1-WT, EK, or NS stress granules from live MEFs cells expressing GFP-TIA1, EK, or NS in (Figure 2E). The circle indicates the photobleached area. Scale is 1 μ m.

3.4.3 SQSTM1 participates in stress granule protein clearance.

To explore the role of SQSTM1 in SG formation and clearance, we immunostained endogenous TIA1 and G3BP1 in control MEFs and MEFs lacking SQSTM1 (p62^{-/-}-MEFs). Individual cells were considered as a total number of cells while cells containing TIA1/G3BP1 SGs were counted. Untreated control or p62^{-/-}-MEFs did not form TIA1/G3BP1 positive SGs (Figure 3A-B). Following 1hr HS, ~95% of control MEFs and 70% of p62^{-/-}-MEFs contained SGs (Figure 3A-B). 20 mins after re-incubating cells at 37°C, ~50% of SGs disappeared in control MEFs and ultimately dissipated by one hour. In contrast, p62^{-/-}-MEFs had a slower SG clearance, with some cells maintaining SGs after 180 minutes (Figure 3A-B). Persistent TIA1 positive SGs in p62^{-/-}-MEFs co-immunolocalized with an antibody that recognizes ubiquitin conjugates (Figure S3A). Consistent with SQSTM1 mediating the clearance of SGs via an autophago-lysosomal pathway, we found that incubation of p62^{-/-}-MEFs with the lysosomal inhibitor BafilomycinA during HS recovery did not further augment the decrease in SG clearance seen with loss of SQSTM1 (Figure S3B).

To explore a direct connection between TIA1 and SQSTM1, we immunostained for endogenous SQSTM1 in MEFs expressing GFP-TIA1-WT, -NS, or -EK after 1hr HS and following 30 mins recovery to 37°C. Individual GFP-TIA1 SGs puncta were considered as a total number of SGs and the number of GFP-TIA1 SGs puncta co-localized with endogenous SQSTM1 was counted at indicated time points. A subset of GFP-TIA1-WT SGs co-localized with SQSTM1. The co-localization of SQSTM1 and GFP-TIA1 was greater in GFP-TIA1-NS or -EK compared to GFP-TIA1-WT expressing MEFs (Figure 3C-D).

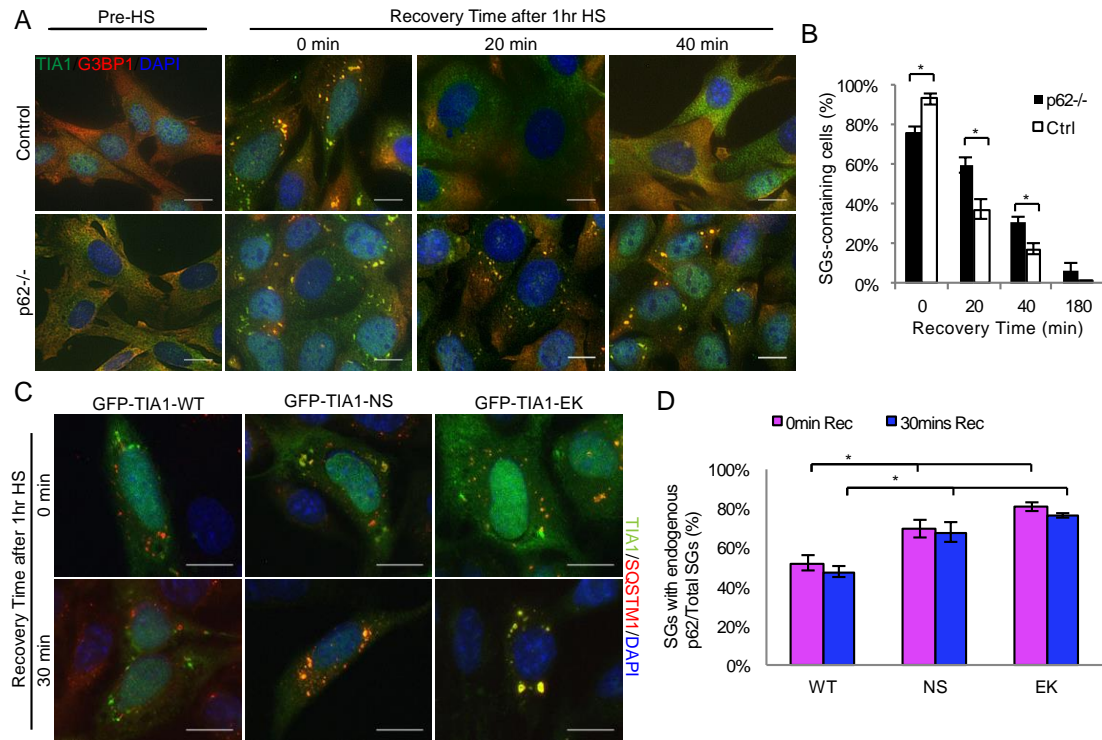


Figure 3. SQSTM1 is necessary for stress granule homeostasis. A) Immunofluorescent images of control or SQSTM1 knockout MEFs (p62^{-/-}), incubated at 42°C for 1hr and returned to 37°C for indicated times, and immunostained for TIA1 (green) and G3BP1 (red) to detect SGs. B) Graph of the percentage of cells containing TIA1/G3BP1 positive stress granules in (A). Transfected cells were counted and indicated as a total number of cells. Representative data were pooled from three independent experiments (n=150~200). C) Immunofluorescent images of MEFs expressing GFP-TIA1-WT, NS, or EK and immunostained with SQSTM1 antibody following incubation at 42°C for 1hr and re-incubated at 37°C for indicated time. D) Graph of the percentage of GFP-TIA1/SQSTM1 positive SGs puncta in (C). Individual GFP-TIA1 SGs puncta were counted and indicated as a total number of SGs. Representative data were pooled from three independent experiments (n=800~1000). Scale is 5µm and error bars are mean± SEM for all figures. *P<0.05.

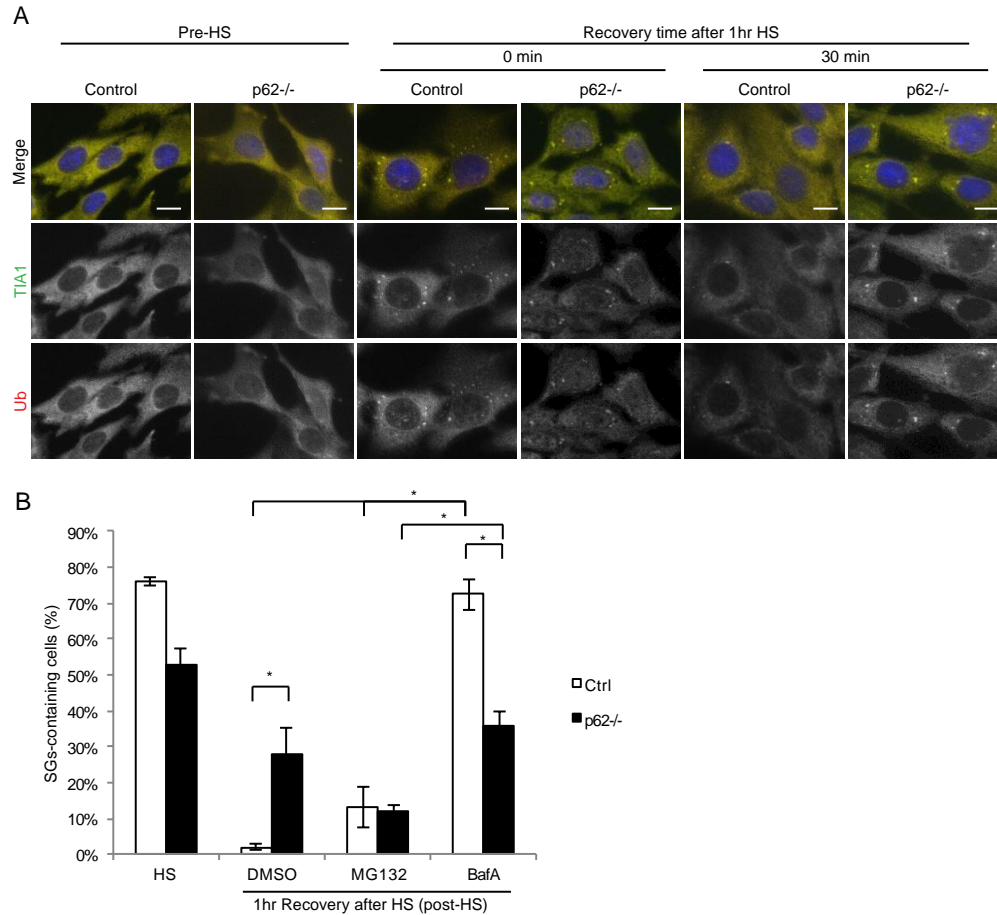


Figure S3. Immunostaining of stress granules accumulating ubiquitin conjugates and bar graph of cells treated with proteasomal inhibitor (MG132) or lysosomal autophagic inhibitor (BafilomycinA). A) Immunofluorescent images of control or p62^{-/-} MEFs for TIA1 and ubiquitin (FK2) before HS, after incubation at 42°C for 1hr and following 30 min HS recovery. Representative data were pooled from three independent experiments (n=150~200). Blue color indicates DAPI staining. B) Bar graph of the percentage of MEFs cells containing TIA1/G3BP1 positive SGs. Control of p62^{-/-} MEFs were incubated at 42°C for 1hr (HS). They were subsequently returned to 37°C and incubated with DMSO, MG132, or BafilomycinA for 1hr. All error bars are mean ± SEM. * denotes p value <0.05.

3.4.4 The presence of aggregated proteins increases TIA SG persistence in the presence of TIA1 mutations or loss of SQSTM1.

Defective ribosomal products (DRiPs) are prematurely terminated and/or misfolded polypeptides [73, 114]. They may form transient inclusions that co-localize with SQSTM1 and are targeted for clearance via the proteasome or autophagy [73, 114-116]. DRiPs may also accumulate adjacent to and within SGs, which may lead to altered SG kinetics [73, 114]. To see if SQSTM1 mediates the clearance of DRiP-containing SGs, we treated control and p62^{-/-}-MEFs with OP-puromycin to generate and label DRiPs. Individual TIA1 positive SGs puncta were considered as a total number of SGs and the number of TIA1 SGs puncta stained with DRiPs were counted. After 1hr HS, ~30% of SGs co-localized with DRiPs in control MEFs and ~45% of SGs co-localized with DRiPs in p62^{-/-}-MEFs (Figure 4A-B). Surprisingly, after 30mins of HS recovery, DRiP containing SGs significantly decreased in control MEFs but DRiP containing SGs accumulated in p62^{-/-}-MEFs, suggesting that the clearance of aberrant SGs with DRiPs is SQSTM1-dependent (Figure 4A-B). Similarly, we treated MEFs expressing GFP-TIA1-WT, -NS, or -EK with OP-puromycin to generate and label DRiPs as above. Following 1 hr HS, ~35% of GFP-TIA1-WT SGs co-localized with DRiPs, this number decreased upon HS recovery (Figure 4C-D). In contrast, GFP-TIA1-NS and -EK SGs co-localized more robustly with DRiPs following HS and this association persisted upon HS recovery (Figure 4C-D).

We reasoned that since DRiPs were misfolded proteins, TIA1 may similarly accumulate with other misfolded and aggregated proteins at SGs. To test this, we expressed an aggregation prone 25kDa C-terminal TDP-43 fragment with an mCherry tag (mCherry-TDP-CTF) in control or p62^{-/-} MEFs and subjected them to 1 hr HS followed by 30 minutes of recovery. Individual TIA1 positive SGs puncta were considered as a total number of SGs and the number of TIA1 SGs puncta co-localized with mCherry-TDP-CTF was counted. Immunofluorescence for

endogenous TIA1 found that upon HS, TIA1 and mCherry-TDP-CTF co-localized in both cell types (Figure 4E-F). However, upon recovery in the p62^{-/-} MEFs, ~80% of persistent TIA1 positive SGs also contained mCherry-TDP-CTF as compared with ~20% in control MEFs (Figure 4E-F).

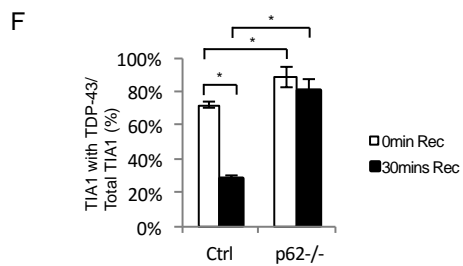
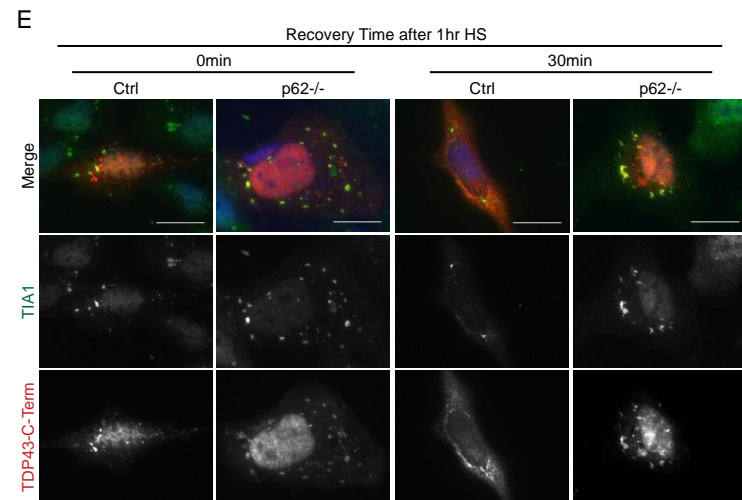
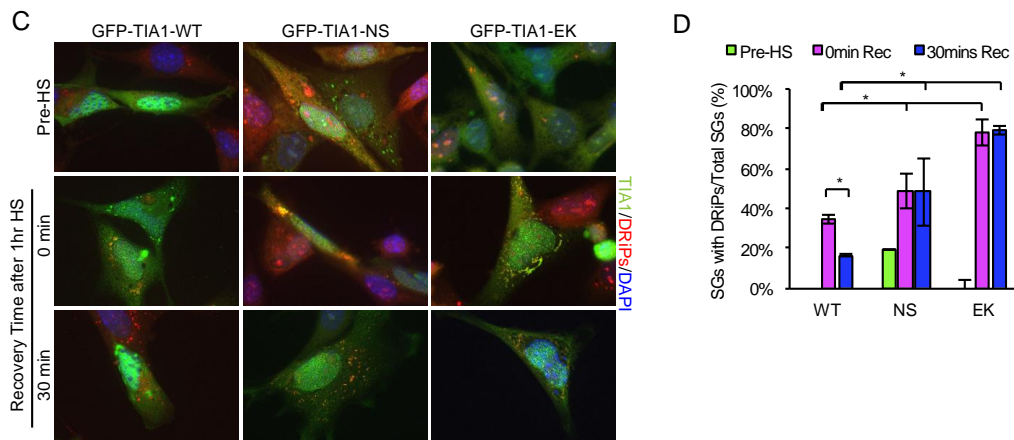
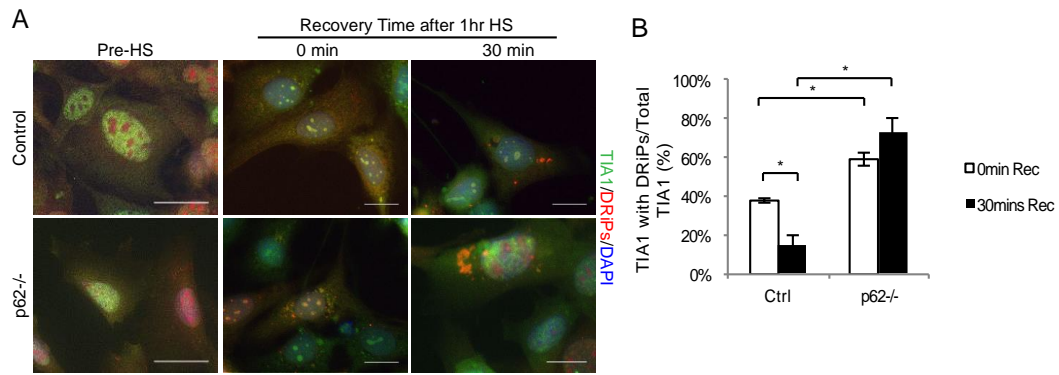


Figure 4. The presence of aggregated proteins increases TIA SG persistence in the presence of TIA1 mutations or loss of SQSTM1. A) Immunofluorescent images of control or p62^{-/-}-MEFs expressing labeled with Alexa594-Azide (red) to detect DRiPs after incubation at 42°C for 1hr and following 30 min HS recovery. Representative data were pooled from three independent experiments (n=350~450). B) Graph of the percentage of TIA1 SGs puncta labeled with Alexa594-Azide (red) that detect defective DRiPs in control or SQSTM1 knockout MEFs (p62^{-/-}), incubated at 42°C for 1hr and returned to 37°C for 30 minutes. Individual TIA1 SGs puncta (green) were counted and indicated as total number of TIA1 SGs. Representative data were pooled from three independent experiments (n=350~450). C) Immunofluorescent images of MEFs expressing GFP-TIA1-WT, NS, or EK and labeled with Alexa594-Azide (red) to detect DRiPs before HS, after incubation at 42°C for 1hr and following 30 min HS recovery. Representative data were pooled from three independent experiments (n=350~450). D) Graph of the percentage of TIA1 SGs puncta labeled with DRiPs in (C). Individual TIA1 SGs puncta (green) were counted and indicated as a total number of TIA1 SGs. E) Immunofluorescent images of endogenous TIA1 (green) from control or p62^{-/-}-MEFs transfected with an mCherry tagged TDP-43 C-terminal fragment (red) after incubation at 42°C for 1hr and following 30 min HS recovery. Representative data were pooled from three independent experiments (n=350~450). F) Graph of the percentage of TIA1 SGs puncta with mCherry TDP-43 c-terminal fragment in control or p62^{-/-}-MEFs from (E). Individual TIA1 SGs puncta (green) were counted and indicated as a total number of TIA1 SGs. Blue color indicates DAPI nuclear staining. Scale is 5 μm and error bars are mean± SEM for all figures. *P<0.05.

3.4.5 MSP associated SQSTM1 mutations impair TIA1 positive stress granule homeostasis.

To investigate whether SQSTM1 disease mutations identified in MSP patients affected the clearance of TIA1-containing SGs, MEFs expressing mCherry, mCherry-SQSTM1-WT, or mCherry-SQSTM1 carrying an MSP mutation, SQSTM1-P392L (PL), SQSTM1-M404V (MV), or SQSTM1-A390X (AX) were immunostained with antibodies to endogenous TIA1. Without HS, MEFs expressing mCherry or mCherry-SQSTM1-WT did not form SGs (Figure 5A). In contrast, even without HS, MEFs expressing mCherry-SQSTM1 disease mutations (PL, MV, or AX) had TIA1 positive SGs (Figure 5A). As expected, most cells contained SGs following 1 hour HS and after 30 min post HS recovery, ~50% of SGs were cleared in MEFs expressing mCherry or mCherry-SQSTM1-WT. In contrast, following 30 mins HS recovery, MEFs expressing mCherry-SQSTM1-PL, -MV, or -AX had persistent SGs in 80% of cells, suggesting that disease-associated SQSTM1 mutations delay SG clearance (Figure 5A).

To explore the synergy of a SQSTM1 disease mutation and the *TIA1*-N357S variant, we utilized patient derived fibroblasts from two control patients (#112, #409), two patients carrying the *TIA1*-N357S variant (#107, #319) and one patient carrying both a *SQSTM1* c.1165+1 G>A mutations which generates a truncated SQSTM1-A390X mutation and a *TIA1*-N357S variant (#483). We treated low passage fibroblasts with 0.5mM AsIII for 1hr and then replaced AsIII-containing media for 40 minutes. Fibroblasts were immunostained for endogenous TIA1 and G3BP1. Untreated fibroblasts had no detectable SGs. Following one hour of AsIII treatment, all fibroblasts formed TIA1/G3BP1 positive SGs (Figure 5B-C). These SGs dissipated in all fibroblasts but were significantly increased in fibroblast line #483 that contains both disease variants (Figure 5B-C).

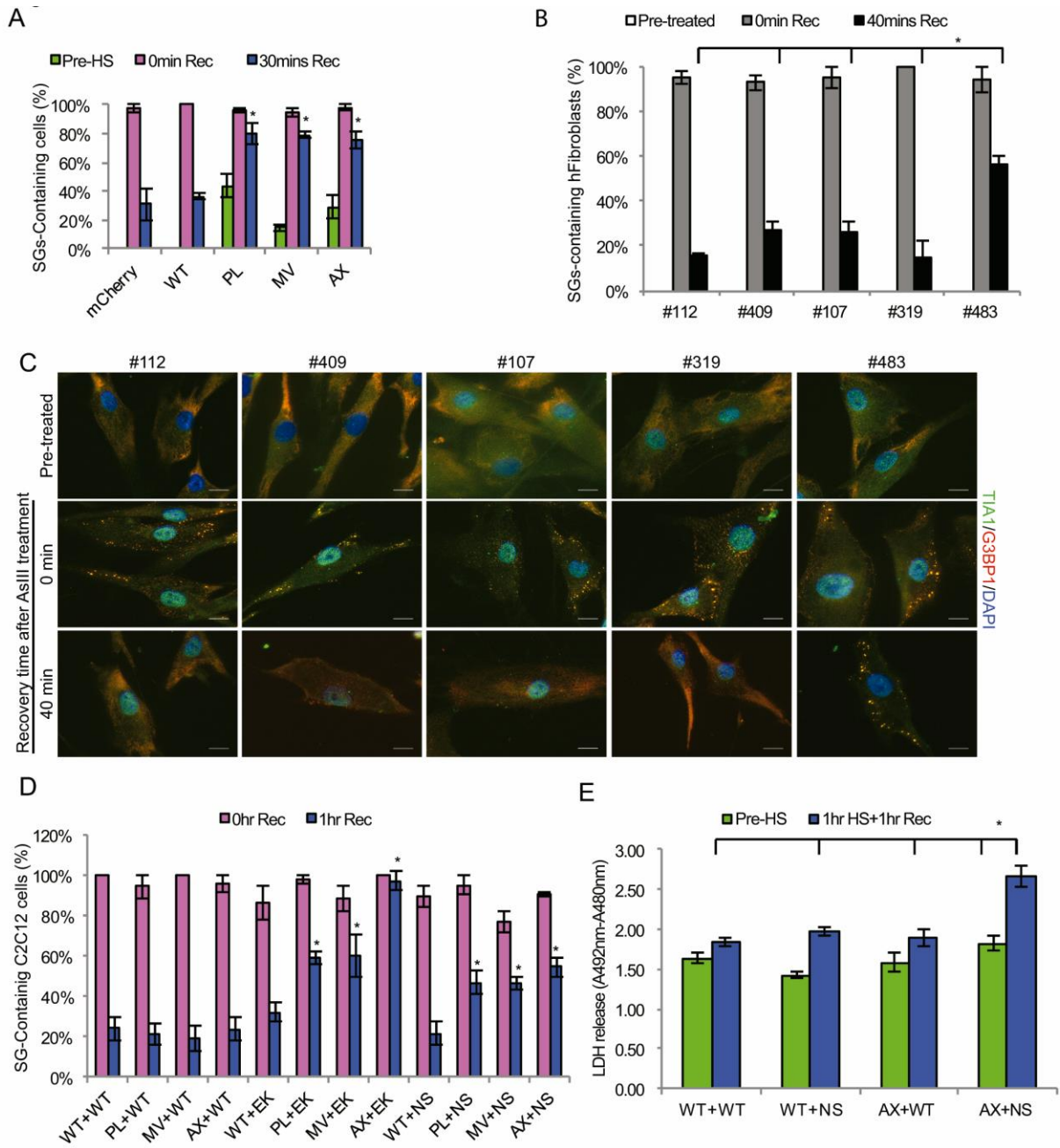


Figure 5. SQSTM1 disease mutations alter SG kinetics and synergistically mediate myotoxicity with TIA1-N357S. A) Bar graph of the percentage of MEFs cells containing endogenous TIA1 positive SGs. MEFs were transfected with mCherry, mCherry-SQSTM1-WT, or one of three different disease mutations (PL, MV or AX) incubated at 42°C for one hour and subsequently returned to 37°C for the indicated time. Transfected cells were counted and indicated as total number of cells. Representative data were pooled from three independent experiments (n=450~550). B) Bar graph of the percentage of fibroblasts containing TIA1/G3BP1 positive SGs from the fibroblasts of control patients (#112, #409), patients carrying the TIA1-N357S variant (#107, #319) and a patient carrying both a SQSTM1-A390X mutation and a TIA1-N357S variant (#483) immediately following 0.5mM Arsenite (AsIII) treatment for one hour or following 40 mins of recovery. C) Immunofluorescent images of patient fibroblasts detailed in (B) immunostained with TIA1 (green) and G3BP1 antibodies (red) before, immediately following 0.5mM AsIII treatment for one hour or following 40 mins of recovery. Blue color indicates DAPI nuclear staining. Scale is 5µm. Representative data were pooled from three independent experiments (n=120~150). D) Bar graph of the percentage of C2C12 myoblasts containing TIA1 positive SGs. C2C12 myoblasts were co-transfected with mCherry, mCherry-SQSTM1-WT or mCherry-SQSTM1 with one of three different disease mutations (PL, MV or AX) and GFP-TIA1-WT or one of two variants (EK or NS) incubated at 42°C for one hour and subsequently returned to 37°C for the indicated time. E) Bar graph of LDH release from C2C12 myoblasts similar to those in (D) before HS and following 1hr HS with an additional 1hr recovery at 37°C. The absorbance of the samples was measured at 492nm. The reference wavelength at 680nm was measured. Representative data were pooled from three independent experiments (n=150~200) and error bars are mean± SEM for all figures. * denotes p value <0.05.

3.4.6 Co-expression of MSP associated SQSTM1 mutations and TIA1-N357S is myotoxic.

To see if the synergistic effect of *SQSTM1* mutations and *TIA1* variants occurred in muscle cells, we co-transfected C2C12 myoblasts with plasmids expressing mCherry-SQSTM1-WT, or mCherry-SQSTM1 carrying an MSP mutation (PL, MV, or AX) and GFP-TIA1-WT or GFP-TIA1 carrying a distal myopathy variant (EK or NS). Following 60 min HS, ~100% of myoblasts had TIA1-GFP positive SG regardless of mutation or variant (Figure 5D). In contrast, after 60 min of HS recovery, myoblasts expressing a disease associated SQSTM1 mutation with a TIA1 variant had an increase in persistent SGs as compared with mCherry-SQSTM1-WT expressing myoblasts (Figure 5D). To see if co-expression of SQSTM1-AX and TIA1-NS synergistically enhanced myotoxicity, we performed a lactate dehydrogenase (LDH) release assay on C2C12 myoblasts co-transfected with plasmids expressing mCherry-SQSTM1-WT, or mCherry-SQSTM1-AX and GFP-TIA1-WT or GFP-TIA1-NS before HS and following 60 min HS with an additional 60 min HS recovery a timepoint when persistent SG are present. Consistent with a synergistic effect, SQSTM1-AX and TIA1-NS expressing myoblasts had an increase in LDH release as compared with SQSTM1-WT or TIA1-WT transfectants (Figure 5E).

3.5 Discussion

The present study identified fourteen patients from nine families with a distal myopathy and RV-IBM pathology that all carried a previously reported pleotropic mutation in *SQSTM1* and a rare *TIA1*-N357S variant. These patients did not manifest other phenotypes associated with *SQSTM1* mutations such as PDB, ALS or FTD at the time of examination. Importantly, *SQSTM1* and *TIA1* accumulated with TDP-43 in patient muscle tissue suggesting they participate in disease pathogenesis. While the connection between SG clearance and autophagic protein degradation has been previously suggested, the present study provides human genetic evidence for a pathologic interaction [73, 109]. These data support that inheritance of a *TIA1* variant can shift the phenotypic spectrum of *SQSTM1* mutations to myodegeneration.

Mutations in *SQSTM1* were initially identified in patients with familial PDB and included the *SQSTM1*-P392L and c.1165+1 G>A splice acceptor mutations [3]. Notably the *SQSTM1*-P392L mutation was found in ~9% of sporadic PDB patients making it the most common genetic cause of PDB [3]. Later reports identified other missense mutations in or truncations of *SQSTM1*'s UBA domain including the M404V mutation as causative in familial and sporadic PDB [111]. Subsequently, *SQSTM1* mutations including the P392L and c.1165+1 G>A were identified in patients with familial ALS and FTD [4, 5, 117]. In 2015, we described three patients with a distal myopathy and RV-IBM pathology with the *SQSTM1* c.1165+1 G>A mutation [75]. Since the same *SQSTM1* mutation can generate distinct phenotypes in different patients, we suggested that *SQSTM1*-associated disease be termed multisystem proteinopathy type 4 (MSP4) [75]. MSP defines a pleotropic genetic disease in which a single gene and mutation can manifest with distinct disease phenotypes that include PDB, RV-IBM, ALS and FTD.

We previously reported a *TIA1*-E384K founder mutation as the cause of WDM, an autosomal dominant distal myopathy with RV-IBM pathology [61]. The phenotype of WDM patients is similar to the *SQSTM1*-*TIA1* patients described in this report. WDM is a progressive late onset myopathy that typically manifests in the fifth decade. Rare WDM patients that are homozygous for the *TIA1*-E384K variant have an earlier onset and more rapid disease progression suggesting that the *TIA1*-E384K mutation exerts a dose dependent dominant effect [118]. Similarly, we identified one patient in our cohort with a distal myopathy that was homozygous for the *TIA1*-N357S variant. This patient did not have a second mutation in *SQSTM1*. The *TIA1*-N357S was overrepresented in our myopathy cohort and was present in 20% of our distal myopathy patients. These data support that the *TIA1*-N357S may itself be a risk factor for distal myopathy.

The findings in our study may relate to other forms of MSP. Specifically, mutations in *VCP*, a ubiquitin segregase necessary for autophagic protein degradation, were the first identified cause of MSP (originally termed IBMPFD for inclusion body myopathy associated with Paget's disease of the bone and fronto-temporal dementia) [97]. Recent studies confirm the original report that 90% of patients develop RV-IBM, 42% PDB, 30% FTD but also expands the degenerative phenotypes to include 9% with ALS and 4% with parkinsonism [119]. Why some patients with *VCP* mutations develop RV-IBM and others PDB is not clear, but similar to our study likely relates to oligogenic inheritance. For example patients manifesting with *VCP* associated dementia are more likely to carry an *APOE4* allele [120]. Some *VCP* mutations, like the *SQSTM1*-P392L mutation have low minor allele frequencies in the general population. Rare variants in *VCP* and *SQSTM1* are identified as overrepresented in large cohorts of sporadic PDB,

IBM, ALS and dementia patients suggesting that they may be risk factors for disease or have reduced penetrance [4, 5, 112, 121-125].

Digenic inheritance can manifest in several ways. For example, the inheritance of second genetic variant can affect the primary genes mutant phenotype by modifying its severity or age of onset. Another example occurs when a single genetic mutation may have a reduced penetrance and the inheritance of a mutation in a second gene unmasks the variable expressivity of the primary mutation. Examples of true digenic inheritance in which the inheritance of two variants on two different genes are necessary to manifest disease are rare and challenging to prove. One recent example is in some forms of facioscapulohumeral muscular dystrophy type 2 (FSHD2) where a patient must inherit both a permissive D4Z4 allele and an *SMCHD1* variant on different chromosomes [126]. The strength of this example relates to its presence in multiple families and the convincing mechanistic interaction between the two alleles.

While autophagy has been implicated in SG clearance, this is the first report to demonstrate a role for SQSTM1 in SG dynamics. RNA binding proteins such as TIA1 initiate granule formation via their LCDs by promoting reversible LLPS [127]. Persistent SGs may occur when LLPS converts the LCD into an irreversible amyloid like structure [67]. Our data suggests that while the TIA-EK and NS variants promote phase separation, only the TIA1-EK variant enhances its amyloidogenic conversion. This may explain why heterozygous *TIA1*-E384K mutations lead to WDM yet *TIA1*-N357S variants require a SQSTM1 mutant environment for penetrance. Loss of SQSTM1 or SQSTM1 mutant expression leads to the accumulation of undegraded, ubiquitinated and insoluble proteins [18]. The presence of misfolded and aggregate prone proteins increases SG formation and persistence in cell culture [72, 114]. We similarly found that in the setting of SQSTM1 knockout or mutant expression,

TIA1 persistent SGs co-localized with aggregated proteins such as DRiPs and a C-terminal TDP-43 fragment. While it is possible that SQSTM1 directly shuttles ubiquitinated and aggregated TIA1 to the autophagosome, we propose an alternate model. Specifically, the presence of SQSTM1 mutations leads to the cytosolic accumulation of aggregated proteins that then serve as a nidus for RNA granule conversion to an irreversible state.

The mechanism whereby disturbances in RNA granule dynamics and persistence of poorly-dynamic SGs impair cell function in general or cause muscle degeneration in particular remains unclear. One possibility is that disturbance of the SG dynamics results in impairment of functions normally conducted within these complex membrane-less organelles (e.g. remodeling of mRNPs or participating in intracellular signaling cascades). Alternatively, the condensed liquid environment of the SG may promote untoward fibrillization of RNA-binding proteins to produce insoluble, pathological species. Indeed, in vitro LLPS promotes rapid fibrillization of RNA-binding proteins that occurs within the condensed liquid phase, resulting in the accumulation of potentially toxic species [67].

An enigmatic feature of the syndrome MSP and most of the constituent diseases (ALS, FTD and RV-IBM) is the prominence of TDP-43 pathology despite tremendous heterogeneity in genetic etiology. Thus, mutations in genes as diverse as *VCP*, *SQSTM1*, *C9ORF72*, *HNRNPA1*, *HNRNPA2B1*, *TARDBP* and *TIA1* culminate in highly similar histopathology in which cytoplasmic deposition of fibrillar TDP-43 is a prominent feature. Notably, even when disease mutations occur in other RNA-binding proteins prone to fibrillization, such as TIA1, the histopathological picture is dominated by TDP-43 pathology [60]. A likely explanation for this phenomenon is differences in the stability of fibrils assembled from various RNA-binding proteins. Indeed, it was recently demonstrated that recruitment of TDP-43 to SGs results in

abrupt reduction in mobility of this protein and conversion to an SDS-resistant, poorly soluble species, whereas other RNA-binding proteins recruited to the same SGs remain mobile and soluble [60].

Cytosolic TDP-43 accumulation has been demonstrated to elicit cellular toxicity via several mechanisms including disruptions in RNA transport, splicing and nucleocytoplasmic shuttling [128]. Interestingly, autophagic inhibition leads to the cytosolic accumulation in TDP-43 [129]. This effect also occurs in differentiated skeletal muscle, further connecting autophagic impairment with SG pathology [129]. Interestingly, enhancing autophagy has been demonstrated to be protective in the setting of TDP-43 accumulation [130].

MSP may represent an alternative manifestation of digenic inheritance. Specifically, a mutation on gene X (i.e. *SQSTM1* or *VCP*) can lead to variable expressivity of multiple phenotypes (PDB, ALS, FTD or RV-IBM). Inheritance of a variant on gene Y (*TIA1*) while impenetrant alone, dictates the phenotypic expression of gene X (distal myopathy with RV-IBM pathology). This model explains the genetics of MSP but may also relate to the phenotypic penetrance seen within the ALS-FTD spectrum. In addition, our model supports a pathomechanistic connection between stress granule homeostasis and ubiquitin mediated autophagic degradation.

Chapter 4: General Conclusion and Future direction

4.1 The butterfly effect of a small protein, ubiquitin.

Minor perturbation in a small state such as the flapping of wings of a distant butterfly can cause a major disruption in a large state, a tornado formation. This present dissertation showed that a small change on a protein (ubiquitination on SQSTM1) can alter a cellular event (protein degradation). This work demonstrated that SQSTM1 is regulated via its UBA domain ubiquitination. In addition, K420 within UBA domain is ubiquitinated by Keap1/Cul3 E3 ligase complex. Deletion of UBA domain or substitution of K420 to arginine decreases its ubiquitination, decreasing the size of SQSTM1 bodies, the number of ubiquitinated inclusion bodies, the interaction with LC3B, and the cell viability against ubiquitinated aggregates. The overexpression of Keap1/Cul3 increases the size of SQSTM1 bodies and enhances the formation of ubiquitinated inclusion bodies. Also, this increases the association with LC3B, consequently the degradation of SQSTM1. Keap1/Cul3 overexpression can rescue cell viability against proteotoxicity. Therefore, this dissertation proposed a model that SQSTM1's UBA domain ubiquitination by Keap1/Cul3 E3 ligase enhances its sequestering activity, recruits phagophores, and subsequently increases the degradation of SQSTM1 bodies (Figure1).

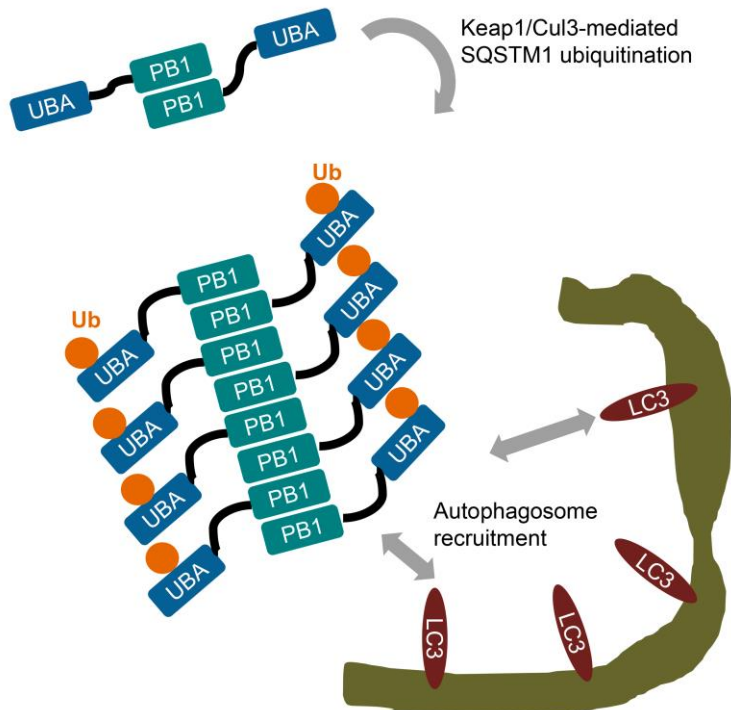


Figure 1. UBA domain ubiquitination regulates SQSTM1's functions.

Cellular functions of high-ordered structures have been emphasized. Post-translational modification on high-ordered structure is one of common regulatory mechanisms [54]. This work also parallels to this idea that ubiquitination within the UBA domain can modulate the dynamics of high-ordered SQSTM1 oligomers. The SQSTM1 oligomers would sequester ubiquitinated proteins and initiate the assembly of phagophore membranes, degrading the substrates. It becomes clear that different E3 ligases regulate the structure and function of SQSTM1, but how these E3 ligases cross talk to fine tune SQSTM1's oligomerization and functions still remains elucidated. It is possible that ubiquitination at different lysines of SQSTM1 can be regulated in a cargo-depending manner. Parkin is a stereotypical mitophagy E3 ligase, which ubiquitinates the outer surface of mitochondria along with the PB1 domain of SQSTM1 [36]. In contrast, upon oxidative stress, TRIM21 ubiquitinates the PB1 domain of SQSTM1 to inhibit its sequestering activity [37]. The other remaining question is how ubiquitination selectively regulates the SQSTM1's interaction with other autophagy adaptor proteins such as NBR1, OPTN and NDP52 upon different cargoes. To this end, which autophagy adaptors are recruited to specific cargoes such as mitochondria, ubiquitinated protein aggregates will be examined by utilizing genome-edited cell lines to knock out multiple autophagy adaptors. For controls, ATG5^{-/-} cells and single autophagy adaptor-knockout cells will be used.

4.2 Ubiquitination status of SQSTM1 disease mutants as a unifying disease feature

This work seeks to answer a question: how do dominantly inherited SQSTM1 disease mutations contribute to MSP pathogenesis? Most of identified SQSTM1 mutations are clustered within its UBA domain. Along with the previous report on ubiquitin binding affinity of SQSTM1 mutants,

we suggest that the reduced ubiquitination status of SQSTM1 mutants may be a unifying feature of pathogenesis with reduced ubiquitin binding affinity [76]. Purified SQSTM1-K420R decreases its binding to ubiquitin *in vitro* compared to naïve SQSTM1-WT while the c-terminus of SQSTM1 enhances its binding to ubiquitin *in vitro*, suggesting the loss of ubiquitination disrupts the ubiquitin binding [39]. Additionally, this study demonstrated that the ubiquitin binding of UBA domain may be linked to its dimerization and ubiquitination. Purified SQSTM1-K420R/E409A, which is neither ubiquitinated nor dimerized, binds much more strongly to ubiquitin than any other purified SQSTM1 proteins. This finding supports our model that once UBA domain ubiquitination at K420 would disrupt its dimerization with a neighboring UBA domain, SQSTM1 forms its “open” SQSTM1 body structure, allowing increased ubiquitin binding. However, it is not clear whether SQSTM1 disease mutants or SQSTM1-K420R are still dimerized and remain as a “close” structure to bind less effectively to ubiquitin. To answer this, *in vitro* structural studies such as Cryo-EM of purified SQSTM1-K420R and other disease mutants in absence/present with ubiquitin should be continued.

Generating a MSP-mouse model can further expand our understanding on MSP diseases. From our own lab, we are pursuing to generate muscle-specific VCP knock-out mouse model as well as neuron-specific VCP knock-out mouse model. We hope to understand the function of VCP and how its mutation manifests MSP in a tissue-specific manner by virally introducing a VCP disease-causing mutation. Homogeneous population of muscle cells or neuronal cells from these models will be isolated and analyzed. For controls, homogenous population of non-MSP affected tissues will be analyzed. Also, several time points to isolate the tissues will be considered since aging is one of the major risk factors of MSP and related to increased somatic

mutations in post-mitotic cells [131]. Along with this work, SQSTM1 mouse models can be generated and analyzed in parallel.

All SQSTM1 disease mutants showed decreased their sequestering function and cell viability against proteotoxicity. Interestingly, the overexpression of Keap1/Cul3 in SQSTM1-disease mutant transfected cells rescued cells against polyglutamine toxicity, suggesting that SQSTM1's UBA domain ubiquitination modulates selective autophagy and further connects to SQSTM1 to Keap1-Nrf2 signaling. SQSTM1 mutations from ALS and FTD patients were identified in KIR domain, showing the loss of binding to Keap1 and reduced Nrf2 activity [94]. Notably, Nrf2 activation can be cytoprotective in several diseases including neurodegenerative disease, liver disease, and cancer [96, 132, 133]. Also, a recent study reported that chemical modulation of Keap1 can selectively drive mitophagy [134]. This chemical treatment disrupts the Keap1 association with Nrf2, allowing the Nrf2 translocation and accumulation in the nucleus. Nrf2 then activates one of its target genes, SQSTM1 and SQSTM1 is subsequently recruited to damaged mitochondria along with other autophagic machinery proteins [45]. This compound does not disturb general macro-autophagy process, but only targets damaged mitochondria. This compound has not been tested in MSP-disease model, but it will be reasonable to administer this chemical to examine the effect on SQSTM1 ubiquitination and protein aggregates clearance.

4.3 SQSTM1 mediates the clearance of SGs.

This present dissertation also provides genetic evidence that TIA1 variants can shift the phenotype spectrum of SQSTM1-driven MSP to myodegeneration. 14 patients with RV-IBM and distal myopathy from 9 families were identified to have both TIA1 and SQSTM1 mutations. These patients did not manifest other phenotypes of MSP such as ALS, FTD, or PDB. One

important note is that, 50 PDB patients carrying SQSTM1-P392L mutation do not have a TIA1 mutation and show no muscle weakness or any other relevant myopathy symptoms. However, what drives other phenotypes of SQSTM1-mediated MSP such as ALS, FTD, and PDB is still unclear and other digenic inheritance may explain this. More genetic studies in SQSTM1-mediated ALS, FTD and PDB should be continued to answer this question.

Together with human genetic data, this dissertation shows that SQSTM1 is linked to both systems: protein quality control (autophagy) and RNA quality control (SGs homeostasis) are connected. The specific mechanism of SGs homeostasis still remains unclear but several studies suggest that chaperones and autophagy machineries participate in this process as a part of their protein-quality control (PQC) functions [109, 114]. However, with MSP-protein mutations and/or under stress conditions, the PQC machineries are overwhelmed and SGs accumulate with misfolded proteins such as TDP-43 in the cytosol. This brings up an important question: what triggers persistent SGs formation and converts them into pathological aggregates? An intriguing hypothesis is that the presence of aggregation-prone proteins in SGs promotes LLPS and the formation of persistent SGs, irreversibly converted into pathological fibers. Also, this might create a condensed environment for locally recruiting and accumulating more aggregation-prone proteins such as TDP-43 to amplify the whole aggregation process.

4.4 Proposed model of SGs homeostasis

Aggregated proteins on SGs have been speculated as one of the major LLPS driving factors, which generate persistent SGs. Mateju et al. reported that SGs co-assembles with SOD1, promoting LLPS and generating poor-dynamic SGs [72]. Interestingly, after SOD1 mutants accumulate within SGs, these mutants also become immobile. The previous study from

Mackenzie et al. suggests that the TDP-43 pathology commonly seen in MSP-affected tissues can be explained by this hypothesis. ALS/FTD-causing TIA1 mutations enhance LLPS and the formation of persistent SGs, and accumulate with TDP-43, which becomes insoluble. *In vitro* LLPS studies also supports that increased LLPS produces pathological SGs [67]. In contrast, a chaperone complex, HSPB8/BAG3/HSP70, is recruited to SGs and aids to disassemble SGs [114]. Inhibition or depletion of this complex disrupts the disassembly of SGs, which contain aggregated proteins such as FUS. A recent interactome study also supports this interaction between aggregation-prone proteins, SGs, and the PQC machineries [135]. The proteomic analysis of polyglutamine repeat of Huntingtin mutants (HttQ) showed that most of soluble HttQ interactors are RNA-binding proteins containing the LCD domain. Surprisingly, once soluble HttQ oligomers become insoluble, they are less interactive and only small number of chaperones and cochaperones e.g. DnaJB can access to these insoluble HttQ, preventing aberrant interaction between HttQ oligomers and others. Similarly, Shorter group reported that Hsp104 solubilizes and disassembles SGs containing RNA-binding proteins such as FUS or TDP-43 [136].

Here, we proposed an extended model of SGs homeostasis (Figure2). 1. Aggregation-prone proteins accumulate within SGs. 2. E3 ligases such as TRIM21, TRIM25 interacting with VCP catalyze these aggregated proteins [137, 138] 3. VCP and its cofactor segregate these ubiquitinated proteins from SGs and shuttle them to the PQC machineries for their re-folding or degradation, while SGs are disassembled by a chaperone complex, HSPB8/BAG3/HSP70. 4. However, if the segregation or disassembly of SGs is failed, SQSTM1 recognizes and sequesters these aberrant SGs with ubiquitinated proteins into inclusion bodies. 6. Aberrant SGs are degraded via autophagy.

We will further investigate whether VCP-recruited SGs fails to be cleared in p62^{-/-}-MEFs. VCP is recruited to SGs upon heat shock, but the depletion or chemical inhibition of VCP accumulates SGs with misfolded proteins e.g. TDP-43 and DRiPs, suggesting that VCP mediates the disassembly and/or clearance of SGs [73, 109]. To this end, p62^{-/-}-MEFs and control MEFs will be incubated for 1hour at 42°C for heat shock, and returned to 37°C for their recovery. Cells will be co-stained with TIA1, G3BP (for SGs detection), and VCP. TIA1/G3BP1-positive SGs will be counted as a total number of SGs and VCP/TIA1/G3BP1-positive SGs will be counted.

Whether the inhibition of VCP accumulates aberrant SGs (SGs containing ubiquitinated proteins) together with SGs (SGs without ubiquitinated proteins) will be further examined. Different VCP chemical inhibitors such as DBeQ, ML240 and EeyarestatinI will be treated in p62^{-/-}-MEFs and control MEFs along with heat shock. Mock-treated cells and chaperone inhibitor e.g. VER-155008 treated cells will be used as controls [72, 109, 114]. Cells will be co-stained with SGs markers, VCP, and ubiquitin. The expected result is shown in Figure3.

We expect that chaperones inhibitor-treated p62^{-/-}-MEFs will accumulate more SGs without ubiquitiated proteins compared to mock-treated p62^{-/-}-MEFs since chaperone-mediated SGs disassembly will be failed after VCP and its cofactors remove ubiquitianted proteins from SGs. We also expect that VCP inhibitor-treated p62^{-/-}-MEFs will accumulate both SGs (SGs without ubiquitinated protiens) and aberrant SGs (SGs with ubiquitinated proteins). To avoid off-target effect of the chemical inhibitors, VCP siRNA can be utilized. Also, the inhibition of VCP may disrupt the recruitment of E3 ligase catalyzing misfolded proteins within SGs. In this case, we will examine TDP-43, FUS, or DRiPs accumulation within SGs instead of ubiquitinated proteins.

We will further confirm this in MSP-disease models. Cells carrying MSP-disease mutation accumulate VCP-recruited SGs [109]. In human fibroblast with disease-causing TDP-43 mutations, SGs were persistent with recruited chaperone complexes [114]. We hypothesize that VCP-recruited SGs also contain SQSTM1 along with chaperone complexes. To test this, we will utilize U2OS cells expressing disease-causing VCP mutations and human fibroblasts derived from MSP patients. Those cells will be co-stained with SGs marker, VCP, and SQSTM1.

Several E3 ligases have been reported as SGs interactors upon virus infection. However, identifying SGs-interacting proteins has been challenging since the assembly/disassembly of SGs occurs rapidly but the components of SGs can be diverse [139]. Also in our scheme, impaired VCP activity may disrupt the recruitment of SQSTM1 and other interactors such as E3 ligases to aberrant SGs. To bypass this, a quantitative experiment with enzyme-catalyzed proximity labeling such as *proximity-dependent biotin identification* (BioID) or *ascorbate peroxidase* (APEX)-mediated labeling will be performed. The advantage of proximity labeling is that the labeling process can be done in live cells under physiological conditions within a short period of time [140]. To identify an interacting E3 ligase, *APEX-GFP* will be fused with *TIA1*. This *TIA1-APEX-GFP* plasmid will be expressed in stable isotope labelled-p62^{-/-}-MEFs and control MEFs upon heat shock as well as biotin-phenol and H₂O₂, while the expression of the plasmid will be visually confirmed. After cells lysis, biotinylated proteins will be enriched with streptavidin beads, digested by trypsin, and analyzed by mass spectrometry.

The proximity-labeling can be done in cell type-specific context. Investigating cell type-specific proteomics is important because components of SGs are diverse in a cell-type specific manner, which may answer a question: why certain tissues such as muscle and CNS are more vulnerable to MSP-causing mutations than others? One possible answer can be found from two

recent studies [138]. These studies successfully applied the proximity-labeling proteomics and identified SGs-interacting proteins in several cell lines including ALS patient-derived neural progenitor cells. They confirmed the presence of previously reported PQC factors within SGs in several cell types. They estimated that up to 20% of components are recruited to SGs in a cell type-specific or stress-specific manner. Interestingly, neuronal cells contain the most diverse components enriched with PQC machineries and about 75% of SGs components were not previously reported as SGs components, suggesting that neuronal cells may need more PQC factors to tightly regulate its protein homeostasis upon environmental stresses. However, muscle-specific proteomic information is still lacking. A systemic approach will broaden but specify our aspects about how diverse SGs components are in different tissues.

Modulating disaggregase activity i.e. Hsp104 or DNaJB6 may provide a therapeutic strategy to prevent MSP pathogenesis since aberrant interaction of SGs with misfolded proteins can be prevented by chaperones [135, 136]. Also, chemically inducing autophagy reduces the number of SGs in ALS patient-derived iPS cells and iPSC-derived neurons [141]. To test whether disaggregase prevent the accumulation of SGs, Hsp104 or DNaJB6 can be expressed in human fibroblast from MSP patients or mouse model expressing MSP-disease causing mutation. Also, autophagy inducers i.e. Rapamycin can be tested to examine the rescue effect in MSP-disease models.

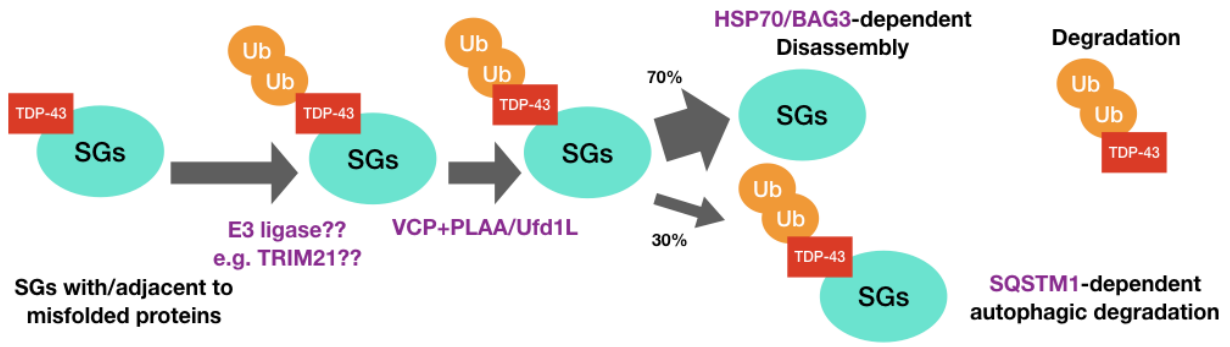


Figure 2. Proposed model for SGs homeostasis.

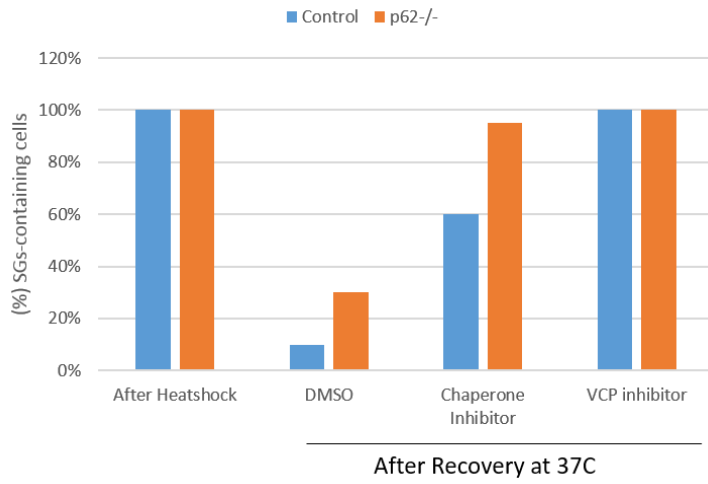


Figure 3. Expected result

4.5 Concluding remarks

Life is full of stress. However, cells always find their own ways to reduce their stress level and keep their own peace. They have developed a sophisticated system to control proteins upon different stresses. This work has investigated protein homeostasis by focusing on how proteins are aggregated and degraded (Chapter 2). Also, this work demonstrated that the biology of protein homeostasis is complex since it is temporally and spatially regulated with RNA metabolism (Chapter 3). The introduction of a single genetic mutation can disrupt this whole system but is very unpredictable, suggesting that many future studies should be coming along from multiple angles. However, understanding of MSP genetics has been paving the way for researchers to focus on various cellular pathways. More genetic studies together with molecular studies should be continued to delineate underlying mechanism of MSP.

References

1. Balch, W.E., et al., *Adapting proteostasis for disease intervention*. Science, 2008. **319**(5865): p. 916-9.
2. Taylor, J.P., *Multisystem proteinopathy: intersecting genetics in muscle, bone, and brain degeneration*. Neurology, 2015. **85**(8): p. 658-60.
3. Hocking, L.J., et al., *Domain-specific mutations in sequestosome 1 (SQSTM1) cause familial and sporadic Paget's disease*. Hum Mol Genet, 2002. **11**(22): p. 2735-9.
4. Fecto, F., et al., *SQSTM1 mutations in familial and sporadic amyotrophic lateral sclerosis*. Arch Neurol, 2011. **68**(11): p. 1440-6.
5. Le Ber, I., et al., *SQSTM1 mutations in French patients with frontotemporal dementia or frontotemporal dementia with amyotrophic lateral sclerosis*. JAMA Neurol, 2013. **70**(11): p. 1403-10.
6. Evila, A., et al., *Targeted next-generation sequencing assay for detection of mutations in primary myopathies*. Neuromuscul Disord, 2016. **26**(1): p. 7-15.
7. Klionsky, D.J., *Autophagy revisited: a conversation with Christian de Duve*. Autophagy, 2008. **4**(6): p. 740-3.
8. Galluzzi, L., et al., *Molecular definitions of autophagy and related processes*. EMBO J, 2017. **36**(13): p. 1811-1836.
9. Stolz, A., A. Ernst, and I. Dikic, *Cargo recognition and trafficking in selective autophagy*. Nat Cell Biol, 2014. **16**(6): p. 495-501.
10. Hara, T., et al., *Suppression of basal autophagy in neural cells causes neurodegenerative disease in mice*. Nature, 2006. **441**(7095): p. 885-9.
11. Komatsu, M., et al., *Homeostatic levels of p62 control cytoplasmic inclusion body formation in autophagy-deficient mice*. Cell, 2007. **131**(6): p. 1149-63.
12. Nezis, I.P., et al., *Ref(2)P, the Drosophila melanogaster homologue of mammalian p62, is required for the formation of protein aggregates in adult brain*. J Cell Biol, 2008. **180**(6): p. 1065-71.
13. Masiero, E., et al., *Autophagy is required to maintain muscle mass*. Cell Metab, 2009. **10**(6): p. 507-15.
14. Seibenhener, M.L., et al., *Sequestosome 1/p62 is a polyubiquitin chain binding protein involved in ubiquitin proteasome degradation*. Mol Cell Biol, 2004. **24**(18): p. 8055-68.

15. Zatloukal, K., et al., *p62 Is a common component of cytoplasmic inclusions in protein aggregation diseases*. Am J Pathol, 2002. **160**(1): p. 255-63.
16. Bjorkoy, G., et al., *p62/SQSTM1 forms protein aggregates degraded by autophagy and has a protective effect on huntingtin-induced cell death*. J Cell Biol, 2005. **171**(4): p. 603-14.
17. Shin, J., *P62 and the sequestosome, a novel mechanism for protein metabolism*. Arch Pharm Res, 1998. **21**(6): p. 629-33.
18. Pankiv, S., et al., *p62/SQSTM1 binds directly to Atg8/LC3 to facilitate degradation of ubiquitinated protein aggregates by autophagy*. J Biol Chem, 2007. **282**(33): p. 24131-45.
19. Kirkin, V., et al., *A role for NBR1 in autophagosomal degradation of ubiquitinated substrates*. Mol Cell, 2009. **33**(4): p. 505-16.
20. Mostowy, S., et al., *p62 and NDP52 proteins target intracytosolic Shigella and Listeria to different autophagy pathways*. J Biol Chem, 2011. **286**(30): p. 26987-95.
21. Wild, P., et al., *Phosphorylation of the autophagy receptor optineurin restricts Salmonella growth*. Science, 2011. **333**(6039): p. 228-33.
22. Thurston, T.L., et al., *Galectin 8 targets damaged vesicles for autophagy to defend cells against bacterial invasion*. Nature, 2012. **482**(7385): p. 414-8.
23. Dikic, I., S. Wakatsuki, and K.J. Walters, *Ubiquitin-binding domains - from structures to functions*. Nat Rev Mol Cell Biol, 2009. **10**(10): p. 659-71.
24. Hicke, L., H.L. Schubert, and C.P. Hill, *Ubiquitin-binding domains*. Nat Rev Mol Cell Biol, 2005. **6**(8): p. 610-21.
25. Komander, D. and M. Rape, *The ubiquitin code*. Annu Rev Biochem, 2012. **81**: p. 203-29.
26. Akutsu, M., I. Dikic, and A. Bremm, *Ubiquitin chain diversity at a glance*. J Cell Sci, 2016. **129**(5): p. 875-80.
27. Woelk, T., et al., *Molecular mechanisms of coupled monoubiquitination*. Nat Cell Biol, 2006. **8**(11): p. 1246-54.
28. Hoeller, D., et al., *Regulation of ubiquitin-binding proteins by monoubiquitination*. Nat Cell Biol, 2006. **8**(2): p. 163-9.
29. Harper, J.W., A. Ordureau, and J.M. Heo, *Building and decoding ubiquitin chains for mitophagy*. Nat Rev Mol Cell Biol, 2018. **19**(2): p. 93-108.

30. Heo, J.M., et al., *The PINK1-PARKIN Mitochondrial Ubiquitylation Pathway Drives a Program of OPTN/NDP52 Recruitment and TBK1 Activation to Promote Mitophagy*. Mol Cell, 2015. **60**(1): p. 7-20.
31. Richter, B., et al., *Phosphorylation of OPTN by TBK1 enhances its binding to Ub chains and promotes selective autophagy of damaged mitochondria*. Proc Natl Acad Sci U S A, 2016. **113**(15): p. 4039-44.
32. Matsumoto, G., et al., *Serine 403 phosphorylation of p62/SQSTM1 regulates selective autophagic clearance of ubiquitinated proteins*. Mol Cell, 2011. **44**(2): p. 279-89.
33. Liu, Z., et al., *Ubiquitylation of autophagy receptor Optineurin by HACE1 activates selective autophagy for tumor suppression*. Cancer Cell, 2014. **26**(1): p. 106-20.
34. Jongasma, M.L., et al., *An ER-Associated Pathway Defines Endosomal Architecture for Controlled Cargo Transport*. Cell, 2016. **166**(1): p. 152-66.
35. Heath, R.J., et al., *RNF166 Determines Recruitment of Adaptor Proteins during Antibacterial Autophagy*. Cell Rep, 2016. **17**(9): p. 2183-2194.
36. Song, P., et al., *Parkin promotes proteasomal degradation of p62: implication of selective vulnerability of neuronal cells in the pathogenesis of Parkinson's disease*. Protein Cell, 2016. **7**(2): p. 114-29.
37. Pan, J.A., et al., *TRIM21 Ubiquitylates SQSTM1/p62 and Suppresses Protein Sequestration to Regulate Redox Homeostasis*. Mol Cell, 2016. **61**(5): p. 720-33.
38. Lin, Q., et al., *The HECT E3 ubiquitin ligase NEDD4 interacts with and ubiquitylates SQSTM1 for inclusion body autophagy*. J Cell Sci, 2017. **130**(22): p. 3839-3850.
39. Peng, H., et al., *Ubiquitylation of p62/sequestosome1 activates its autophagy receptor function and controls selective autophagy upon ubiquitin stress*. Cell Res, 2017. **27**(5): p. 657-674.
40. Komatsu, M., et al., *The selective autophagy substrate p62 activates the stress responsive transcription factor Nrf2 through inactivation of Keap1*. Nat Cell Biol, 2010. **12**(3): p. 213-23.
41. Ichimura, Y., et al., *Phosphorylation of p62 activates the Keap1-Nrf2 pathway during selective autophagy*. Mol Cell, 2013. **51**(5): p. 618-31.
42. Lau, A., et al., *A noncanonical mechanism of Nrf2 activation by autophagy deficiency: direct interaction between Keap1 and p62*. Mol Cell Biol, 2010. **30**(13): p. 3275-85.
43. Furukawa, M. and Y. Xiong, *BTB protein Keap1 targets antioxidant transcription factor Nrf2 for ubiquitination by the Cullin 3-Roc1 ligase*. Mol Cell Biol, 2005. **25**(1): p. 162-71.

44. Kobayashi, A., et al., *Oxidative and electrophilic stresses activate Nrf2 through inhibition of ubiquitination activity of Keap1*. Mol Cell Biol, 2006. **26**(1): p. 221-9.
45. Jain, A., et al., *p62/SQSTM1 is a target gene for transcription factor NRF2 and creates a positive feedback loop by inducing antioxidant response element-driven gene transcription*. J Biol Chem, 2010. **285**(29): p. 22576-91.
46. Long, J., et al., *Dimerisation of the UBA domain of p62 inhibits ubiquitin binding and regulates NF-kappaB signalling*. J Mol Biol, 2010. **396**(1): p. 178-94.
47. Lim, J., et al., *Proteotoxic stress induces phosphorylation of p62/SQSTM1 by ULK1 to regulate selective autophagic clearance of protein aggregates*. PLoS Genet, 2015. **11**(2): p. e1004987.
48. Lu, K., F. den Brave, and S. Jentsch, *Receptor oligomerization guides pathway choice between proteasomal and autophagic degradation*. Nat Cell Biol, 2017. **19**(6): p. 732-739.
49. Wurzer, B., et al., *Oligomerization of p62 allows for selection of ubiquitinated cargo and isolation membrane during selective autophagy*. Elife, 2015. **4**: p. e08941.
50. Zaffagnini, G., et al., *p62 filaments capture and present ubiquitinated cargos for autophagy*. EMBO J, 2018.
51. Ciuffa, R., et al., *The selective autophagy receptor p62 forms a flexible filamentous helical scaffold*. Cell Rep, 2015. **11**(5): p. 748-58.
52. Narendra, D., et al., *p62/SQSTM1 is required for Parkin-induced mitochondrial clustering but not mitophagy; VDAC1 is dispensable for both*. Autophagy, 2010. **6**(8): p. 1090-106.
53. Itakura, E. and N. Mizushima, *p62 Targeting to the autophagosome formation site requires self-oligomerization but not LC3 binding*. J Cell Biol, 2011. **192**(1): p. 17-27.
54. Wu, H. and M. Fuxreiter, *The Structure and Dynamics of Higher-Order Assemblies: Amyloids, Signalosomes, and Granules*. Cell, 2016. **165**(5): p. 1055-66.
55. Rea, S.L., et al., *SQSTM1 mutations--bridging Paget disease of bone and ALS/FTLD*. Exp Cell Res, 2014. **325**(1): p. 27-37.
56. Cavey, J.R., et al., *Loss of ubiquitin-binding associated with Paget's disease of bone p62 (SQSTM1) mutations*. J Bone Miner Res, 2005. **20**(4): p. 619-24.
57. Goode, A., et al., *Defective recognition of LC3B by mutant SQSTM1/p62 implicates impairment of autophagy as a pathogenic mechanism in ALS-FTLD*. Autophagy, 2016. **12**(7): p. 1094-104.

58. Wright, T., et al., *The S349T mutation of SQSTM1 links Keap1/Nrf2 signalling to Paget's disease of bone*. Bone, 2013. **52**(2): p. 699-706.
59. Kurihara, N., et al., *Contributions of the measles virus nucleocapsid gene and the SQSTM1/p62(P392L) mutation to Paget's disease*. Cell Metab, 2011. **13**(1): p. 23-34.
60. Mackenzie, I.R., et al., *TIA1 Mutations in Amyotrophic Lateral Sclerosis and Frontotemporal Dementia Promote Phase Separation and Alter Stress Granule Dynamics*. Neuron, 2017. **95**(4): p. 808-816 e9.
61. Hackman, P., et al., *Welander distal myopathy is caused by a mutation in the RNA-binding protein TIA1*. Ann Neurol, 2013. **73**(4): p. 500-9.
62. Kim, H.J., et al., *Mutations in prion-like domains in hnRNPA2B1 and hnRNPA1 cause multisystem proteinopathy and ALS*. Nature, 2013. **495**(7442): p. 467-73.
63. Vieira, N.M., et al., *A defect in the RNA-processing protein HNRPDL causes limb-girdle muscular dystrophy 1G (LGMD1G)*. Hum Mol Genet, 2014. **23**(15): p. 4103-10.
64. Gitcho, M.A., et al., *TDP-43 A315T mutation in familial motor neuron disease*. Ann Neurol, 2008. **63**(4): p. 535-8.
65. Kwiatkowski, T.J., Jr., et al., *Mutations in the FUS/TLS gene on chromosome 16 cause familial amyotrophic lateral sclerosis*. Science, 2009. **323**(5918): p. 1205-8.
66. Alberti, S., et al., *A systematic survey identifies prions and illuminates sequence features of prionogenic proteins*. Cell, 2009. **137**(1): p. 146-58.
67. Molliex, A., et al., *Phase separation by low complexity domains promotes stress granule assembly and drives pathological fibrillization*. Cell, 2015. **163**(1): p. 123-33.
68. Protter, D.S. and R. Parker, *Principles and Properties of Stress Granules*. Trends Cell Biol, 2016. **26**(9): p. 668-79.
69. Anderson, P. and N. Kedersha, *RNA granules*. J Cell Biol, 2006. **172**(6): p. 803-8.
70. Decker, C.J. and R. Parker, *P-bodies and stress granules: possible roles in the control of translation and mRNA degradation*. Cold Spring Harb Perspect Biol, 2012. **4**(9): p. a012286.
71. Ryu, H.H., et al., *Autophagy regulates amyotrophic lateral sclerosis-linked fused in sarcoma-positive stress granules in neurons*. Neurobiol Aging, 2014. **35**(12): p. 2822-2831.
72. Mateju, D., et al., *An aberrant phase transition of stress granules triggered by misfolded protein and prevented by chaperone function*. EMBO J, 2017. **36**(12): p. 1669-1687.

73. Seguin, S.J., et al., *Inhibition of autophagy, lysosome and VCP function impairs stress granule assembly*. Cell Death Differ, 2014. **21**(12): p. 1838-51.
74. Rogov, V., et al., *Interactions between autophagy receptors and ubiquitin-like proteins form the molecular basis for selective autophagy*. Mol Cell, 2014. **53**(2): p. 167-78.
75. Bucelli, R.C., et al., *SQSTM1 splice site mutation in distal myopathy with rimmed vacuoles*. Neurology, 2015. **85**(8): p. 665-74.
76. Layfield, R., et al., *p62 mutations, ubiquitin recognition and Paget's disease of bone*. Biochem Soc Trans, 2006. **34**(Pt 5): p. 735-7.
77. Kim, W., et al., *Systematic and quantitative assessment of the ubiquitin-modified proteome*. Mol Cell, 2011. **44**(2): p. 325-40.
78. Kang, M.I., et al., *Scaffolding of Keap1 to the actin cytoskeleton controls the function of Nrf2 as key regulator of cytoprotective phase 2 genes*. Proc Natl Acad Sci U S A, 2004. **101**(7): p. 2046-51.
79. Rodriguez, A., et al., *Mature-onset obesity and insulin resistance in mice deficient in the signaling adapter p62*. Cell Metab, 2006. **3**(3): p. 211-22.
80. Mosesson, Y., et al., *Monoubiquitinylation regulates endosomal localization of Lst2, a negative regulator of EGF receptor signaling*. Dev Cell, 2009. **16**(5): p. 687-98.
81. Cullinan, S.B., et al., *The Keap1-BTB protein is an adaptor that bridges Nrf2 to a Cul3-based E3 ligase: oxidative stress sensing by a Cul3-Keap1 ligase*. Mol Cell Biol, 2004. **24**(19): p. 8477-86.
82. Fuentealba, R.A., et al., *Interaction with polyglutamine aggregates reveals a Q/N-rich domain in TDP-43*. J Biol Chem, 2010. **285**(34): p. 26304-14.
83. Weihl, C.C., et al., *Inclusion body myopathy-associated mutations in p97/VCP impair endoplasmic reticulum-associated degradation*. Hum Mol Genet, 2006. **15**(2): p. 189-99.
84. Wagner, S.A., et al., *A proteome-wide, quantitative survey of in vivo ubiquitylation sites reveals widespread regulatory roles*. Mol Cell Proteomics, 2011. **10**(10): p. M111 013284.
85. Mertins, P., et al., *Integrated proteomic analysis of post-translational modifications by serial enrichment*. Nat Methods, 2013. **10**(7): p. 634-7.
86. Singer, J.D., et al., *Cullin-3 targets cyclin E for ubiquitination and controls S phase in mammalian cells*. Genes Dev, 1999. **13**(18): p. 2375-87.
87. Soucy, T.A., et al., *An inhibitor of NEDD8-activating enzyme as a new approach to treat cancer*. Nature, 2009. **458**(7239): p. 732-6.

88. Lau, A., et al., *Arsenic inhibits autophagic flux, activating the Nrf2-Keap1 pathway in a p62-dependent manner*. Mol Cell Biol, 2013. **33**(12): p. 2436-46.
89. Watanabe, Y., et al., *p62/SQSTM1-dependent autophagy of Lewy body-like alpha-synuclein inclusions*. PLoS One, 2012. **7**(12): p. e52868.
90. Fan, W., et al., *Keap1 facilitates p62-mediated ubiquitin aggregate clearance via autophagy*. Autophagy, 2010. **6**(5): p. 614-21.
91. Lo, S.C. and M. Hannink, *PGAM5, a Bcl-XL-interacting protein, is a novel substrate for the redox-regulated Keap1-dependent ubiquitin ligase complex*. J Biol Chem, 2006. **281**(49): p. 37893-903.
92. Lo, S.C., et al., *Structure of the Keap1:Nrf2 interface provides mechanistic insight into Nrf2 signaling*. EMBO J, 2006. **25**(15): p. 3605-17.
93. Haack, T.B., et al., *Absence of the Autophagy Adaptor SQSTM1/p62 Causes Childhood-Onset Neurodegeneration with Ataxia, Dystonia, and Gaze Palsy*. Am J Hum Genet, 2016. **99**(3): p. 735-43.
94. Goode, A., et al., *ALS-FTLD associated mutations of SQSTM1 impact on Keap1-Nrf2 signalling*. Mol Cell Neurosci, 2016. **76**: p. 52-58.
95. Ishimura, R., K. Tanaka, and M. Komatsu, *Dissection of the role of p62/Sqstm1 in activation of Nrf2 during xenophagy*. FEBS Lett, 2014. **588**(5): p. 822-8.
96. Gan, L. and J.A. Johnson, *Oxidative damage and the Nrf2-ARE pathway in neurodegenerative diseases*. Biochim Biophys Acta, 2014. **1842**(8): p. 1208-18.
97. Watts, G.D., et al., *Inclusion body myopathy associated with Paget disease of bone and frontotemporal dementia is caused by mutant valosin-containing protein*. Nat Genet, 2004. **36**(4): p. 377-81.
98. Johnson, J.O., et al., *Mutations in the Matrin 3 gene cause familial amyotrophic lateral sclerosis*. Nat Neurosci, 2014. **17**(5): p. 664-666.
99. Deng, H.X., et al., *Mutations in UBQLN2 cause dominant X-linked juvenile and adult-onset ALS and ALS/dementia*. Nature, 2011. **477**(7363): p. 211-5.
100. Maruyama, H., et al., *Mutations of optineurin in amyotrophic lateral sclerosis*. Nature, 2010. **465**(7295): p. 223-6.
101. Lee, Y., et al., *Keap1/Cullin3 Modulates p62/SQSTM1 Activity via UBA Domain Ubiquitination*. Cell Rep, 2017. **19**(1): p. 188-202.
102. Morissette, J., N. Laurin, and J.P. Brown, *Sequestosome 1: mutation frequencies, haplotypes, and phenotypes in familial Paget's disease of bone*. J Bone Miner Res, 2006. **21 Suppl 2**: p. P38-44.

103. Powell, A., et al., *Isolation of pandemic Vibrio parahaemolyticus from UK water and shellfish produce*. Microb Ecol, 2013. **65**(4): p. 924-7.
104. Ju, J.S. and C.C. Weihl, *Inclusion body myopathy, Paget's disease of the bone and frontotemporal dementia: a disorder of autophagy*. Hum Mol Genet, 2010. **19**(R1): p. R38-45.
105. Weihl, C.C., et al., *TDP-43 accumulation in inclusion body myopathy muscle suggests a common pathogenic mechanism with frontotemporal dementia*. J Neurol Neurosurg Psychiatry, 2008. **79**(10): p. 1186-9.
106. Salajegheh, M., et al., *Sarcoplasmic redistribution of nuclear TDP-43 in inclusion body myositis*. Muscle Nerve, 2009. **40**(1): p. 19-31.
107. Nogalska, A., et al., *p62/SQSTM1 is overexpressed and prominently accumulated in inclusions of sporadic inclusion-body myositis muscle fibers, and can help differentiating it from polymyositis and dermatomyositis*. Acta Neuropathol, 2009. **118**(3): p. 407-13.
108. Hiniker, A., et al., *Comparative utility of LC3, p62 and TDP-43 immunohistochemistry in differentiation of inclusion body myositis from polymyositis and related inflammatory myopathies*. Acta Neuropathol Commun, 2013. **1**: p. 29.
109. Buchan, J.R., et al., *Eukaryotic stress granules are cleared by autophagy and Cdc48/VCP function*. Cell, 2013. **153**(7): p. 1461-74.
110. Lek, M., et al., *Analysis of protein-coding genetic variation in 60,706 humans*. Nature, 2016. **536**(7616): p. 285-91.
111. Falchetti, A., et al., *Two novel mutations at exon 8 of the Sequestosome 1 (SQSTM1) gene in an Italian series of patients affected by Paget's disease of bone (PDB)*. J Bone Miner Res, 2004. **19**(6): p. 1013-7.
112. Cuyvers, E., et al., *Genetic variability in SQSTM1 and risk of early-onset Alzheimer dementia: a European early-onset dementia consortium study*. Neurobiol Aging, 2015. **36**(5): p. 2005 e15-22.
113. Langston, A.L., et al., *Randomized trial of intensive bisphosphonate treatment versus symptomatic management in Paget's disease of bone*. J Bone Miner Res, 2010. **25**(1): p. 20-31.
114. Ganassi, M., et al., *A Surveillance Function of the HSPB8-BAG3-HSP70 Chaperone Complex Ensures Stress Granule Integrity and Dynamism*. Mol Cell, 2016. **63**(5): p. 796-810.
115. Meriin, A.B., N. Zaarur, and M.Y. Sherman, *Association of translation factor eEF1A with defective ribosomal products generates a signal for aggresome formation*. J Cell Sci, 2012. **125**(Pt 11): p. 2665-74.

116. Schubert, U., et al., *Rapid degradation of a large fraction of newly synthesized proteins by proteasomes*. Nature, 2000. **404**(6779): p. 770-4.
117. Teyssou, E., et al., *Mutations in SQSTM1 encoding p62 in amyotrophic lateral sclerosis: genetics and neuropathology*. Acta Neuropathol, 2013. **125**(4): p. 511-22.
118. Welander, L., *Homozygous appearance of distal myopathy*. Acta Genet Stat Med, 1957. **7**(2): p. 321-5.
119. Al-Obeidi, E., et al., *Genotype-phenotype study in patients with VCP valosin-containing protein mutations associated with multisystem proteinopathy*. Clin Genet, 2017.
120. Mehta, S.G., et al., *APOE is a potential modifier gene in an autosomal dominant form of frontotemporal dementia (IBMPFD)*. Genet Med, 2007. **9**(1): p. 9-13.
121. Weihl, C.C., et al., *Targeted sequencing and identification of genetic variants in sporadic inclusion body myositis*. Neuromuscul Disord, 2015. **25**(4): p. 289-96.
122. Gang, Q., et al., *Rare variants in SQSTM1 and VCP genes and risk of sporadic inclusion body myositis*. Neurobiol Aging, 2016. **47**: p. 218 e1-218 e9.
123. Abramzon, Y., et al., *Valosin-containing protein (VCP) mutations in sporadic amyotrophic lateral sclerosis*. Neurobiol Aging, 2012. **33**(9): p. 2231 e1-2231 e6.
124. Lucas, G.J., et al., *Evaluation of the role of Valosin-containing protein in the pathogenesis of familial and sporadic Paget's disease of bone*. Bone, 2006. **38**(2): p. 280-5.
125. Beyens, G., et al., *Evaluation of the role of the SQSTM1 gene in sporadic Belgian patients with Paget's disease*. Calcif Tissue Int, 2004. **75**(2): p. 144-52.
126. Lemmers, R.J., et al., *Digenic inheritance of an SMCHD1 mutation and an FSHD-permissive D4Z4 allele causes facioscapulohumeral muscular dystrophy type 2*. Nat Genet, 2012. **44**(12): p. 1370-4.
127. Kedersha, N.L., et al., *RNA-binding proteins TIA-1 and TIAR link the phosphorylation of eIF-2 alpha to the assembly of mammalian stress granules*. J Cell Biol, 1999. **147**(7): p. 1431-42.
128. Ratti, A. and E. Buratti, *Physiological functions and pathobiology of TDP-43 and FUS/TLS proteins*. J Neurochem, 2016. **138** Suppl 1: p. 95-111.
129. Ju, J.S., et al., *Valosin-containing protein (VCP) is required for autophagy and is disrupted in VCP disease*. J Cell Biol, 2009. **187**(6): p. 875-88.
130. Scotter, E.L., et al., *Differential roles of the ubiquitin proteasome system and autophagy in the clearance of soluble and aggregated TDP-43 species*. J Cell Sci, 2014. **127**(Pt 6): p. 1263-78.

131. Lodato, M.A., et al., *Aging and neurodegeneration are associated with increased mutations in single human neurons*. *Science*, 2018. **359**(6375): p. 555-559.
132. Bae, S.H., et al., *Sestrins activate Nrf2 by promoting p62-dependent autophagic degradation of Keap1 and prevent oxidative liver damage*. *Cell Metab*, 2013. **17**(1): p. 73-84.
133. Deshmukh, P., et al., *The Keap1-Nrf2 pathway: promising therapeutic target to counteract ROS-mediated damage in cancers and neurodegenerative diseases*. *Biophys Rev*, 2017. **9**(1): p. 41-56.
134. Georgakopoulos, N.D., et al., *Reversible Keap1 inhibitors are preferential pharmacological tools to modulate cellular mitophagy*. *Sci Rep*, 2017. **7**(1): p. 10303.
135. Kim, Y.E., et al., *Soluble Oligomers of PolyQ-Expanded Huntingtin Target a Multiplicity of Key Cellular Factors*. *Mol Cell*, 2016. **63**(6): p. 951-64.
136. Yasuda, K., et al., *FUS inclusions disrupt RNA localization by sequestering kinesin-1 and inhibiting microtubule detyrosination*. *J Cell Biol*, 2017. **216**(4): p. 1015-1034.
137. Hauler, F., et al., *AAA ATPase p97/VCP is essential for TRIM21-mediated virus neutralization*. *Proc Natl Acad Sci U S A*, 2012. **109**(48): p. 19733-8.
138. Markmiller, S., et al., *Context-Dependent and Disease-Specific Diversity in Protein Interactions within Stress Granules*. *Cell*, 2018. **172**(3): p. 590-604 e13.
139. Aulas, A., et al., *Stress-specific differences in assembly and composition of stress granules and related foci*. *J Cell Sci*, 2017. **130**(5): p. 927-937.
140. Rhee, H.W., et al., *Proteomic mapping of mitochondria in living cells via spatially restricted enzymatic tagging*. *Science*, 2013. **339**(6125): p. 1328-1331.
141. Marrone, L., et al., *Isogenic FUS-eGFP iPSC Reporter Lines Enable Quantification of FUS Stress Granule Pathology that Is Rescued by Drugs Inducing Autophagy*. *Stem Cell Reports*, 2018.